REPORT DOCUMENTATION PAGE

READ INSTRUCTIONS BEFORE COMPLETING FORM

1. REPORT NUMBER: AFIT/CI/NR 88- 62
2. GOVT ACCESSION NO.:
3. RECIPIENT'S CATALOG NUMBER:

TITLE (and Subtitle): OPTIMIZATION OF MICROWAVE MAGNETOELASTIC DELAY LINES

5. TYPE OF REPORT & PERIOD COVERED: MS THESIS
6. PERFORMING ORG. REPORT NUMBER:

AUTHOR(s): BRUCE FRANK FELDMAN

8. CONTRACT OR GRANT NUMBER(s):

PERFORMING ORGANIZATION NAME AND ADDRESS: AFIT STUDENT AT: MASSACHUSETTS INSTITUTE OF TECHNOLOGY

10. PROGRAM ELEMENT, PROJECT, TASK AREA & WORK UNIT NUMBERS:

CONTROLLING OFFICE NAME AND ADDRESS:

12. REPORT DATE: 1988
13. NUMBER OF PAGES: 127

14. MONITORING AGENCY NAME & ADDRESS (if different from Controlling Office): AFIT/NR, Wright-Patterson AFB OH 45433-6583

15. SECURITY CLASS. (of this report): UNCLASSIFIED
15a. DECLASSIFICATION/DOWNGRADING SCHEDULE:

16. DISTRIBUTION STATEMENT (of this Report): DISTRIBUTED UNLIMITED: APPROVED FOR PUBLIC RELEASE

17. DISTRIBUTION STATEMENT (of the abstract entered in Block 20, if different from Report): SAME AS REPORT

18. SUPPLEMENTARY NOTES: Approved for Public Release: IAW AFR 190-1
LYNN E. WOLAVER 19 July 88
Dean for Research and Professional Development
Air Force Institute of Technology
Wright-Patterson AFB OH 45433-6583

19. KEY WORDS (Continue on reverse side if necessary and identify by block number):

20. ABSTRACT (Continue on reverse side if necessary and identify by block number): ATTACHED

Title: OPTIMIZATION OF MICROWAVE MAGNETOELASTIC DELAY LINES

Author: Bruce Frank Feldman
Capt, USAF

Year: 1988

Institution: Massachusetts Institute of Technology
Cambridge, MA 02139

Degree Awarded: MSEE

Number of Pages: 126

Abstract:

A new ray tracing computer program which optimizes the design of linearly dispersive, two-port magnetoelastic delay lines operating at microwave frequencies has been developed. The simulation shows that delay line line bandwidth and dynamic range can be separately optimized for the value of a wave focussing parameter within a limited range. Whereas previous work had demonstrated that there are a potentially infinite number of synthesized magnetic fields which produce the desired linear delay function, choice of magnetic field can now be made to obtain a desired value of the wave focussing parameter and thereby optimize delay line performance.

The computer simulation is correlated with experimental magnetoelastic delay line results. Previously, linearly dispersive two-port magnetoelastic delay lines with synthesized magnetic fields had been built in both a Strauss type configuration and with a novel, "buried-antenna" design where the antennas were wires inserted through separate holes drilled by laser in a YIG rod. The validity of the ray tracing is confirmed by the experimental data and, additionally, the simulation elucidates the causes of the differences in bandwidth performance between the design types.

The critical factors in optimizing bandwidth/dynamic range are shown to be the axial and radial magnetic field gradients which control both the focussing parameter and the time evolution of wavelength. A simple predictive model for bandwidth is developed as well as a closed form solution for the magnetic field which maximizes bandwidth.

Thesis Supervisor: Professor Frederic Morgenthaler
Department of Electrical Engineering and Computer Science (EECS)
Massachusetts Institute of Technology
Cambridge, MA 02139

Bibliography:
of Key References:

[1] Addison, R.C., Auld, B.A., and Collins, J.H., "Ray Theory Analysis of Magnetoelastic Delay Lines," Journal of Applied Physics, Vol. 39, No. 3, pp. 1828-1839, February 1968.

[2] Borgeaud, M., "An Improved Two-Port Magnetoelastic Delay Line," Technical Report 48 (SM Thesis), Microwave and Quantum Mechanics Group, Massachusetts Institute of Technology, January 1984.

OPTIMIZATION OF MICROWAVE MAGNETOELASTIC DELAY LINES

by

BRUCE FRANK FELDMAN

B.A., Chemistry
Yale University
(1978)

and

B.S.E.E., Electrical Engineering
Air Force Institute of Technology
(1983)

Submitted to the Department of
Electrical Engineering and Computer Science
in Partial Fulfillment of the Degree of
Master of Science

at the

Massachusetts Institute of Technology

May 1988

Signature of Author.....
Department of Electrical Engineering and Computer Science
April 25, 1988

Certified by.....
Frederic R. Morgenthaler
Professor, EECS
Thesis Supervisor

Accepted by.....
Arthur C. Smith
Professor, EECS
Chairman, Committee of Graduate Admissions

OPTIMIZATION OF MICROWAVE MAGNETOELASTIC DELAY LINES

by

BRUCE FRANK FELDMAN

Submitted to the Department of
Electrical Engineering and Computer Science
on May 6, 1988 in partial fulfillment of the
requirements for the Degree of Master of Science
in Electrical Engineering

ABSTRACT

A new ray tracing computer program which optimizes the design of linearly dispersive, two-part magnetoelastic delay lines operating at microwave frequencies has been developed. The simulation shows that delay line bandwidth and dynamic range can be separately optimized for the value of a wave focusing parameter within a limited range. Whereas previous work had demonstrated that there are a potentially infinite number of synthesized magnetic fields which produce the desired linear delay function, choice of magnetic field can now be made to obtain a desired value of the wave focusing parameter and thereby optimize delay line performance.

The computer simulation is correlated with experimental magnetoelastic delay line results. Previously, linearly dispersive two-port magnetoelastic delay lines with synthesized magnetic fields had been built in both a Strauss type configuration and with a novel, "buried-antenna" design where the antennas were wires inserted through separate holes drilled by laser in a YIG rod. The validity of the ray tracing is confirmed by the experimental data and, additionally, the simulation elucidates the causes of the differences in bandwidth performance between the design types.

The critical factors in optimizing bandwidth/dynamic range are shown to be the axial and radial magnetic field gradients which control both the focusing parameter and the time evolution of wavelength. A simple predictive model for bandwidth is developed as well as a closed form solution for the magnetic field which maximizes bandwidth.

Thesis Supervisor: Prof. Frederic Morgenthaler

Title: Professor of Electrical Engineering

ACKNOWLEDGMENTS

This thesis would not have been possible without the direction and support given me by my thesis advisor, Professor F.R. Morgenthaler. I am forever in his debt.

My MIT experience and education was made possible by the United States Air Force through its Senior Commanders Sponsored Education Program. This program, and the corporate dedication to excellence it represents, is just one more reason why I am proud to serve my country in the uniform of the U.S. Air Force.

It has been a pleasure knowing the faculty and staff of MIT's U.S. Air Force Reserve Officer Training Corps Detachment. My appreciation for their encouragement and support.

I also wish to thank Mr. Paul Martin of the Physics Department for both his intellectual companionship and the late night coffee breaks.

Finally, this thesis would not have been possible without the love, dedication, and support of my wife, Jean, and my children, Matthew and Jessica. Words cannot express my love.

FOR JEAN

TABLE OF CONTENTS

Page

LIST OF FIGURES

LIST OF PRINCIPAL SYMBOLS

a	$\frac{\omega_M}{\omega}$
a_n	coefficient of inner magnetic potential/field expansion
$\bar{B}$	magnetic flux
b	magnetoelastic splitting constant
b_n	coefficient of inner magnetization expansion
C	nonlinearity constant in synthesized magnetic field
C_p, C_p'	coefficients of outer magnetic potential/field expansion
C_{44}, C_{12}	Lamé constants
D	dispersive delay rate in TD(f)
$\bar{D}$	electric flux
D_c	density
$\bar{E}$	electric field
$\bar{e}$	small signal component of electric field
f	frequency
f_z	$\frac{\omega_z}{2\pi}$
f_M	$\frac{\omega_M}{2\pi}$
$\bar{H}$	magnetic field
$\bar{H}_A, \bar{H}_{DEM}, \bar{H}_{EX}$	components of magnetic field
H_0	static component of magnetic field
H_r, H_z	magnetic field in cylindrical coordinates
H_0', H_0''	derivatives of H_0 with respect to z
$\bar{h}, \bar{h}_{rf}$	small signal RF component of $\bar{H}$
$\bar{h}_{me}$	magnetoelastic components of $\bar{H}$
$\bar{k}$	wave vector

k_{cp}, k_{tp}	wavenumber at crossover point, turning point
k_0	$\omega(\mu_0 \epsilon)^{1/2}$
k_r, k_z	wavevector in cylindrical coordinates
$\bar{M}$	magnetization
M_0	static component of magnetization
M_r, M_z	magnetization in cylindrical coordinates
$\bar{m}$	small signal component of magnetization
P_n^*	external magnetic potential function
Q	focusing parameter
Q_n^*	external magnetic potential function
$\bar{r}, \bar{z}$	unit vectors in cylindrical coordinates
R	rod radius
T	time (with subscripts for elastic wave, spin wave)
TD(f)	dispersive delay function
T_0	fixed delay in dispersive delay function
$\bar{v}$	velocity (with subscripts for elastic wave, spin wave)
v_g	group velocity
v_p	phase velocity
v_r, v_z	components of $\bar{v}$ in cylindrical coordinates
YIG	Yttrium Iron Garnet
z_{cp}, z_{tp}	axial location of crossover point, turning point
α_n, β_n	coefficients of polynomial inner magnetic potential/field expansion
γ	gyromagnetic constant
ϵ	permittivity
$\bar{\xi}$	elastic displacement vector
κ, μ	components derived from Polder Tensor
λ_{ex}	spin exchange constant

μ_0	permeability of free space
θ	angle between $\bar{K}$ and $\bar{M}$
η	efficiency
ψ	scalar magnetic potential
ω	angular frequency
ω_z	$\gamma\mu_0 H_0$
ω_M	$\gamma\mu_0 M_0$
$\bar{\bar{x}}$	Polder Tensor

PREFACE

The increasing cost and complexity of microwave signal generating and processing systems continues to spur interest in the development of components which operate directly at microwave frequencies. Currently, many microwave signal processing systems require elaborate frequency conversion schemes wherein microwave signals are heterodyned down to VHF/UHF and are then processed by a wide variety of existing RF signal processing devices. The explosive growth in Surface Acoustic Wave (SAW) devices, for example, is a direct result of the advent of large microwave systems utilizing downconversion to RF. These downconversion methods, however, can be extraordinarily expensive (as when extremely coherent downconversion is required) and lack the extremely wide bandwidths which are a fundamental design objective in microwave system design. A case in point is wideband linear FM modulated (CHIRP) radar which suffers from hardware bandwidth limitations even today.

Magnetostatic and magnetoelastic wave devices hold the promise of addressing some of these issues. Components utilizing the propagation and conversion of magnetostatic and acoustic waves offer the advantages of direct operation at microwave frequencies, nonreciprocal spatial propagation, relatively long delay times, and frequency dispersion. Although many common devices utilize these and other magnetostatic effects (i.e., YIG filters and oscillators, isolators, circulators, etc.), development of linearly dispersive delay lines with user selectable characteristics has been limited by difficulties in synthesizing the requisite internal magnetic fields.

Within the last 10 years a technique for synthesizing a desired magnetic field in a YIG rod or disc has become available [1]. The method involves the defining of the equipotential surfaces both within and without the medium. Polepieces which are equipotentials outside the rod are then built and matched to the rod; energizing the pole pieces creates corresponding internal potential and magnetic fields.

As a result of this field synthesis technique, magnetoelastic delay lines with linear dispersion can be made and optimized to application [2,3]. These delay lines are extremely small, and have attenuations and bandwidths suitable for most signal processing applications. This thesis recapitulates the theory of operation of these delay lines, summarizes the experimental work performed to date, and describes the optimization technique which makes delay line design practicable.

Chapter I

INTRODUCTION

I.A Thesis Objectives

The goal of this research is to determine whether the design of a ferrite device, the magnetoelastic delay line, can be improved so as to maximize output bandwidth and dynamic range. The purpose of the thesis document itself is to evaluate the method, results, and conclusions of computer simulation of that type of delay line, and to describe the requirements for successful optimization. The computer program which is the analytical tool for simulating the magnetoelastic delay line, the model which resulted from consideration of the data, and the conclusions on optimizing delay line performance are all discussed as part of the presentation.

This introductory chapter is intended to provide a perspective from which to view the work accomplished. The chapter includes a short history of the discovery of magnetostatic and magnetoelastic waves and their immediate application in microwave delay devices. Also, a survey is made of a variety of magnetoelastic devices. Finally, the chapter concludes with a somewhat closer look at the predecessor work upon which this thesis is based.

Chapter II ("Theory of Magnetoelastic Waves") and Appendix A of this thesis constitute an abbreviated discussion of the underlying theory of magnetoelastic waves. Included therein are a review of magnetostatic and magnetoelastic wave dispersion relations, wave behaviors, and coupling effects. Chapter III ("The Magnetoelastic Delay Line") and Appendices B

and C provide a discussion of the operation of the magnetoelastic delay line, the magnetic field anisotropy of the YIG rod which is the medium of propagation, and the field parameters required for synthesis of the desired linear delay function. Although Chapters II and III extensively reference the appendices, they are intended to be a self-contained introduction sufficient to allow understanding of the problem and subsequent chapters.

Chapter IV ("Ray Tracing") presents the theory and techniques used in the ray tracing. Because the magnetic field in the ferrite rod is anisotropic, the propagation of energy depends upon position in the medium and assumptions more complex than those of simple optics must be made. The validity of the assumptions which allow ray tracing to be used in an anisotropic medium is discussed and the equations which describe the time evolution of the wave are presented. Also, the computer program which performs the ray tracing is outlined.

Chapter V ("Results and Conclusions") provides a brief summary of the raw data and presents conclusions in the form of a simple model. Predictions which extend the model to other substances are also made, and the ultimate goal of the thesis research, optimizing delay line design, is discussed in the context of the model.

Chapter VI ("Conclusions and Recommended Future Work") concludes the thesis with some suggestions for future work.

I.B History of the Magnetoelastic Delay Line

Although spin waves had been extensively considered previously, it was Ernst Schlömann who, in 1961, noted that naturally occurring

nonuniform magnetic fields in YIG rods and disks could be used to couple electromagnetic energy to magnetostatic spin waves [4]. His observation was that long wavelength spin waves should exist near surface regions of net magnetic dipole moment. They would then propagate into the sample towards regions of lesser magnetic field while simultaneously decreasing in wavelength. Eshbach subsequently verified this prediction and also noted that under certain conditions of magnetic field, the spin waves could be converted into elastic waves [5]. The experimental fact that the internal magnetic field controlled conversion of spin waves to elastic waves, and thus the propagation time, led to proposals by Schlömann [6] and others [7,8] for a magnetoelastic delay line. These proposals envisioned a delay line in which delay would be controlled by tuning the magnitude of the external magnetic field.

The delay line designs of Schlömann and Strauss reflected the simplicity of using the naturally occurring nonuniform internal magnetic fields. Schlömann inserted the ends of a YIG rod into cavities. Strauss' design [7], of greater utility, mounted a wire against the end face of a rod in an axial magnetic field; the wire served to both transmit and receive microwave pulses. Subsequent designs have often been based upon Strauss' original single ended conception with improvements. Both these designs, however, produced nonlinear dispersive delay functions over bandwidths typical of microwave systems.

Continued work in magnetoelastic delay lines has focused upon two issues: (a) synthesizing internal magnetic fields which can provide linear or other desired delay functions, and (b) improving efficiency and feedthrough isolation between input and output. In the former case, efforts have been made to produce linear fields by adding magnetic

shunts [9] or trying unusual crystal shapes [10]. These approaches have generally proven ineffectual. Work on the latter has included improving the antennas mounted on rod endfaces with orthogonal thin wire coupling antennas [2], etched antenna designs [11], and two-ended polycrystalline YIG-YAG-YIG constructions [12]. Improvements in reproduceability and insertion loss have been seen.

Borgeaud's work (predecessor to this thesis) in magnetoelastic delay line manufacture incorporated two extremely effective improvements [3]. Previously, Morgenthaler had developed a method for synthesizing any desired on-axis magnetic field in a YIG rod or disk [1]. Since the formulae for magnetic fields giving linear delay functions were well established, Morgenthaler and Platzker were able to incorporate this method in the construction of a Strauss type single-ended delay line, and they found much improved bandwidth [2]. Their design, however, still suffered the liabilities of single-ended delay line construction.

Borgeaud and Morgenthaler then extended the magnetic synthesis technique to a two-ended delay line design, wherein the antennas were fine wires inserted through extremely small holes drilled in a YIG rod by laser. The synthesized field was designed to the requirements of two-ended operation. Borgeaud found substantial improvement in isolation and insertion loss but encountered reduced bandwidth for his particular experimental case [3].

The logical extension of Borgeaud's work is to seek greater bandwidth without sacrificing improved insertion loss and isolation. There was no a priori reason to expect Borgeaud's delay line to show reduced bandwidth; the operation of his delay line is identical to that of a single-ended delay line absent the liability of a reflection of

elastic waves. Borgeaud had, however, selected and tested only one of an infinite possibility of synthesized magnetic field profiles and his selection was made prior to the development of computer analysis tools.

The purpose of this thesis, as stated earlier, is to use improved ray tracing techniques to analyze Borgeaud's delay line design. Implicit in that is discovering how to optimize bandwidth without sacrificing improved isolation and insertion loss, and explaining the previously described results. Development of a general model for delay line behavior and consideration of dynamic range are goals included within this topic as well.

Chapter II

THEORY OF MAGNETOELASTIC WAVES

II.A Introduction

Although magnetic spin waves and their coupling to both electromagnetic and acoustic waves have been studied extensively [13,14,15], it is only recently that the two-port "buried-antenna," linearly dispersive magnetoelastic delay line could be built and tested [3]. Magnetostatic spin waves (MSW) in ferrites have been investigated thoroughly and theoretical explanations of their behavior have been well formulated. Theoretical work includes analysis of these waves in limiting cases [13,14,15], under the influence of various boundary conditions [16,17], and in the presence of various magnetic field conditions [7,18].

Magnetic spin waves result from the presence of electron spin magnetic moments in certain substances. Under the influence of a time varying, external magnetic field, these spin moments tend to precess around the axis of static magnetization. The precession of these moments can be envisioned as having some phase relative to the spin precessions of other spin moments, and periodicities in the phase relationships appear (Figure 2.1b). These periodicities can be viewed as sums of plane waves which are propagating through the medium. Electric fields are likewise generated and energy propagates through the medium according to a Poynting Vector description [13]. Although the coupling between electromagnetic radiation and magnetic spin wave modes is well understood, the actual field and mode structures are complex to

Electromagnetic waves

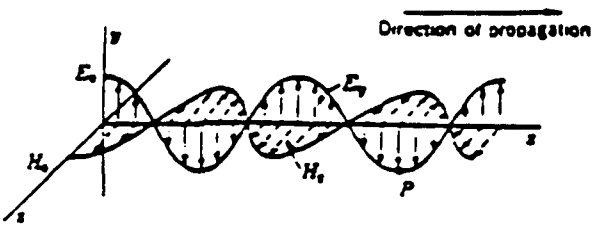

Spin waves

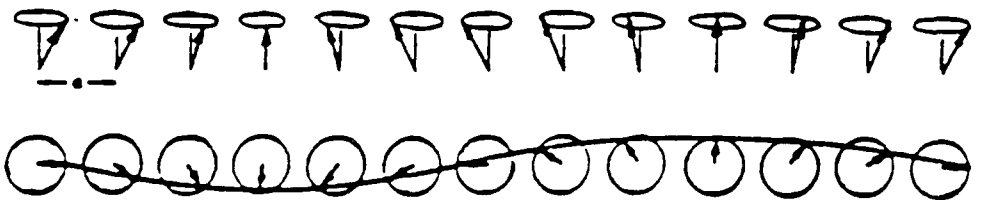

Elastic waves

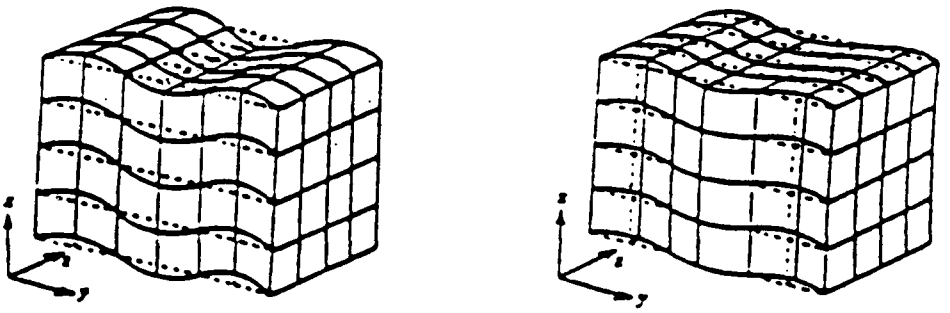

Polarization along x-axis Polarization along z-axis

Figure (2.1) - Waves in ferrite

characterize; it suffices to say that electromagnetic waves couple to MSW's with comparable wavelengths [19].

Acoustic waves in crystal media are well understood as propagating vibrations in the crystal lattice (Figure 2.1c) [7]. In fact, magnetic spin waves and acoustic waves are inherently coupled together, as the magnetic forces produce lattice strain ("magnetostriction") and a conversion of energy from magnetic spin wave to elastic wave [20]. Any propagation of magnetic or elastic energy in a ferrimagnetic actually contains an admixture of both; thus the term "magnetoelastic" waves. Practically, however, the proportions of one or the other type of wave tend to be small except under the specific conditions which convert one wave type to the other. This conversion can be effected with high efficiency under restricted conditions [20].

Spin waves can thus be envisioned as a bridge between electromagnetic and elastic waves. Indeed, spin waves are an extraordinarily effective bridge because: (a) they have wavenumbers which vary with local magnetic field, allowing coupling at different positions within the same medium to modes with different wavelengths; (b) they couple to both EM and elastic waves with very high efficiencies; (c) they have well defined characteristics which lend themselves to theoretical and computer modeling; and (d) they propagate with relatively low attenuation. As analysis will show, these properties of spin waves and the development of a magnetic field synthesis method led to the design of single ended magnetoelastic delay lines and, ultimately, to two-port magnetoelastic delay lines which are the subject of this work.

The delay line itself is a single crystal rod made of Yttrium Iron Garnet ($Y_3Fe_5O_{12}$), also called YIG. YIG is ferrimagnetic, having two

interleaved magnetic sublattices with net electron spin moments, and is optimum for this application. Its properties include:

(a) High resistivity: This allows for penetration of electromagnetic energy into the rod and high efficiency coupling of electromagnetic to spin energy.

(b) Low saturation magnetization: Magnetic domains are eliminated at relatively low values of external magnetic field.

(c) Relatively slow relaxation time: Magnetic and acoustic linewidths are small and attenuation from consequent damping is small.

(d) Easy synthesis: YIG is grown into large single crystals relatively easily.

YIG crystals are commercially available in very pure form.

II.B Magnetic Spin Wave Theory

In the presence of an applied magnetic field ($\bar{H}$), a magnetization field ($\bar{M}$) is induced in ferrimagnetic substances. This magnetization field is caused by the alignment of individual electron spin magnetic moments and is effectively a volume magnetic dipole moment. If a static magnetic field is applied, then both magnetization and magnetic fields are present inside the crystal. The magnetization reaches saturation when essentially all the electron spin moments are aligned.

Magnetic spin waves in ferrimagnetics are a consequence of the existence of this magnetization field and its incorporation into the

constitutive relations. Maxwell's Equations for a sourceless, materially isotropic medium (in MKS units) are:

$$\bar{\nabla} \cdot \bar{D} = 0 \tag{2.1}$$

$$\bar{\nabla} \cdot \bar{B} = 0 \tag{2.2}$$

$$\bar{\nabla} \times \bar{H} = \partial \bar{D} / \partial t \tag{2.3}$$

$$\bar{\nabla} \times \bar{E} = -\partial \bar{B} / \partial t \tag{2.4}$$

The constitutive relations, however, are defined differently from the electromagnetic free space case in that (a) the magnetic flux is proportional to the sum of the magnetic and magnetization fields (Equation 2.5), and (b) time varying magnetic fields interact with the magnetization vector as torques, inducing a time dependence in the magnetization (Equation 2.6 and Figure 2.2):

$$B = \mu_0 (\bar{H} + \bar{M}) \tag{2.5}$$

$$\frac{\partial \bar{M}}{\partial t} = \gamma \mu_0 (\bar{M} \times \bar{H}_{EFF}) \tag{2.6}$$

$$\bar{H}_{EFF} = \bar{H}_0 + \bar{h}_{rf} + \bar{H}_{EX} \tag{2.7}$$

$\frac{\gamma \mu_0}{2\pi} \approx 2.8 \times 10^6$ [Hz/Oe]: gyromagnetic constant

$\bar{H}_{EX} = \lambda_{ex} \nabla^2 \bar{M}$

$\lambda_{ex} \approx 3 \times 10^{-16}$ [m^2]: spin exchange constant

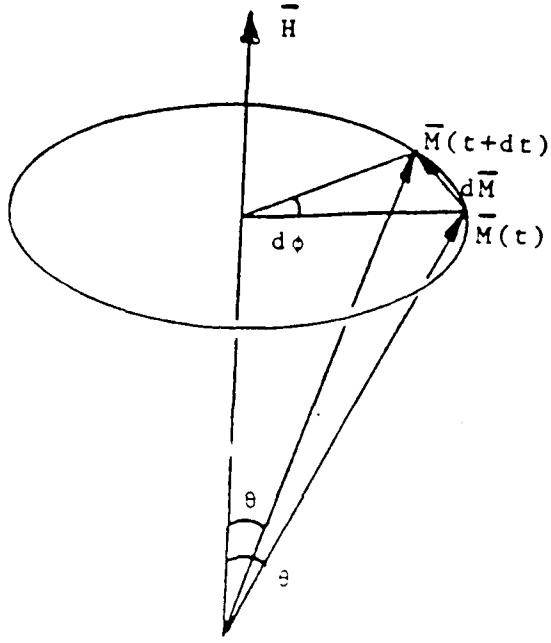

Figure (2.2) - Precession of magnetization around axis of static magnetic field

Equation 2.6 describes the interaction between the internal magnetic field and the magnetization. The presence of a time derivative in the constitutive relation causes anisotropy in the dispersion relation -- as will be seen subsequently, the group velocity and wave vector will not be collinear. As shown by Equation 2.8, the magnitude of $\bar{M}$ is constant and the cone angle (see Figure 2.2) changes as the driving field changes:

$$\frac{\partial \bar{M}}{\partial t} \cdot \bar{M} = \frac{\partial}{\partial t} |\bar{M}|^2 = 0 \qquad (2.8)$$

$\bar{H}_{EFF}$, the effective internal magnetic field in Equation 2.7, can be effectively represented as containing three terms: (a) the static applied magnetic field, $\bar{H}_0$, (b) the applied RF magnetic field, $\bar{h}_{rf}$, and (c) the exchange interaction field, $\bar{H}_{EX}$. Additional terms are

present and discussed in Appendix A, but they are neglected in this approximation.

If it is assumed that (a) the DC components of the magnetization and magnetic fields are $\bar{z}$ directed, (b) the DC components are much larger than the time varying components, and (c) the time varying components can be modeled as plane waves, then:

$$\bar{M} = M_0\bar{z} + \bar{m} \qquad |\bar{M}| = M_0 \qquad (M_0 = 1780\ [\text{Oe}]\ \text{in YIG}) \tag{2.9}$$
$$\bar{H} = H_0\bar{z} + \bar{h} \qquad |\bar{H}| = H_0 \qquad \bar{h} = \bar{h}_{rf} + \lambda_{ex}\nabla^2\bar{m}$$

(H_0 is the z directed internal magnetic field), and:

$$\bar{h}(\bar{r},t) = \bar{h}_0 e^{j(\omega t - \bar{k}\cdot\bar{r})} \tag{2.10}$$
$$\bar{m}(\bar{r},t) = \bar{m}_0 e^{j(\omega t - \bar{k}\cdot\bar{r})}$$

then substitution into the constitutive relation and subsequent manipulation (Equations A.10-A.13) yields the tensor relations between the small signal magnetization and the driving magnetic field. The coefficient matrix is the Polder Tensor:

$$\bar{m} = \begin{pmatrix} \dfrac{\omega_z\omega_M}{\omega_z^2 - \omega^2} & j\dfrac{\omega\omega_M}{\omega_z^2 - \omega^2} \\ -j\dfrac{\omega\omega_M}{\omega_z^2 - \omega^2} & \dfrac{\omega_z\omega_M}{\omega_z^2 - \omega^2} \end{pmatrix} \cdot \bar{h} \tag{2.11}$$

$$\omega_z = \gamma\mu_0 H_0 \qquad \omega_M = \gamma\mu_0 M_0 \qquad \omega = 2\pi f \tag{2.12}$$

The Polder Tensor is hermitian and the medium is gyromagnetic.

Applying the plane wave approximation to Equation 2.6 yields the small signal constitutive relation:

$$j\omega\bar{m} = \gamma\mu_0\bar{z} \times (\omega_M\bar{h} - \omega_z\bar{m} - \omega_M\lambda_{ex}k^2\bar{m}) \tag{2.13}$$

Similarly, applying the plane wave approximation to Maxwell's Equations (A.10-A.19) yields relations for the RF magnetic field as a function of the small signal magnetization field:

$$\bar{h} = \frac{-\bar{k}(\bar{k}\cdot\bar{m}) + k_0^2\bar{m}}{k^2 - k_0^2} \tag{2.14}$$

$$k_0 = \omega(\mu_0\epsilon)^{1/2}$$

These relations define the characteristic waves of the medium and lead to the magnetostatic approximation. It is worth noting that, for propagation along the axis of magnetization, the $\bar{h}$ and $\bar{m}$ fields are transverse and circularly polarized. When propagating perpendicular to the axis of magnetization, the $\bar{h}$ field is elliptically polarized with a longitudinal component and a component transverse to both the axis of magnetization and the direction of propagation. From Maxwell's equations for a plane wave in an electrically isotropic medium (A.15-A.16), however, it is clear that the $\bar{e}$ and $\bar{b}$ fields remain transverse to the direction of propagation [21].

II.C The Magnetostatic Approximation

Rather than substitute Equation 2.14 into Equation 2.13 to obtain a complete dispersion relation (Equation A.21, Figure A.1), a "magnetostatic" approximation can be applied which greatly simplifies the dispersion relation and which is applicable to the delay line problem. As derived in Appendix A (Equation A.20), the small signal electric field is generally proportional to 1/k and a magnetostatic approximation can be made: for $|\bar{k}| >> k_0$ the electric field approaches zero, the curl of the time varying magnetic field approaches zero, $\bar{h}$ can be approximated as the gradient of a scalar potential field, and a magnetostatic approximation relating the time varying magnetic and magnetization fields is available (Equations A.22-A.28):

$$\bar{h} \approx \frac{-\bar{k}(\bar{k}\bullet\bar{m})}{k^2} \tag{2.15}$$

Although the small signal electric field is approximated as zero, $\bar{e} \approx 0$, the small signal energy flow is still accurately described by a small but nonzero Poynting Vector, $\bar{e} \times \bar{h}$.

Substituting Equation 2.15 into Equation 2.13 gives the dispersion relation for an infinite ferrite under the magnetostatic approximation:

$$\omega^2 = (\omega_z + \omega_M\lambda_{ex}k^2)(\omega_z + \omega_M\lambda_{ex}k^2 + \omega_M\sin^2(\theta)) \tag{2.16}$$

$$\sin(\theta) = \frac{\bar{k} \times \bar{M}}{|\bar{k}||\bar{M}|}$$

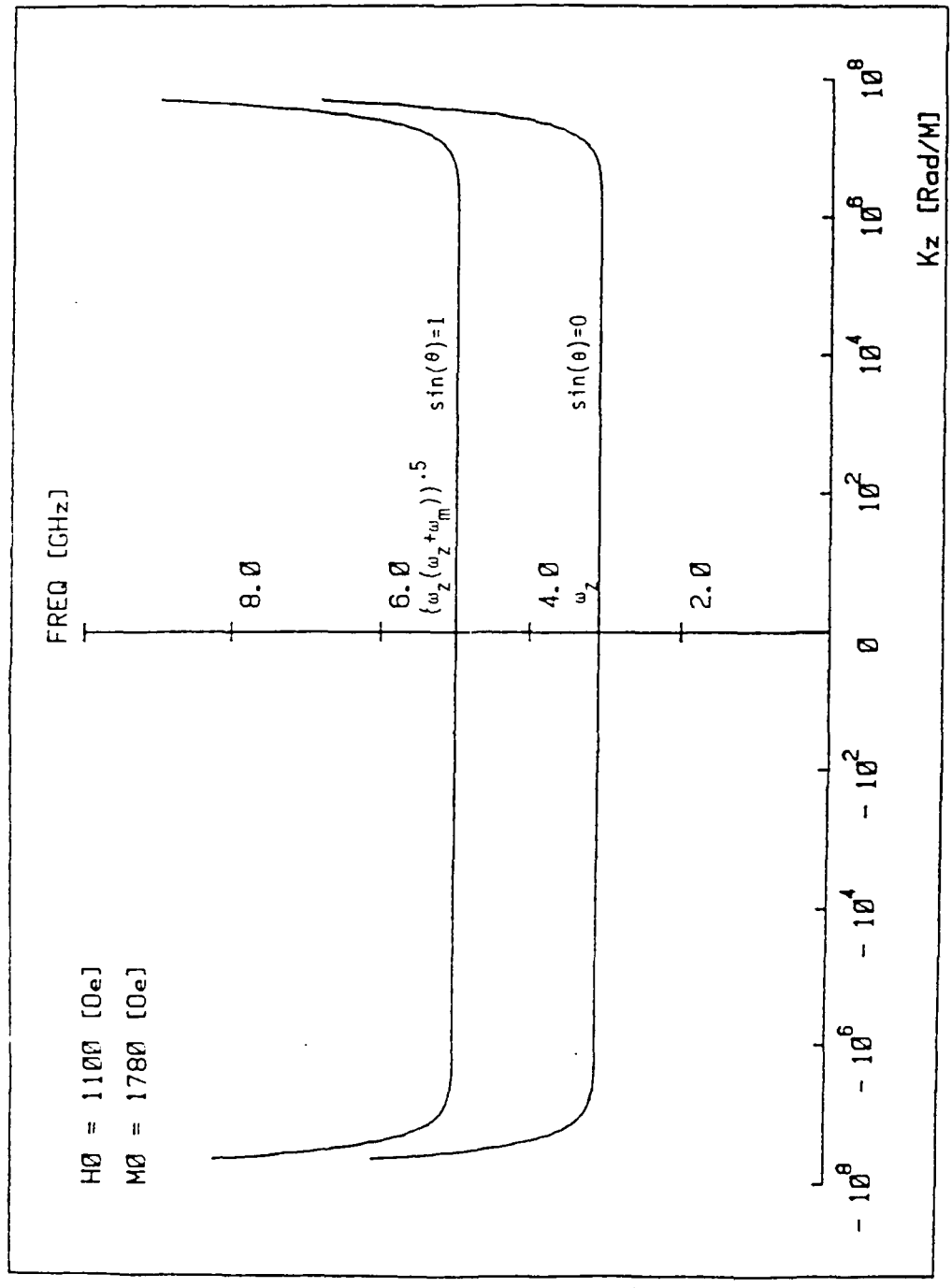

Figure (2.3) - Magnetostatic dispersion relation for an infinite ferrite medium

This dispersion relation (Figure 2.3) is central to the modeling of magnetoelastic delay lines.

Incorporation of the radial boundary conditions for a YIG rod produces an approximate dispersion relation derived by Doane [22] (Figure 2.4):

$$\omega \approx \omega_z + \omega_M \lambda_{ex} k^2 + \frac{\omega_M}{2} \frac{k_r^2}{k_r^2 + k_z^2} \qquad (2.17)$$

$$J_0(k_r R) = 0 \qquad J_0 = \text{zero}^{\text{th}} \text{ order Bessel function}$$

This equation resembles Equation 2.16 with a substitution of the arithmetic mean for the geometric mean. The radial component of $\bar{k}$ is equal to the ratio of the zeroth Bessel function root to the rod radius, as required for continuity of normal $\bar{b}$ and tangential $\bar{h}$ at the cylindrical crystal face. Kittel's original derivation of the dispersion relation for a rod demonstrated the radial wavenumber boundary condition but included the end face boundary conditions [16]. Doane's derivation assumes that the axial wavelength is much smaller than the rod length and finds the same radial wavenumber boundary condition.

It is of interest to superimpose the dispersion relation which includes the radial boundary condition on the magnetostatic dispersion relation for an infinite medium (Figure 2.5). For small values of $\bar{k}$ the wave behaves as if propagating radially, and for large values of $\bar{k}$ the waves propagate axially.

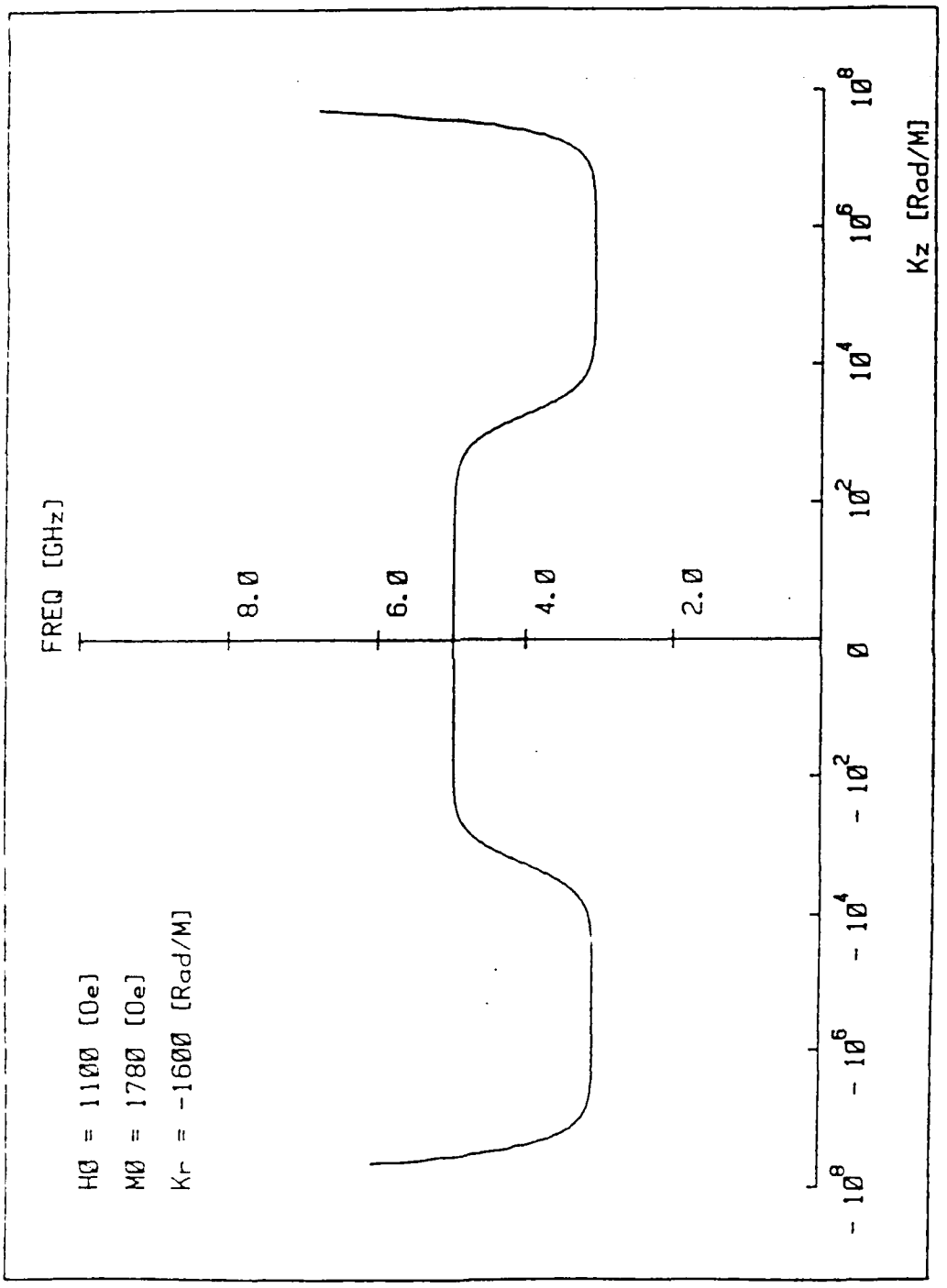

Figure (2.4) - Magnetostatic dispersion relation for a YIG cylinder

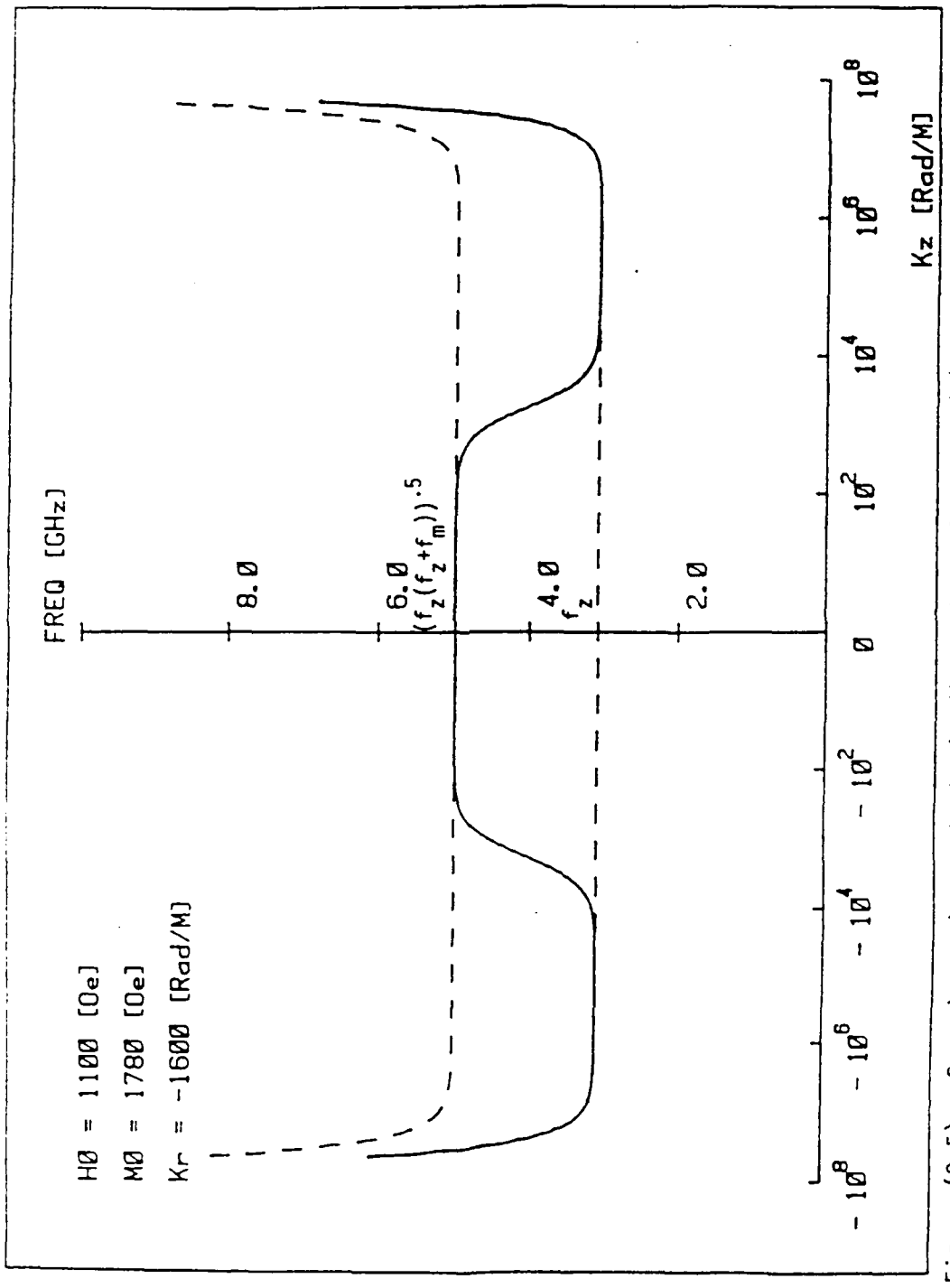

Figure (2.5) - Superimposed magnetostatic dispersion relations: (A) Infinite ferrite - - - -
(B) Ferrite cylinder ——

II.D Properties of Magnetostatic Spin Waves

The magnetoelastic delay line is made possible by special properties of magnetostatic and magnetoelastic waves, including: (a) the dependence of both phase and group velocity on the local magnetic field strength and the wavenumber, and (b) the existence of turning and crossover points. The following sections constitute a brief summary of some of these properties and their importance in delay line conception.

II.D.1 Backward Magnetostatic and Spin Exchange Wave Behaviors

The dispersion relations of Equations 2.16 and 2.17 both allow for dramatically differing wave behaviors as a function of the wavenumber, k. This distinction is defined for "backward magnetostatic waves" (referred to in the literature as Backward Magnetostatic Volume Waves or BMSVW) and "spin exchange waves," although both are manifestations of the magnetostatic approximation for magnetic spin waves. It is these strikingly different behaviors that allows the magnetoelastic delay line to function.

For values of $|\bar{k}| >> k_0$ (to maintain the magnetostatic approximation) but $\lambda_{ex}k^2 << 1$ (the spin exchange contribution negligible), the dispersion relation in Equation 2.17 can be simplified to:

$$\omega \approx \omega_z + \frac{\omega_M}{2} \frac{k_r^2}{k_r^2 + k_z^2} \qquad (2.18)$$

The group velocity for a backward magnetostatic wave propagating in this region is found from Hamilton's equations (see Chapter 4):

$$\bar{v}_g = \frac{\partial \omega}{\partial \bar{k}} \tag{2.19}$$

For values of $|\bar{k}|$ between 10^3-10^5 [rad/m^{-1}] (Figure 2.6):

$$v_z = -\omega_M k_r^2 k_z / k^4 \tag{2.20}$$

$$v_r = \omega_M k_z^2 k_r / k^4 \tag{2.21}$$

$$|\bar{v}_g| \sim 10^3\text{-}10^4 \text{ [m/sec]}$$

The group velocity is large and opposite in sign to the axial wavenumber. The direction of propagation of energy is thus opposite to the direction of phase advance and the wave is a "backward magnetostatic" wave. Also, the components of group velocity are not directly proportional to their corresponding component of the wave vector. The group velocity and phase vector are therefore not parallel and there is a deflection of propagation direction from the axis of phase advance.

For values of $|\bar{k}| > 5 \times 10^6$ [rad/m^{-1}], $\lambda_{ex} k^2 \sim 1$ and the dipolar interaction term becomes dominated by the quantum mechanical exchange term. The dispersion relation can then be approximated:

$$\omega \approx \omega_z + \omega_M \lambda_{ex} k^2 \tag{2.22}$$

This behavior is delineated in Figure 2.6 as the "Spin Exchange" region.

Applying Hamilton's equations gives the components of group velocity for the spin exchange dominated wave:

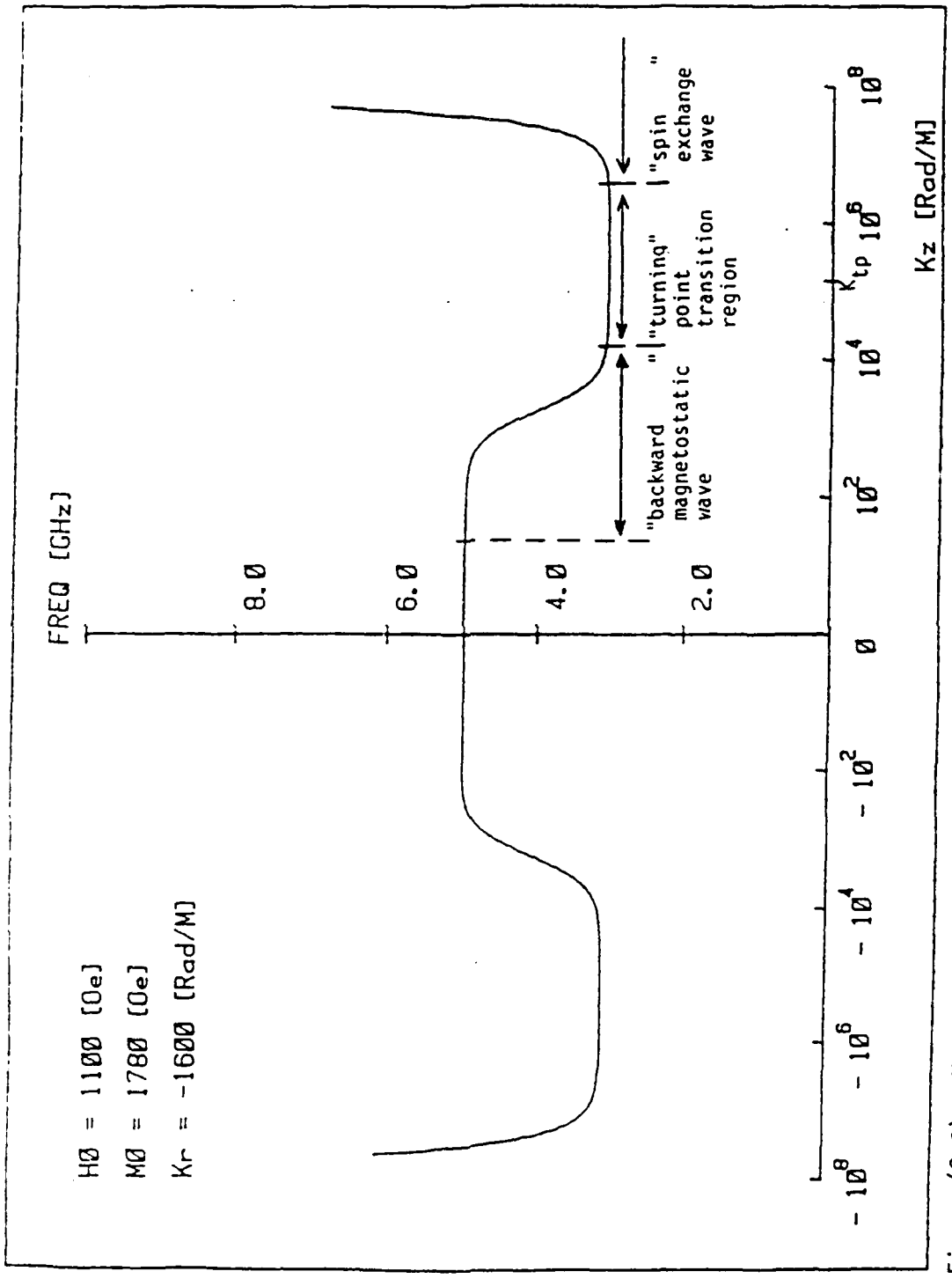

Figure (2.6) - Magnetostatic dispersion relation for a YIG cyliner (labeled)

$$v_z = 2\omega_M \lambda_{ex} k_z \tag{2.23}$$

$$v_r = 2\omega_M \lambda_{ex} k_r \tag{2.24}$$

The group velocity components are directly and equally proportional to their corresponding components of the vector. The group velocity is therefore collinear with the direction of phase advance and the wave is a "forward" wave. Even for very large values of the wavenumber, the spin exchange dominated wave has low group velocity, on the order of 10^1-10^2 [m/sec].

II.D.2 Definition of Turning Point

The transition between the previously described "backward magnetostatic" and "spin exchange" wave behaviors is critical to understanding the operation of the magnetoelastic delay line. Consider a backward magnetostatic wave propagating axially -- (a) at fixed frequency, (b) at high speed, (c) in the positive direction, and (d) with negative wavenumber -- toward a region of increasing magnetic field (Figure 2.7, Point A). From Equation 2.17 and Figure 2.7, the magnitude of the (negative) wavenumber will become larger and the wave will move "down" the dispersion curve. As the wave continues to propagate towards increasing magnetic field, $|\bar{k}|$ will continue to increase until the wave reaches the bottom of the dispersion curve (Figure 2.7, Point B). At this point the wave can continue to propagate in the same direction only with imaginary wavenumber. This point is called the "Turning Point" and it is here that the "backward

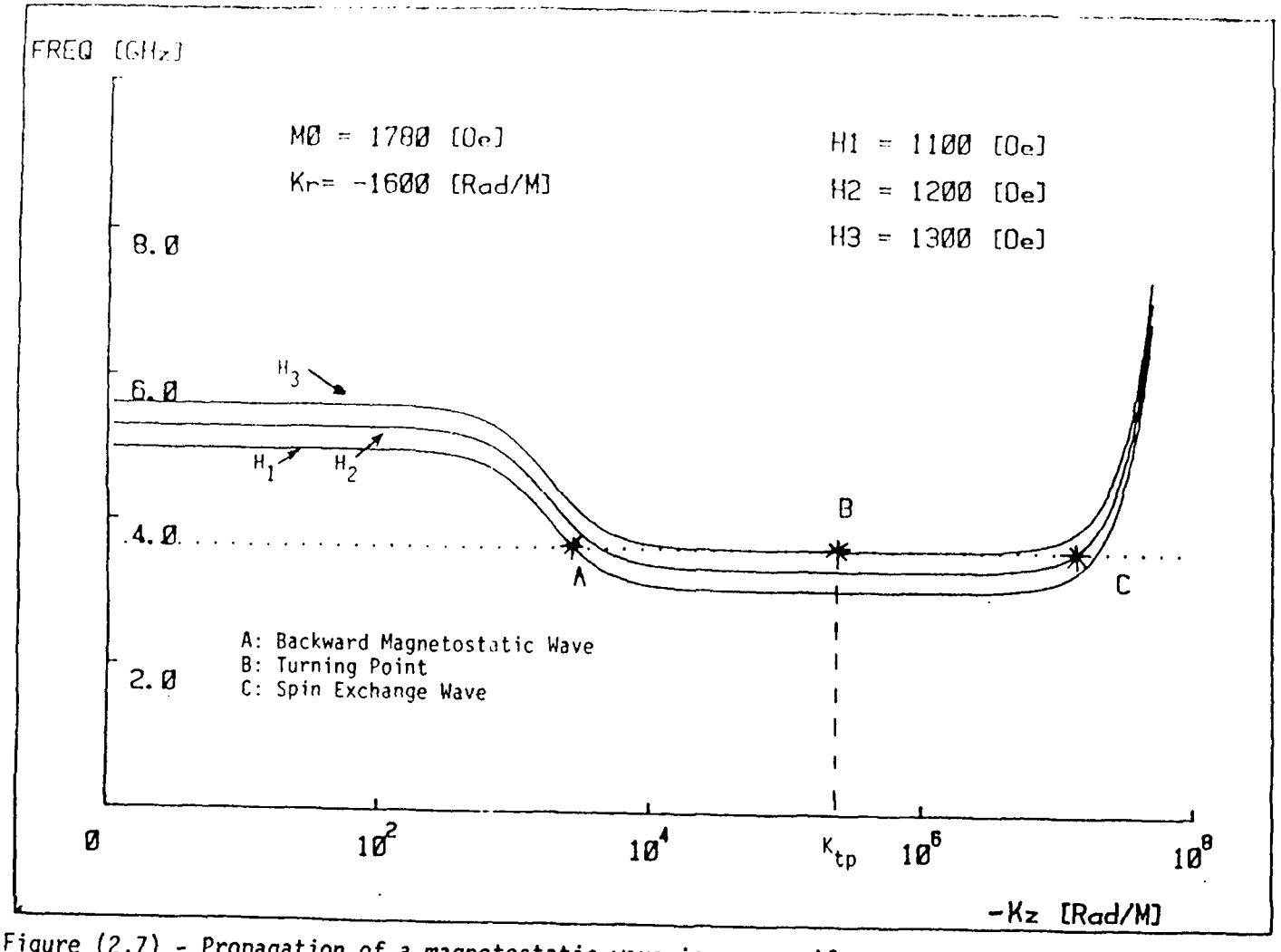

Figure (2.7) - Propagation of a magnetostatic wave in a nonuniform magnetic field

magnetostatic" behavior of the wave decreases and "spin exchange" behavior begins to dominate.

The increasing spin exchange character of the wave, however, introduces fundamental changes in wave behavior. Since the spin exchange wave is a forward wave, the group velocity changes sign and becomes negative -- the direction of energy flow actually turns around and the wave propagates back toward the region of weaker magnetic field (Figure 2.7, Point C). The wavenumber, however, continues to be negative and increase in magnitude -- the "turning" of the wave is unlike a reflection where both power and momentum change direction. Also, the magnitude of the group velocity changes dramatically, from backward magnetostatic wave values of 10^3 [m/sec] to spin exchange wave magnitudes of 10^1 [m/sec].

The point at which the axial group velocity equals zero as it changes from positive to negative is the "Turning Point" and can also be defined by equal and opposite spin exchange and backward magnetostatic contributions to group velocity:

$$2\omega_M \lambda_{ex} k_z - \omega_M k_r^2 k_z / k^4 = 0 \tag{2.25}$$

$$|\bar{k}_{tp}| \approx \left(\frac{k_r^2}{2\lambda_{ex}} \right)^{1/4} \tag{2.26}$$

Typically, $|\bar{k}_{tp}|$ is on the order of 10^5 [rad/m] and, from Equations 2.12, 2.17, and 2.26, the magnetic field strength is:

$$\omega_z \approx \omega \tag{2.27}$$

$$\left(H_0 \approx \frac{2\pi f}{\gamma \mu_0} \right)$$

II.D.3 Definition of Crossover Point

A description of elastic waves and their coupling to magnetostatic spin waves is contained in Appendix A. This conversion between spin and elastic waves, usually with high efficiency, occurs at the "Crossover Point." The crossover point is reached when the wavenumber reaches the value:

$$|\bar{k}_{cp}| = \frac{\omega}{v_{ew}} \tag{2.28}$$

v_{ew} = 3844 [m/sec]: elastic wave velocity

The combined magnetostatic and elastic "magnetoelastic" dispersion relation is shown in Figures 2.8 and 2.9.

For waves at microwave frequencies in YIG, values of wavenumber at crossover are on the order of 10^7 [rad/m]. At this point, the character of the wave changes abruptly from spin exchange to elastic (or vice versa). As described in Appendix A.3, elastic waves are forward waves and the group velocity is collinear with the wave vector.

II.D.4 Transition Between Turning and Crossover Points

From the previous sections it is possible to envision a magnetic spin wave whose backward magnetostatic character evolves to spin exchange behavior and then undergoes transformation to an elastic wave. These changes would occur as the wave propagates into a turning point, reverses direction, and the converts into an elastic wave at the crossover point.

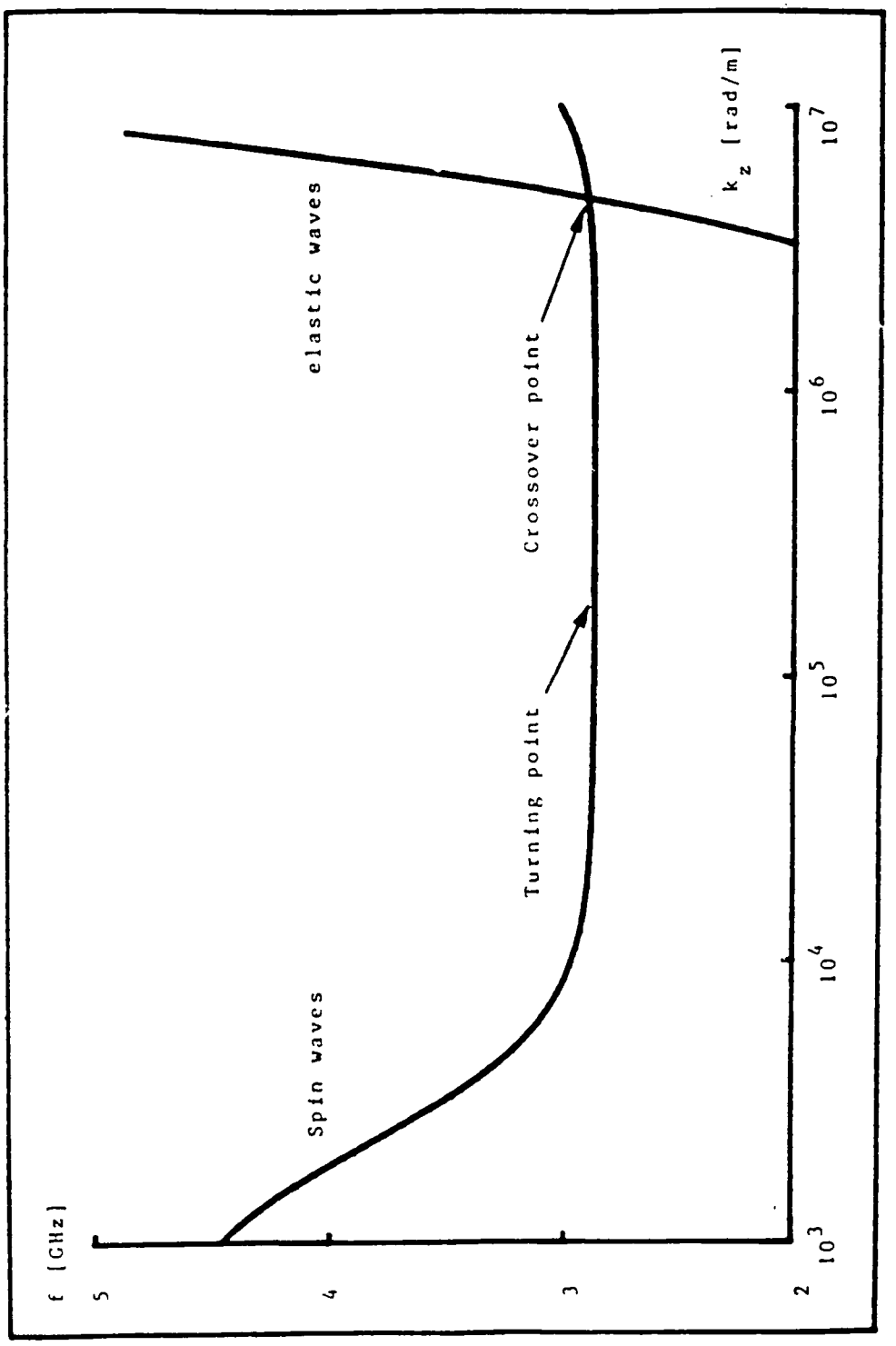

Figure (2.8) - Turning point and crossover point on magnetoelastic dispersion relation.

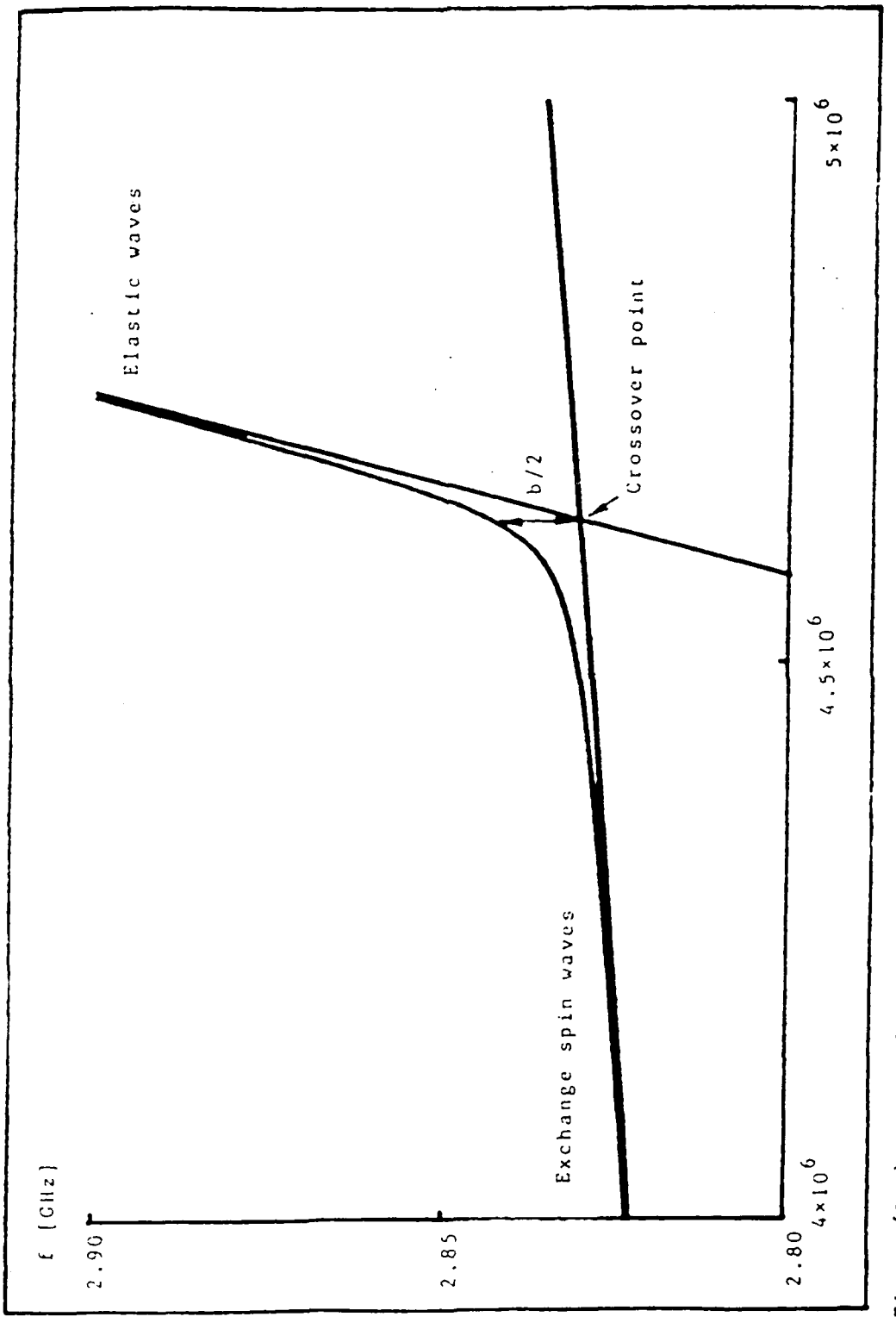

Figure (2.9) - Spin/elastic wave conversion

The cause of the evolution of the wave would be the presence of a spatially inhomogenous magnetic field.

The striking feaure of this behavior is that the magnetic spin wave experiences a large change in wavenumber in the very short distance between turning point and crossover point. As established in previous sections, at the turning point:

$$|\bar{k}_{tp}| \approx 10^5 \text{ [rad/m]}$$
$$|\bar{H}_0| \approx \omega/\gamma\mu_0 \text{ [Oe]}$$

At the crossover point, $|\bar{k}_{cp}| \approx 10^7$ [rad/m]. Applying Equations 2.12, 2.22, and 2.28 gives a magnetic field strength at the crossover point:

$$|\bar{H}_0| \approx \frac{\omega - \omega_M \lambda_{ex} (\omega/v_{ew})^2}{\gamma\mu_0} \tag{2.29}$$

For a nominal frequency of 4 GHz, the change in field strength between the turning and crossover points is a very small 22 Oe. As will be seen in the next chapter, derivatives of axial field profile will typically be on the order of 5×10^5 [Oe/m]. This implies that the magnetic spin wave undergoes a two order of magnitude increase in wavenumber in an axial distance on the order of 0.1 [mm].

Chapter III

THE MAGNETOELASTIC DELAY LINE

III.A Introduction

The design goal for the magnetoelastic delay line is to achieve wave propagation times which are a linear function of frequency:

$$TD(f) = D \cdot f + T_0 \tag{3.1}$$

where TD is the time delay, D is the dispersive delay coefficient, and T_0 is some fixed delay. This linear delay function has numerous practical applications.

The magnetoelastic delay works by converting electromagnetic radiation to long wavelength magnetostatic waves inside a YIG crystal. The YIG crystal has a nonuniform internal magnetic field designed so that the magnetostatic waves will evolve into spin exchange waves, couple with high efficiency to short wavelength elastic waves, and then undergo the exact reverse set of conversions, ending at the isolated output antenna. The internal magnetic field is synthesized to produce a time delay which is a linear function of frequency.

III.B One-Dimensional Model of the Magnetoelastic Delay Line

The operation of the magnetoelastic delay line can be understood by following the path and evolution of a wave packet of energy in a simple one-dimensional model. The model includes the following features:

(a) A symmetric, axially directed, concave upward magnetic field $H_0(z)\bar{z}$ is present (Figure 3.1a).

(b) A constant, axially directed magnetization $M_0\bar{z}$ is present.

(c) The medium is a YIG rod with the dispersion relation of Equation 2.17 (Figure 2.4).

(d) Transducers which convert electromagnetic waves to spin waves are present in the rod but do not interfere with the propagation of elastic waves.

The delay line can be envisioned as operating as follows:

- Electromagnetic energy is converted to a long wavelength, high speed backward magnetostatic wave at an input antenna (Figure 3.1, Point A). Initially, the wave has $k_z < 0$ and propagates in the positive z direction as a backward wave (Equation 2.20).
- As the wave propagates toward greater field strength, the wavenumber increases and the wave slows down until the turning point, z_{tp} (Figure 3.1, Point B), is reached. At z_{tp}, the wave reverses direction (Section II.D) and becomes a forward spin exchange wave traveling in the -z direction.
- The wave continues to travel in the negative z direction until, as described in Section II.D, the wavenumber increases in magnitude sufficiently to permit crossover at the crossover point, z_{cp} (Figure 3.1, Point C). z_{cp} is very close to z_{tp} (within 0.1 [mm]).
- The elastic wave continues in the negative direction, travels through the center of the rod, and then the entire process is

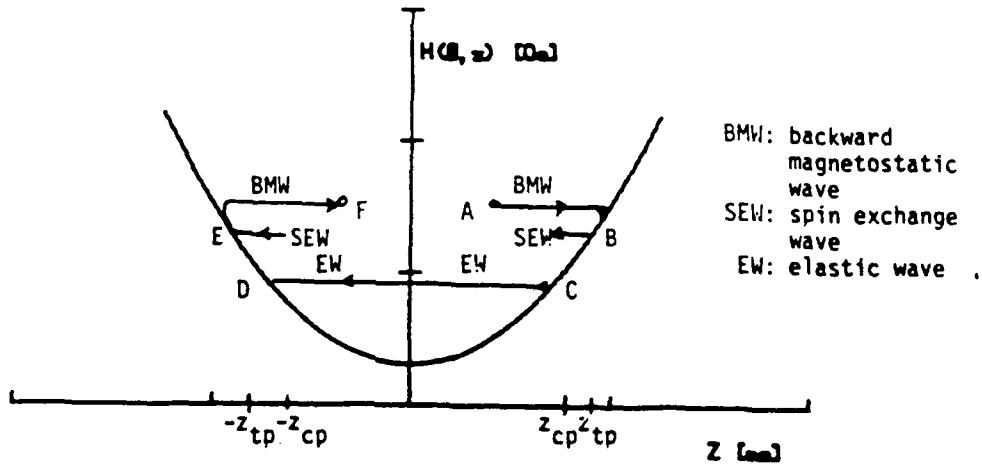

A. Magnetoelastic wave in a nonuniform magnetic field

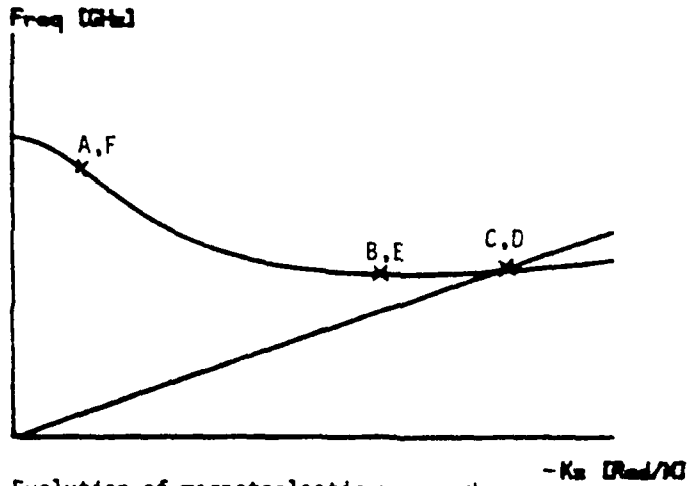

B. Evolution of magnetoelastic wavenumber

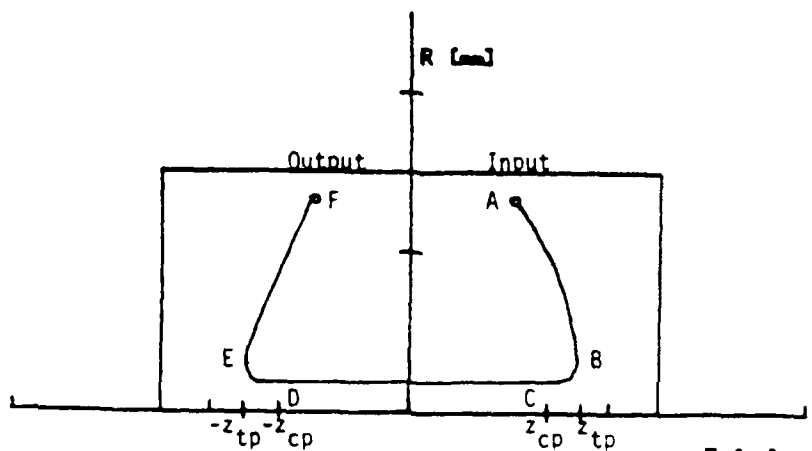

C. Magnetoelastic wave path in the YIG rod

Figure (3.1) - Operation of the magnetoelastic delay line

reversed with a magnetostatic wave arriving at the output antenna (Figure 3.1, Points D-E).

The evolution of the magnetoelastic wave in the delay line is shown in Figure 3.2

III.C The Delay Function and Internal Magnetic Field

Although the propagation path for the magnetoelastic delay line has been described, the means to produce a linearly dispersive time delay has not been defined. This section surveys the rationale for synthesizing a linear delay function by specifying a particular on-axis magnetic field.

The total time for a wave packet to travel from the input antenna to the output antenna in the manner described in Section III.B is readily estimated and is a very good approximation to the actual three-dimensional rod. The time spent in propagation can be broken down into three portions: (a) backward magnetostatic wave; (b) spin exchange wave; and (c) elastic wave. The backward magnetostatic wave, however, is very fast and makes a negligible contribution to the overall trip time. Thus,

$$TD(f) = T_{\text{spin exchange wave}} + T_{\text{elastic wave}} \tag{3.2}$$

Since the elastic wave is insensitive to local magnetic field conditions (except at crossover), the time spent as an elastic wave is simply:

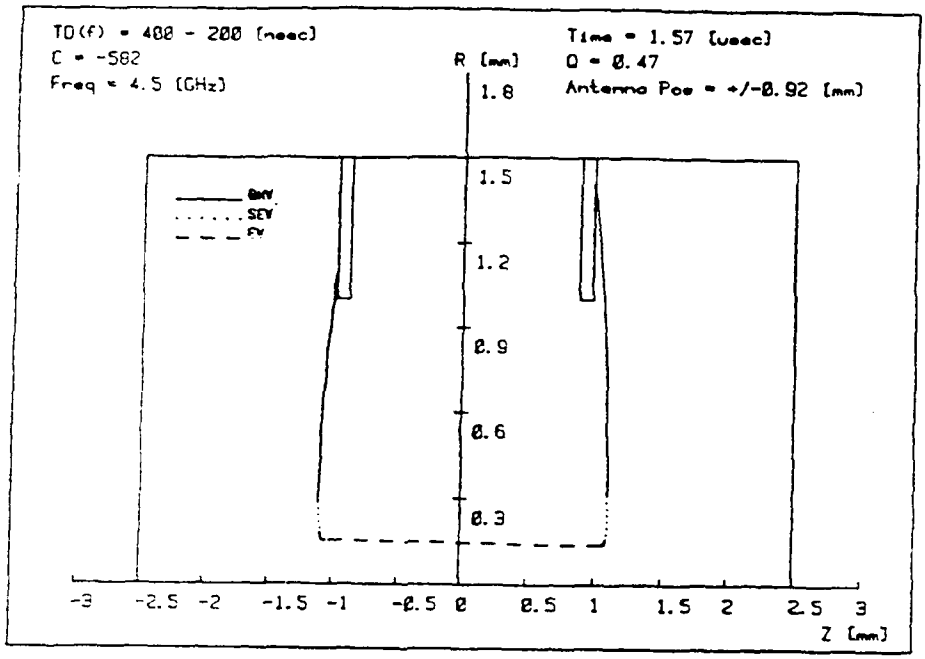

A. Magnetoelastic wave path and character

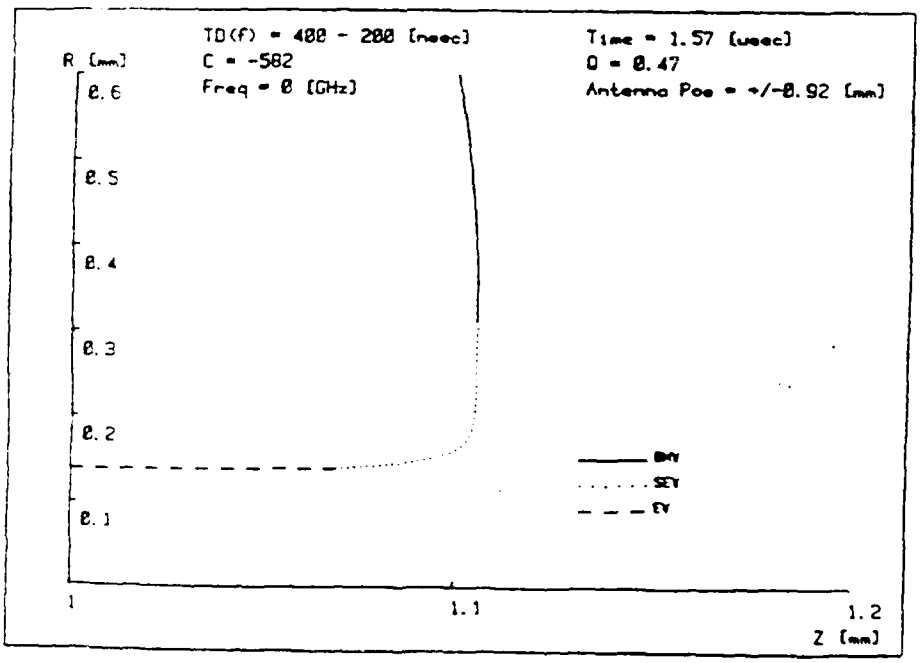

B. Magnetoelastic wave near turning and crossover points

Figure (3.2) - Magnetoelastic delay line ray tracing
BMW: backward magnetostatic wave SEW: spin exhange wave
EW: elastic wave

$$T_{ew} = \frac{2z_{cp}}{v_{ew}} \tag{3.3}$$

The time spent as a spin exchange wave (whose group velocity depends upon the local magnetic field strength) is derived in Appendix B. The result is:

$$T_{sew} = \frac{2}{v_{ew}} \left[\frac{H(z_{cp})}{\frac{\partial H}{\partial z}\Big|_{z=z_{cp}}} \right] \tag{3.4}$$

As shown in Chapter 2, Equation 2.29:

$$H(z_{cp}) \approx \frac{\omega}{\gamma \mu_0} \tag{3.5}$$

and the total time spent is:

$$TD \approx \frac{2}{v_{ew}} \left[z_{cp} + \frac{2\pi f/\gamma\mu_0}{\frac{\partial H}{\partial z}\Big|_{z=z_{cp}}} \right] \tag{3.6}$$

As shown in Appendix B, by carefully locating the crossover point z_{cp} as a function of frequency, the linear dispersion can be obtained:

$$z_{cp} = \left[\frac{Df}{4} + \frac{T_0}{2} + \frac{C}{2f} \right] v_{ew} \tag{3.7}$$

where C is an arbitrary, nonpositive constant.

Generalizing z_{cp} to cover all values within the rod permits complete derivation of the required one-dimensional magnetic field. Synthesis of this on-axis magnetic field produces the desired linearly dispersive delay function:

$$H(z) = \frac{(2|z| - v_{ew}T_0) + \sqrt{2|z| - v_{ew}T_0)^2 - 4v_{ew}^2DC}}{\left(\frac{\gamma\mu_0}{2\pi}\right)\left(\frac{v_{ew}D}{2}\right)} \qquad (3.8)$$

The presence of an arbitrary constant of integration, C, is a critical factor. Theoretically, C can be any nonpositive number and it determines the extent of nonlinearity of the field profile. For C = 0, the field profile is a linear function of z. As C becomes more negative the field becomes more nonlinear. Any delay function therefore has a potentially infinite number of acceptable field profiles. Optimizing the selection of the field profile constant C so as to maximize bandwidth is one objective of this thesis.

III.D Insights into Delay Line Operation

Not all the magnetic spin wave energy arriving at the output antenna is converted back into electromagnetic energy: a fraction of that energy continues to propagate until it reaches the input antenna and repeats the delay process. The presence of second (and higher) order echoes may limit the potential bandwidth of the delay line. For example, the presence of pulse second time around echoes could swamp high frequency leading edge transients of interest. A bandwidth constraint can be

defined by requiring that the second order echo time for the lowest frequency of interest must be greater than the delay time of the highest frequency of interest (Figure 3.3):

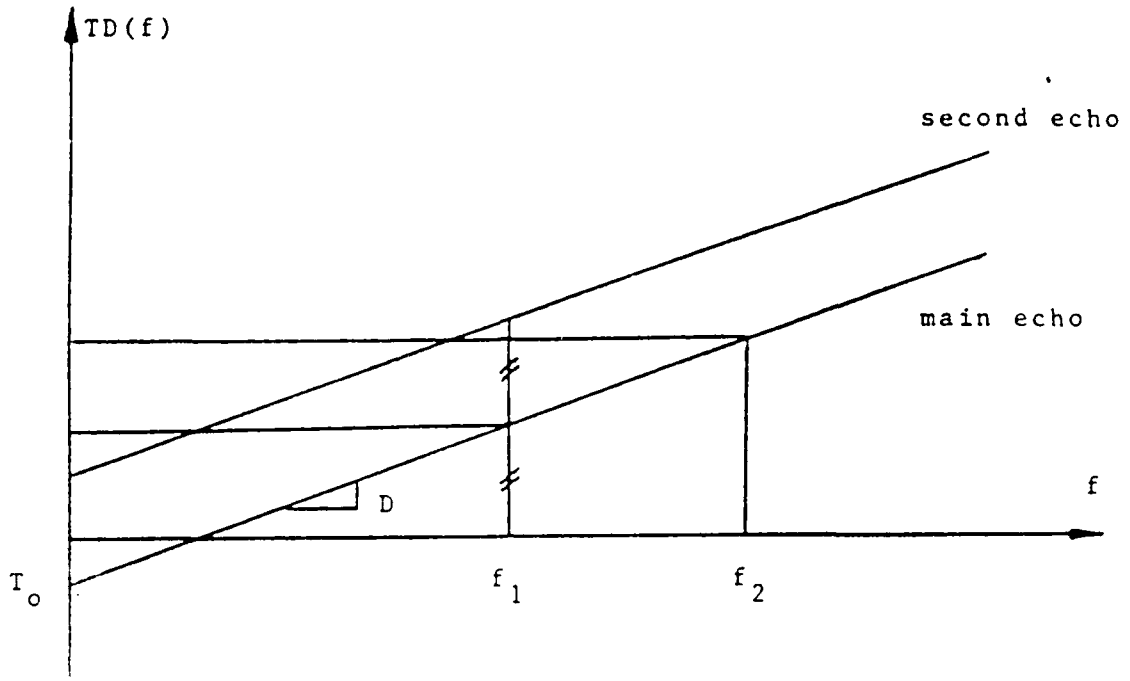

Figure (3.3) - Echo limited bandwidth

$$Df_{hi} + T_0 < 2(Df_{lo} + T_0) \tag{3.9}$$

$$f_{hi} < 2f_{lo} + \frac{T_0}{D}$$

A potential maximum bandwidth can be readily calculated.

Also, the amount of time spent as an elastic wave and as a spin wave can be explicitly solved:

$$T_{ew} = \frac{Df}{2} + T_0 + \frac{C}{f} \tag{3.10}$$

$$T_{sew} = \frac{Df}{2} - \frac{C}{f} \tag{3.11}$$

The fixed delay term T_0 is wholly incorporated into the elastic wave propagation whereas the dispersive propagation time Df is divided equally between the elastic and spin wave regimes. The constant of integration term C adjustably decreases the elastic wave propagation time while adding equally to the spin wave propagation time.

Since the spin wave propagation time is explicitly defined in Equation 3.4 and is accounted for in Equation 3.11, a simple expression for the axial derivative of the magnetic field at crossover can be obtained:

$$H'(z_{cp}) = \frac{2}{v_{ew}} \frac{2\pi f}{\gamma \mu_0} \left[\frac{Df}{2} - \frac{C}{f} \right]^{-1} \tag{3.12}$$

The magnetic field slope at crossover is independent of the fixed delay term T_0 and is inversely proportional to C and D.

III.E Focusing Conditions

Initial work in magnetostatic spin wave delay lines found that the attenuation of the signals varied strongly with the magnetic field profile's characteristics [23]. Theoretical analysis of the behavior of spin waves between z_{tp} and z_{cp}, and ray tracing simulations demonstrated that the spin waves undergo wavefront focusing/defocusing effects which are dependent upon the local magnetic field. Rays which defocus show increased attenuation since the wavefront disperses through the rod.

Morgenthaler has analytically solved for radial position and the ratio of the wavenumber components as a function of time between z_{tp} and z_{cp} [24]. His analysis shows that there is a focusing parameter Q which controls whether a ray will (a) focus, (b) defocus, or (c) oscillate in an overfocused condition. Q is defined by the magnetic fields at the crossover point, z_{cp}:

$$Q = \frac{2H_0M_0}{(H_0 + M_0)^2(H_0')^2}\left[\frac{3}{2}(H_0')^2 - (H_0 + M_0)H_0''\right] \tag{3.13}$$

$$H_0 \approx \frac{\omega}{\gamma\mu_0} \qquad H_0' = \left.\frac{\partial H}{\partial z}\right|_{z=z_{cp}} \qquad H_0'' = \left.\frac{\partial^2 H}{\partial z^2}\right|_{z=z_{cp}}$$

For $Q < 0$, the wave is defocusing; $Q > 1$ is overdamped; and $1 > Q > 0$ is a focusing condition.

The one dimensional delay line approximations in Equation 3.12 can be applied to the definition of Q. The result is an explicit expression for Q as a function of the selected linear dispersion function, the frequency, and the field profile constant:

$$Q = \frac{3a}{(a + 1)^2} + \frac{4a}{a + 1}\left[\frac{Df^2}{2C} - 1\right] \tag{3.14}$$

$$a = \frac{\omega_M}{\omega}$$

For the linear delay line, Q can range between 1 and $-\infty$. An overfocusing condition is not possible with these types of profiles.

Since Q is not defined for negative magnetic field gradients, it is not generally applicable to the complete delay line problem. It does,

however, provide a design criterion which correlates with bandwidth (as will be shown). It is worth noting, however, that D must be greater than zero for a focusing profile ($Q > 0$) to be achieved.

III.F Synthesis of the Magnetic Field

Section III.C derives the general formula for the on-axis magnetic field for any given linear delay function. Appendix C reviews Morgenthaler's approach to synthesis of any on-axis field in a rod or disk. The field is created by manufacturing pole pieces whose surfaces are continuous with the equipotential which would be generated by the specified field (Figures 3.4, 3.5, and 3.6). The pieces are spherically symmetric, made from ferrous material, and energized in an external magnetic field.

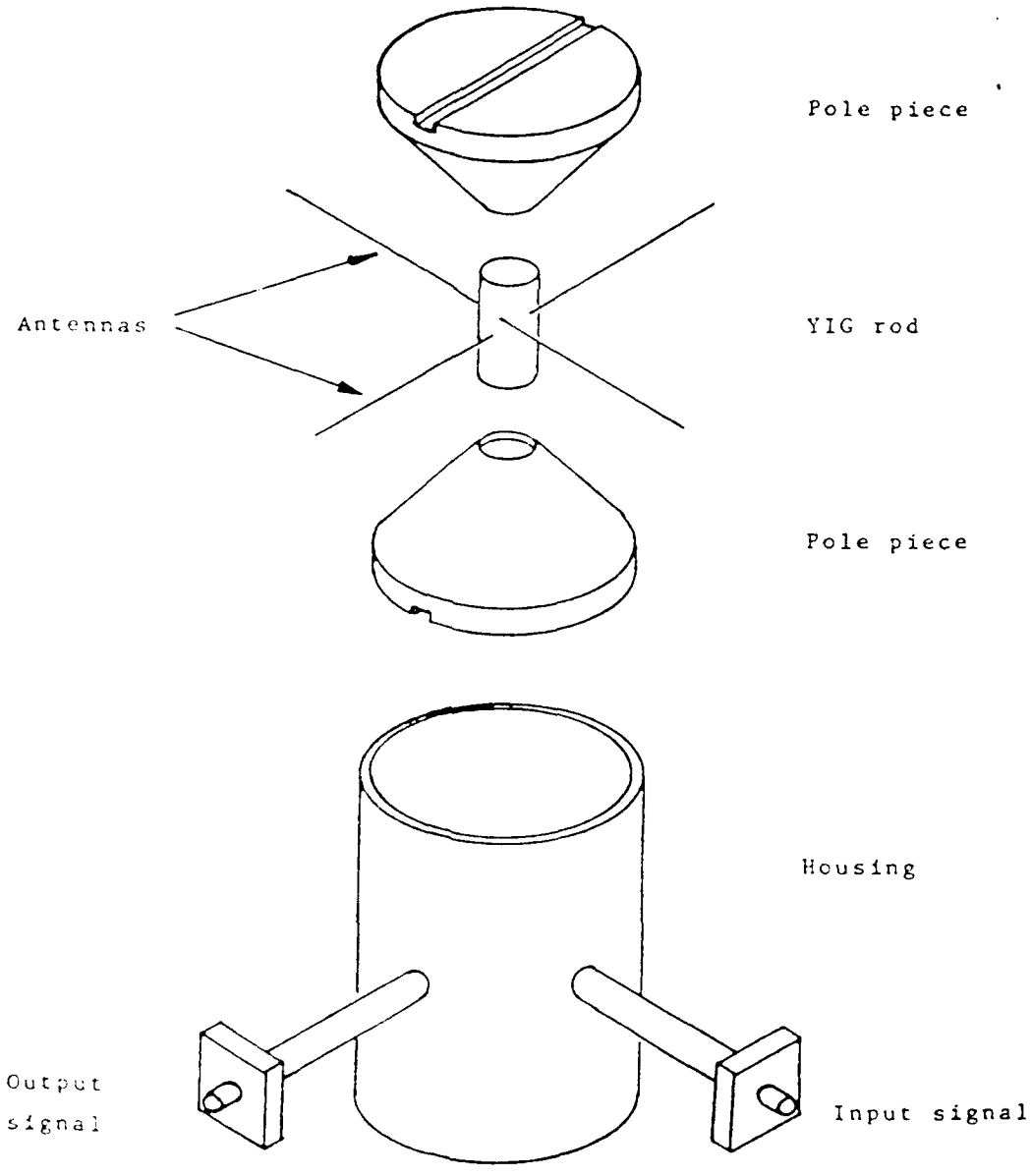

Figure (3.4) - Construction of "buried-antenna" magnetoelastic delay line (Courtesy M. Borgeaud, Ref. 3)

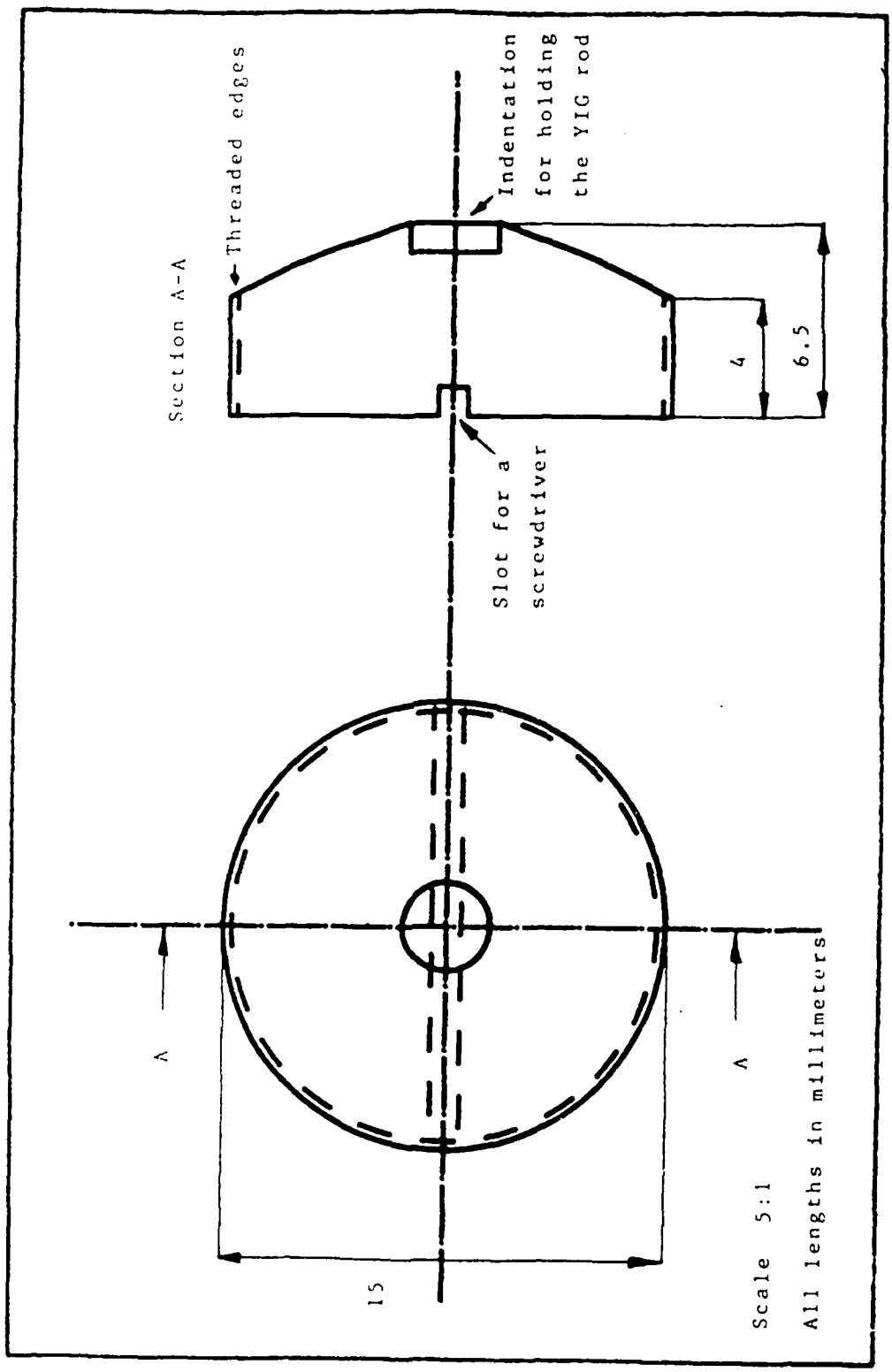

Figure (3.5) - Pole piece design

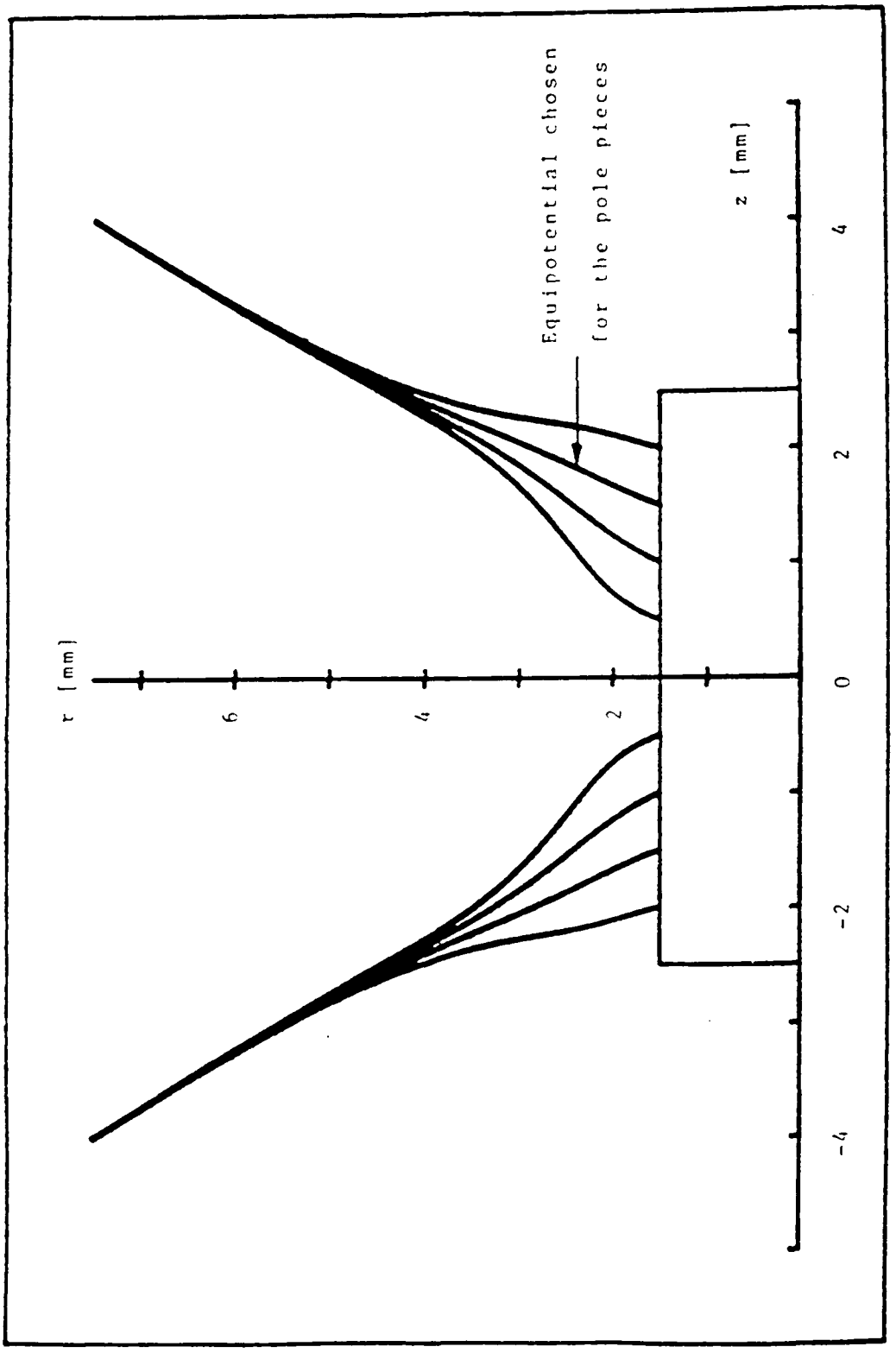

Figure (3.6) - Computer generated equipotential surfaces

Chapter IV

RAY TRACING

IV.A Introduction

Ray tracing is the primary technique used herein for analysis of the isolated two port magnetoelastic delay line. Ray tracing has, of course, been the primary tool in optical analysis for over a century and predates Maxwell's equations. Ray tracing in anisotropic media, however, is somewhat more complex and relies heavily upon some additional assumptions. This chapter will explore the methodology of ray tracing, the underlying assumptions, and the computer program developed for this thesis.

IV.B Theory of Ray Tracing

Ray tracing is based on the idea that if an electromagnetic wave propagating through a medium meets certain conditions, it can be treated as a particle which obeys Newtonian laws of motion, i.e., the particle motion can be approximated by a fixed velocity over small time intervals. This approximation allows the tracing of ray paths which are the "geodesics for the metric where the optical length ... is a measure of the arc ..." [25]. The local nature of the geodesic depends upon the refractive index of the material.

Geometrical optics has been shown to be a valid way of describing the propagation of magnetoelastic waves in nonuniform magnetic fields [20,26]. Morgenthaler has demonstrated that a particle approximation to

magnetoelastic wave propagation in magnetically saturated ferro- and ferrimagnets is a natural consequence of small signal energy and momentum conservation laws [20]. His proof, which incorporates the terms in the complete magnetoelastic wave description given in Equations A.5-A.7, requires only that wavenumber be large compared with both the normalized spatial field derivatives and the rod dimensions:

$$|\bar{k}_0| >> \left| \frac{\nabla H(r,z)}{H(r,z)} \right| \tag{4.1}$$

$$|\bar{k}_0| >> \text{radius, length} \tag{4.2}$$

Given these conditions, the spatial dependence of the small signal fields can be represented by:

$$\bar{\phi}(\bar{r},t) = \bar{\phi}_0 e^{j(\omega t - \int \bar{k} \cdot d\bar{r})} \tag{4.3}$$

and a "quasiparticle" description, based upon a linear sum of plane waves, is acceptable.

Morgenthaler applied the above assumptions to the magnetoelastic wave small signal power-energy and stress-momentum conservation theorems and, after taking a time average over the period, obtained the Hamilton Equations of optics:

$$\bar{v}_g = \frac{d\bar{r}}{dt} = \bar{\nabla}_k \omega \Big|_{\bar{r},t} \tag{4.4}$$

$$\frac{d\bar{k}}{dt} = -\bar{\nabla}_r \omega \Big|_{\bar{k},t} \tag{4.5}$$

Equations 4.4 and 4.5 form the basis for ray tracing techniques. Equation 4.4 is the classical group velocity relation of optics. Equation 4.5 gives the time evolution of the wavenumber as a function of the spatial derivative of the frequency. Ray paths are found by integrating Equations 4.4 and 4.5; although most ray paths are actually found from numerical integration over successive small time increments, closed form solutions are sometimes available.

The time derivative of the wavenumber (the group velocity solution has already been presented in Section II.D) can be found from Equations 2.18 and 2.22:

$$\frac{d\bar{k}}{dt} = -\nabla_r \omega_z = -\gamma\mu_0 \left[\frac{\partial H}{\partial z} \bar{z} + \frac{\partial H}{\partial r} \bar{r} \right] \tag{4.6}$$

The solutions for both backward magnetostatic and spin exchange wave behaviors are approximately the same.

The magnetic fields inside the rod are found from Taylor series expansions of the on-axis field (Appendix C and Figures 4.1 and 4.2). Near the central axis, only the highest order component of each spatial derivative needs to be considered:

$$\nabla \left| \bar{H}(r,z) \right|_{r=0} = \frac{\partial}{\partial z} H(r,z)\Big|_{r=0} \bar{z} + -\frac{1}{4} \left(\frac{1}{a+1} \right) \frac{\partial}{\partial z} H(r,z)\Big|_{r=0} \bar{r} \tag{4.7}$$

$$a = \frac{\omega_M}{\omega}$$

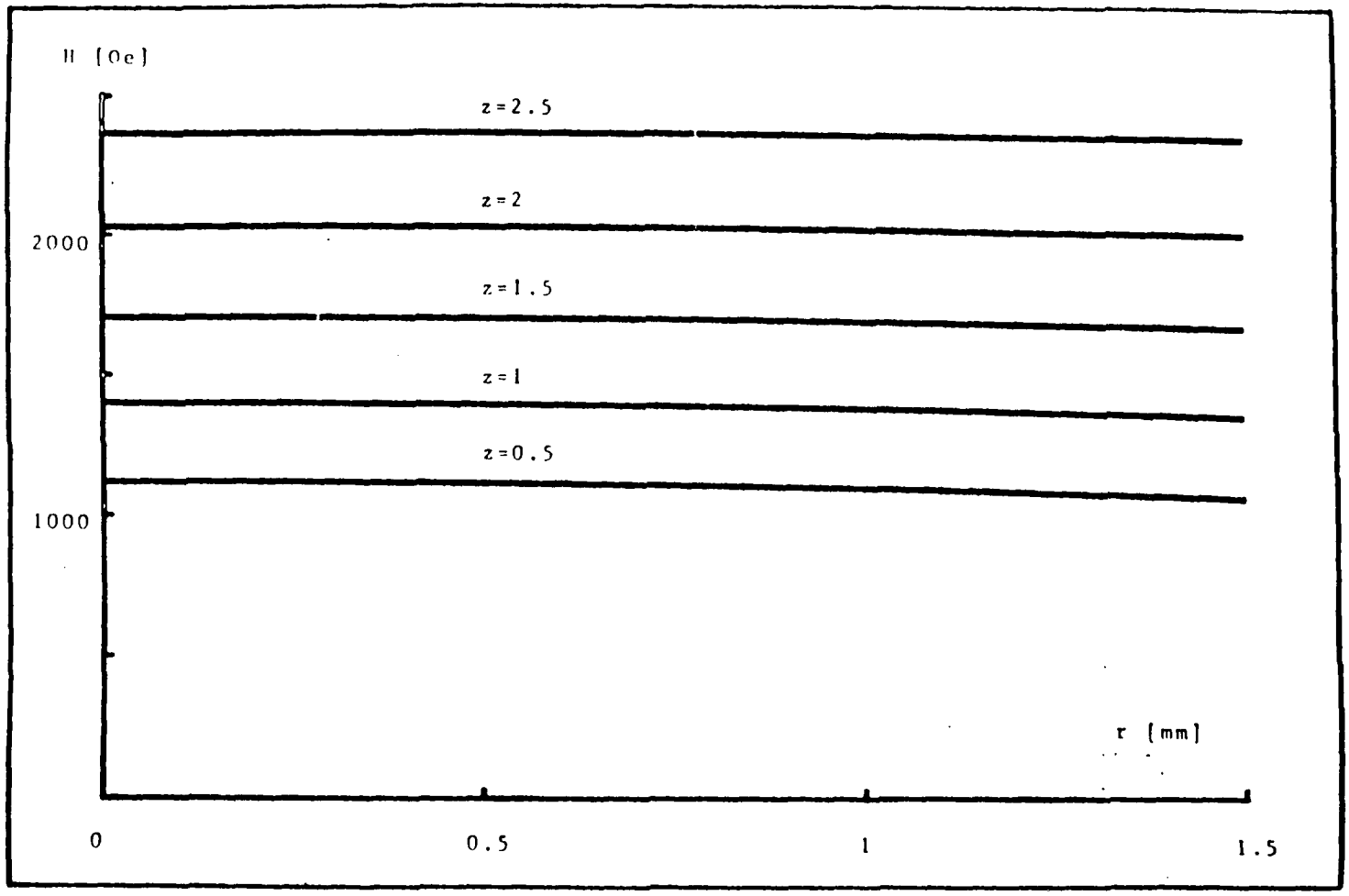

Figure (4.1) - $H(r,z=z_0)$ in the YIG rod

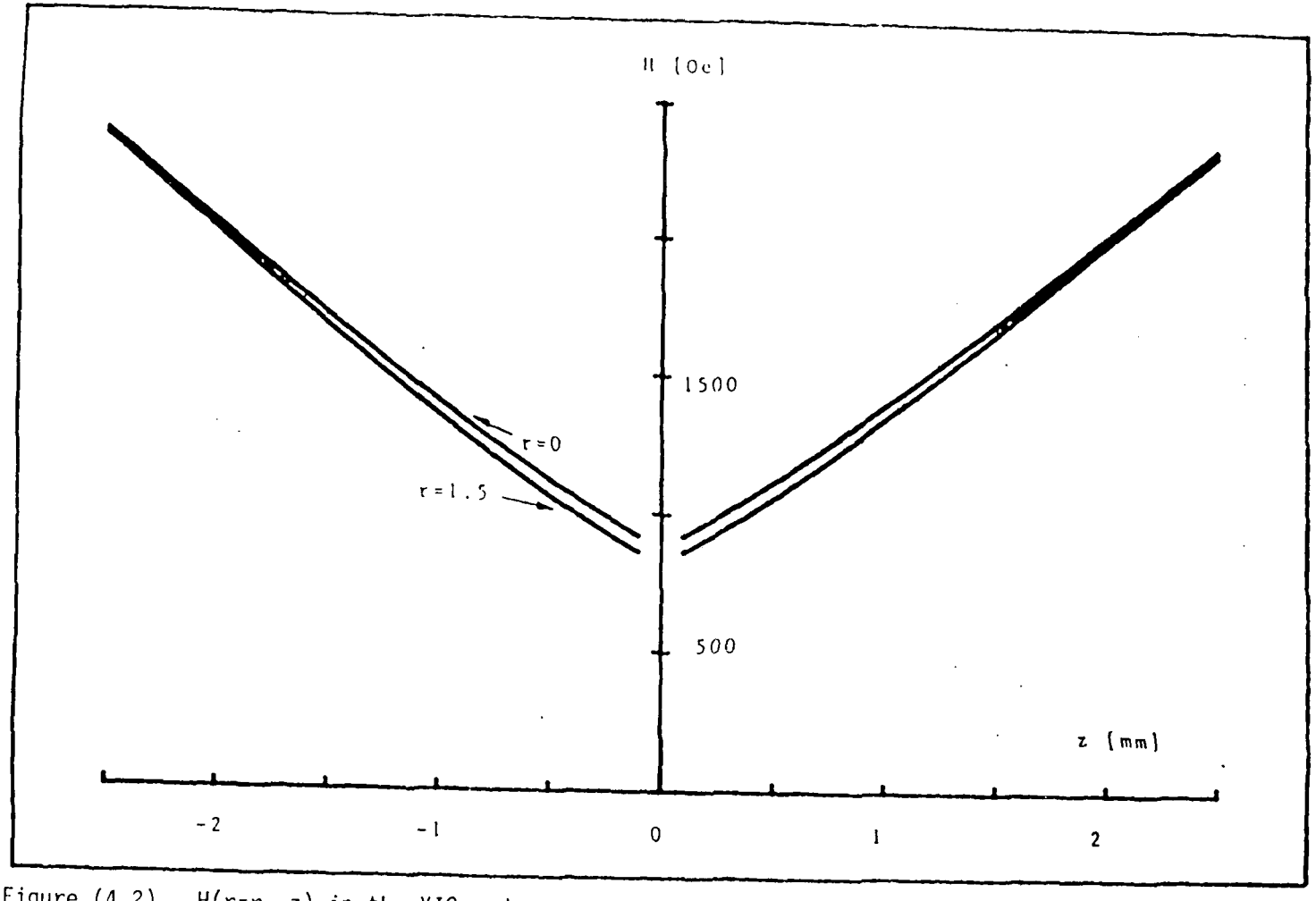

Figure (4.2) - $H(r=r_0,z)$ in the YIG rod

From Equation 3.12, the axial derivative of the on-axis magnetic field at the crossover point can be approximated and substituted into both equations:

$$\frac{dk_z}{dt} = \frac{-2\omega}{v_{ew}} \left[\frac{Df}{2} - \frac{C}{f} \right]^{-1} \quad (4.8)$$

$$\frac{dk_r}{dt} \approx + \frac{1}{4} \left(\frac{1}{a + 1} \right) \frac{2\omega}{v_{ew}} \left[\frac{Df}{2} - \frac{C}{f} \right]^{-1} \quad (4.9)$$

The spatial derivatives throughout the YIG rod remain constant to within an order of magnitude, the rate of time evolution of the axial wavenumber is greater than that of the radial wavenumber, i.e., $|dk_z/dt| >> |dk_r/dt|$, and the magnitude of k_z becomes much larger than the magnitude of k_r. It is in this manner that spatial inhomogeneity of the magnetic field controls the time evolution of wavenumber.

IV.C Dynamic Range and Saturation

Ray tracing can also be used to estimate power handling capability up to levels where saturation effects produce nonlinearities. Since a finite area contains a limited number of precessing atoms, the magnetic spin wave energy density cannot exceed the maximum level called saturation. Above this level, higher order processes are present which produce nonlinear effects [27].

For any plane wave based on Maxwell's Equations, the power flow through a unit normal cross-sectional area (Figure 4.3) is proportional to the following:

$$P \propto Id\Sigma \propto |\bar{A}|^2 v_g d\Sigma \qquad (4.10)$$

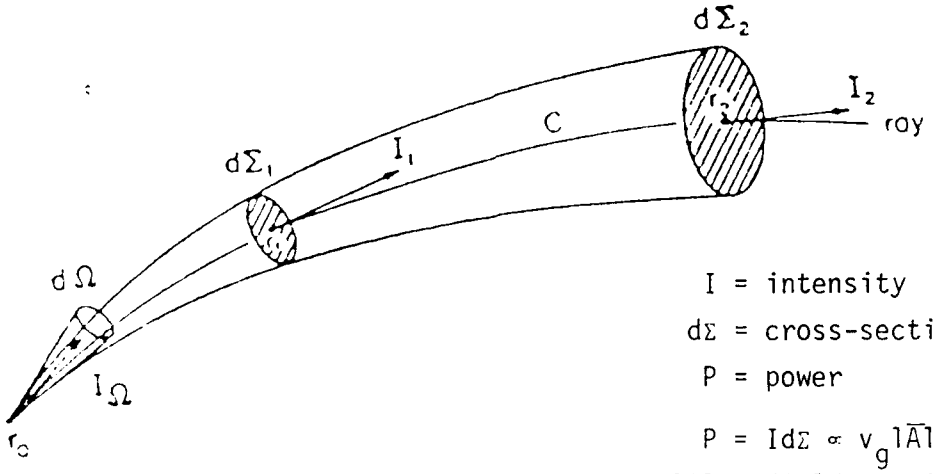

I = intensity

dΣ = cross-sectional area

P = power

$P = Id\Sigma \propto v_g |\bar{A}|^2 d\Sigma$

|A| = field magnitude

Figure (4.3) - Power flow from ray tracing

Ray tracing lends itself well to estimating relative power saturation points through application of Equation 4.10, since the distance between rays can be related to cross-sectional area. Magnetoelastic waves are relatively low loss and the field amplitude can be assumed to be constant. The power can therefore be considered proportional to the product of cross-sectional area and group velocity. Saturation occurs in the ray paths where Equation 4.10 is a minimum.

IV.D Considerations in Ray Tracing

Two important factors in ray tracing are: (a) the causes of ray path bending, and (b) the behavior of rays in isotropic versus

anisotropic media. Brief consideration of these issues is worthwhile for the insight into ray tracing in a gyrotropic medium.

There are two primary causes for ray paths departing from straight line propagation in gyromagnetic media. First, the dispersion relation is anisotropic -- the group velocity and wave vectors are not collinear. This deflection phenomenon is illustrated by considering the wave surface for a gyrotropic medium. The wave surface in Figure 4.4 is defined for the magnetostatic dispersion relation of Equation 2.17 at fixed frequency and magnetic field strength. It can be proven that the group velocity is always perpendicular to the wave surface [28] but is not necessarily parallel to the wave vector:

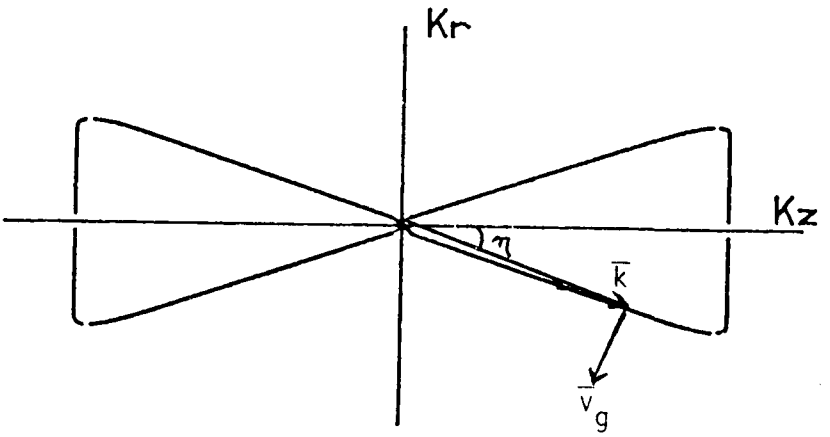

Figure (4.4) - Magnetic Wave Surface and Anisotropy

Clearly, a small shift in the displayed angle η of the wave vector produces a dramatic deflection in the direction of the group velocity and an effective bending of the ray.

The magnetic inhomogeneity of the medium also produces ray refraction. A ray propagating along the central axis of the rod experiences a greater magnetic field than a ray propagating off-axis. For fixed frequency, rays propagating between the turning point and

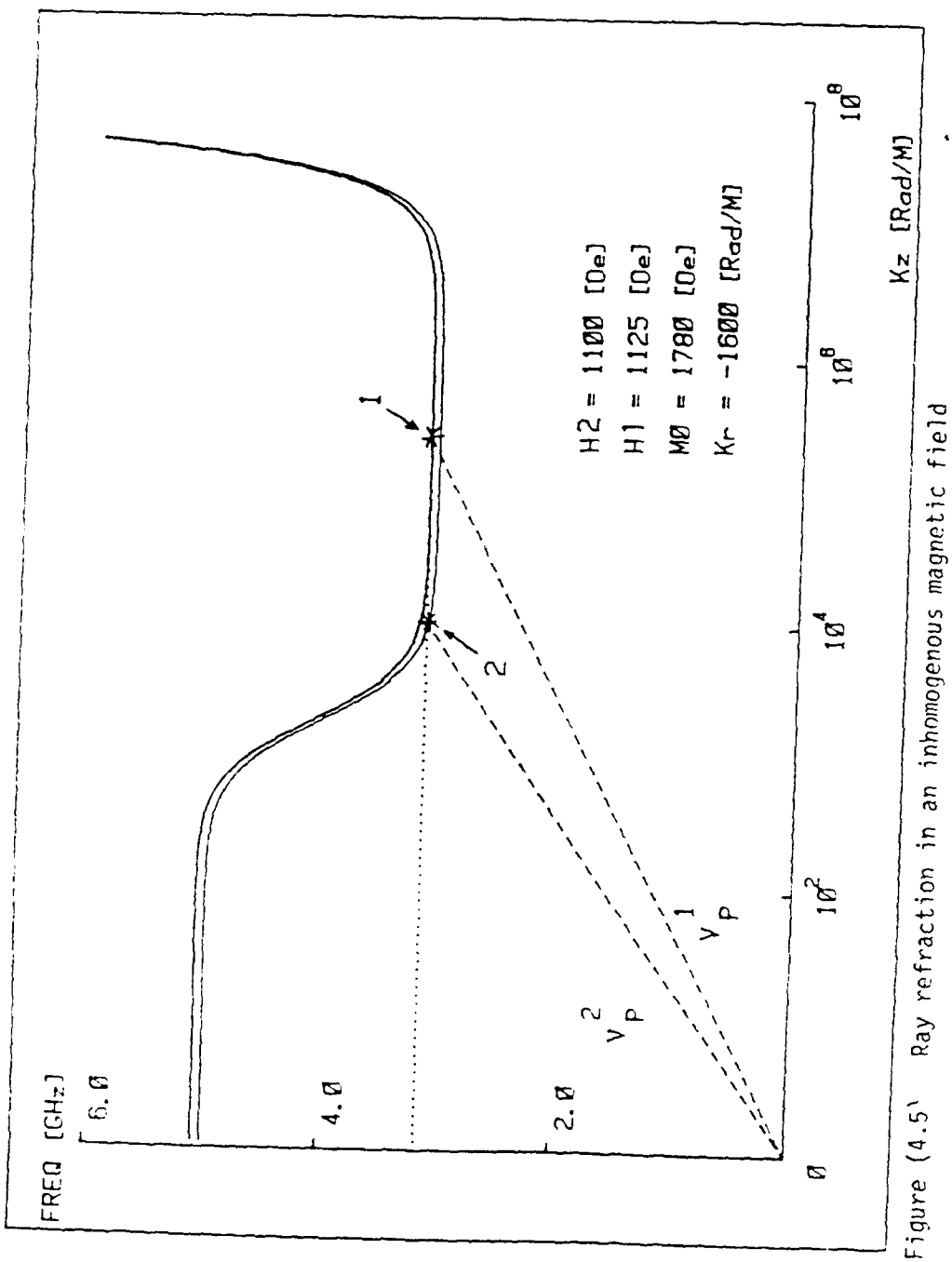

Figure (4.5) Ray refraction in an inhomogenous magnetic field

crossover point may have dramatically different phase velocities but similar group velocities, as shown in Figure 4.5. The result is that the phase front tends to refract and ray paths bend.

The use of wave surfaces as shown in Figure 4.4 is an extremely useful means for visualizing how ray paths evolve. Before going on to analyze the magnetoelastic delay line, however, it is worthwhile to examine a few simple cases.

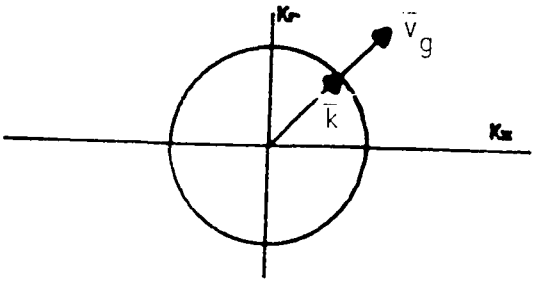

Figure (4.6) - Wave Surface for Electromagnetic Wave in Isotropic Medium

The case shown in Figure 4.6 is the classical optics case, propagation of light in a uniform medium. Because the medium is homogenous and the dispersion relation is isotropic (the constitutive relations contain no time derivatives), the group and phase velocities are collinear.

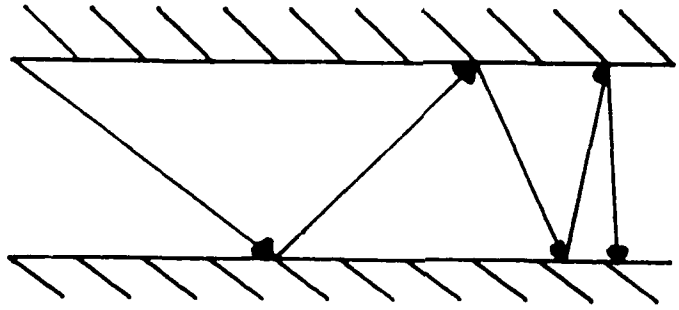

Figure (4.7) - Electromagnetic Radiation in a Waveguide with Spatially Dependent Permittivity

The case shown in Figure 4.7 illustrates the behavior of electromagnetic radiation in a waveguide filled with a substance whose permittivity increases with x. The transverse component of the wavenumber is fixed by the boundary condition. The longitudinal component decreases until it reaches a zero cutoff; at that point the wave is reflected although some energy continues to propagate as a decaying exponential. Spatial dependence of permittivity is analogous to the spatial dependence of susceptibility in the magnetoelastic delay line. The wave surface can be imagined as a circle whose radius shrinks with increasing permittivity.

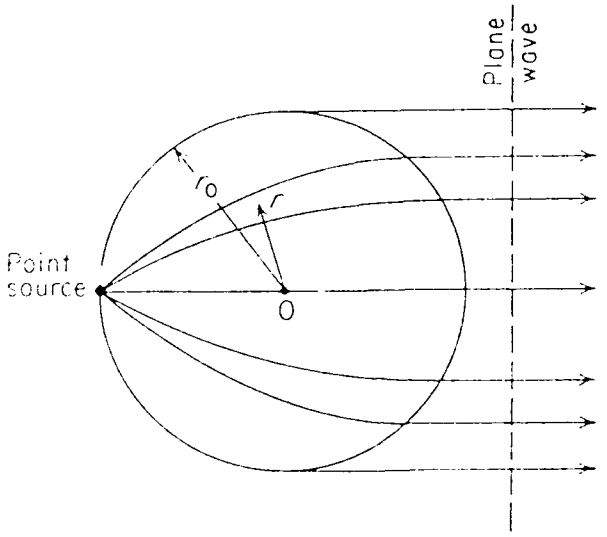

Figure (4.8) - The Luneberg Lens

Figure 4.8 shows the path of rays in a Luneberg Lens, commonly used in antenna systems where aperture blockage is unacceptable [29]. The Luneberg Lens focuses a plane wave onto a surface point through the use of a spatially varying permittivity:

$$\epsilon(r) = 2 - \left(\frac{r}{r_0} \right)^2 \qquad (4.11)$$

Since the dielectric constant at the sphere surface is equal to the dielectric of air, none of the ray path is a result of surface refraction. The range of permittivity variation is not extensive and the Luneberg Lens is relatively simple to build. Ray tracing analysis demonstrates the properties of the Luneberg Lens and is far simpler than full fledged electromagnetic analysis.

IV.E Ray Tracing for the Magnetoelastic Delay Line

The wave surface for magnetoelastic waves (fixed frequency, field strength) is shown in Figure 4.9. The radial portions of the surface correspond to magnetostatic behavior, the circular end portions to spin exchange wave behavior. The area contained inside the surface decreases as $\omega_z \to \omega$. Clearly, backward magnetostatic wave group velocities experience strong deflection from their wave vectors; spin exchange waves have collinear group velocity and wave vectors.

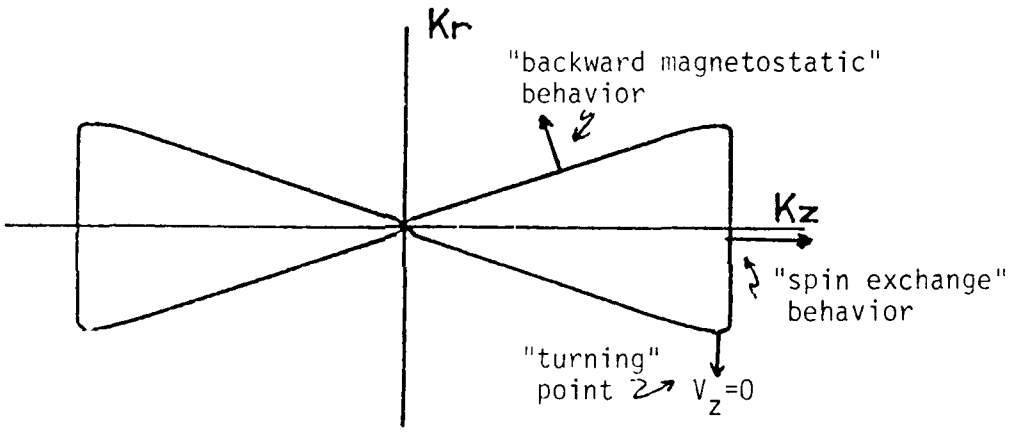

Figure (4.9) - Labeled Wave Surface for Magnetostatic Waves

The wave surface does not give any indication of group velocity magnitude. This, however, is easily visualized from the ω-k dispersion diagram, since the group velocity is the slope of the dispersion curve.

Table 4.1 lists several key quantitites needed to visualize the ray tracing of the magnetoelastic delay line:

	Backward Magnetostatic Waves	Spin Exchange Waves	Elastic Waves
Dispersion Relation	$\omega_z + \frac{\omega_M}{2}\frac{k_r^2}{k^2}$	$\omega_z + \omega_M \lambda_{ex} k^2$	$v_{ew} k$
v_z	$-\omega_M \frac{k_r k_z^2}{k^4}$	$2\omega_M \lambda_{ex} k_z$	$v_{ew} \frac{k_z}{k}$
v_r	$\omega_M \frac{k_r^2 k_z}{k^4}$	$2\omega_M \lambda_{ex} k_r$	$v_{ew} \frac{k_r}{k}$
$\frac{dk_z}{dt}$	$-\gamma\mu_0 \frac{\partial H}{\partial z}$		0
$\frac{dk_r}{dt}$	$-\gamma\mu_0 \frac{\partial H}{\partial r}$		0

$$k_r^{initial} = \frac{-2.405}{radius}$$

Table 4.1 Summary of Backward Magnetostatic Wave, Spin Exchange Wave, and Elastic Wave Relations

Initial value of k_r is defined by Kittel's analysis of magnetostatic propagation in rods [16]. An initial value of k_z is found by solving the magnetostatic (without exchange) dispersion relation in Equation 2.18. Froms Equations 4.8 and 4.9, it is apparent that k_z will evolve much more quickly than k_r.

Figures 4.10a-d show, in parallel, the evolution of the ray path and the corresponding visualization from the wave surface. Since dk_r/dt is always positive and k_r is initially negative, the evolution is not symmetric. The evolution of k_z, however, is roughly symmetric as dk_z/dt changes sign with the sign of z.

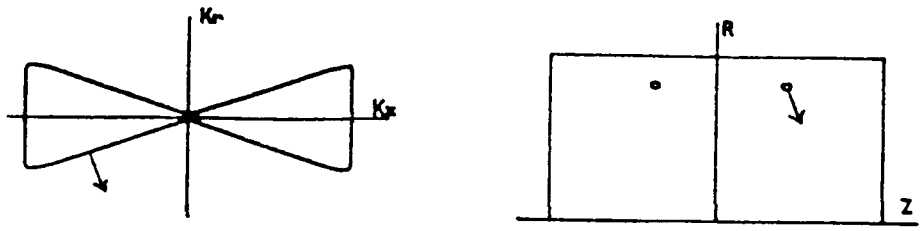

A. Starting point - backward magnetostatic wave

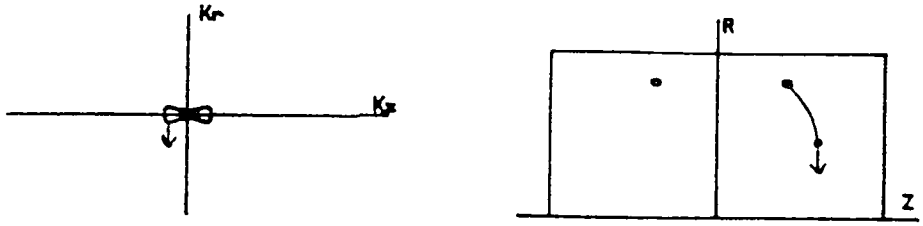

B. First turning point

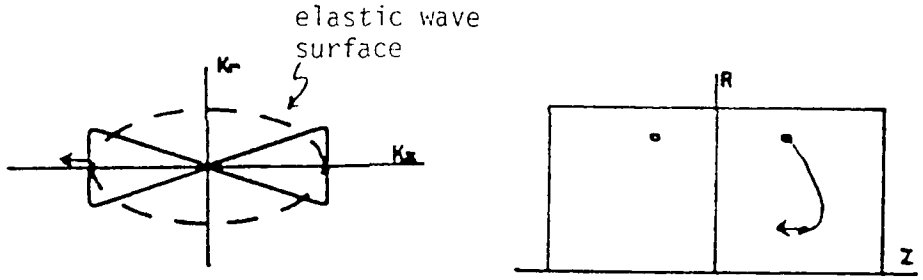

C. First crossover point

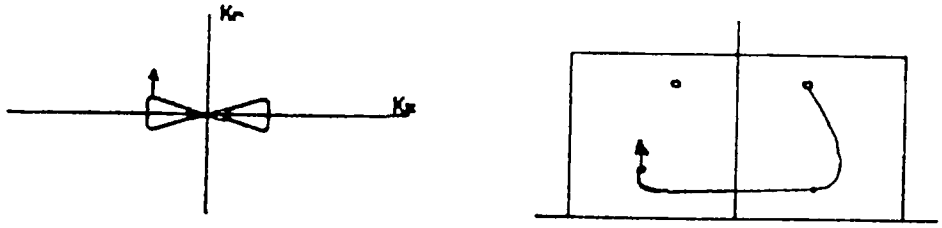

D. Second turning point

Figure (4.10) - Magnetoelastic wave evolution in the delay line

IV.F Ray Tracing Computer Program

The ray tracing computer program iteratively tracks out the ray path using the techniques described above. The dispersion relation used is that of Equation 2.16, magnetostatic waves in an infinite ferrite. Use of this dispersion relation is acceptable because the initial conditions guarantee that the wavelength is virtually always much smaller than the rod dimensions and the medium appears infinite to the wave. Borgeaud's analysis [3] confirms the acceptability of (a) applying ray tracing technqiues to relatively long wavelength magnetoelastic waves in the early stages and (b) using the first root of the zeroth order Bessel function as the initial value of k_r.

The Hamilton equations are applied to this dispersion relation without any simplifying assumptions. The conditions for application are that (a) frequency is constant, and (b) only $\bar{H}$ and $\bar{M}$ are functions of position. In the latter case, $\bar{H}$ and $\bar{M}$ are defined anywhere in the rod by the method described in Appendix C. The ray tracing is implemented as shown in Figure 4.11. At Point 1, the position, wave vector, and group velocity are known. For a time increment on the order of nanoseconds, $\Delta\bar{r}$ and $\Delta\bar{k}$ are calculated from Hamilton's equations. The new position, wave vector, and group velocity are then found.

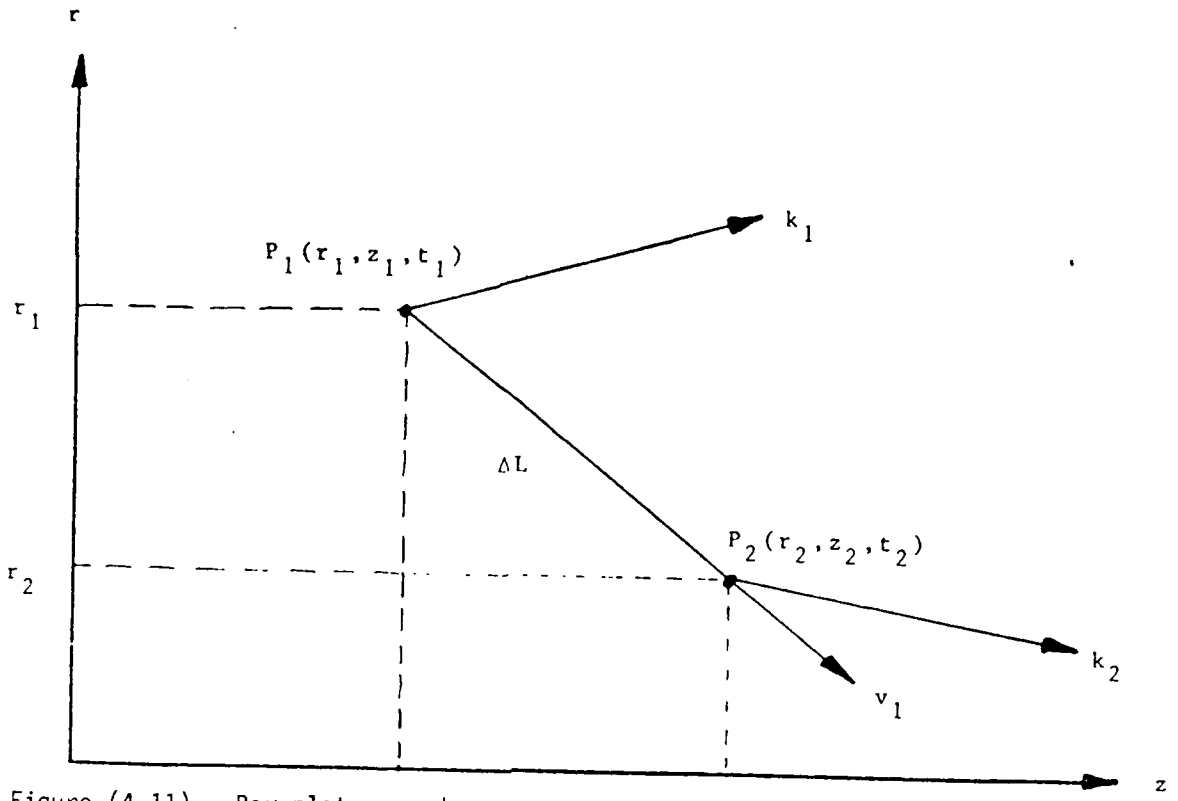

Figure (4.11) - Ray plot procedure

Besides ray tracing, the program also automatically increments frequency for bandwidth determination, locates the antennas, varies user parameters, etc. Additionally, the program identifies turning and crossover points in the propagation path, checks for ray path colliding with sample surfaces, and provides data storage and graphics. Figure 4.12 shows a typical ray tracing product for a particular delay function and field profile constant.

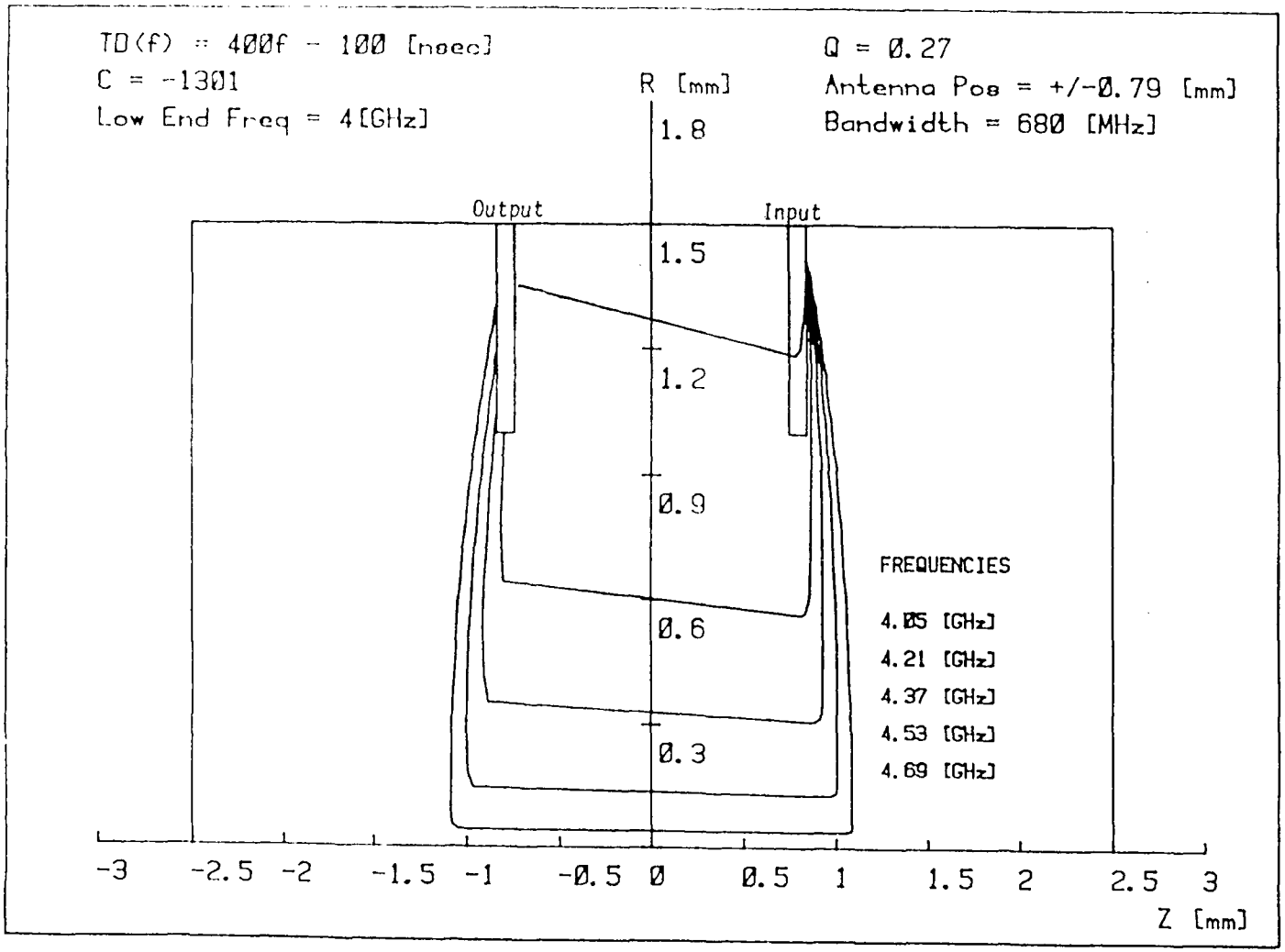

Figure (4.12) - Computer generated ray tracing for bandwidth analysis

Chapter V

RESULTS AND CONCLUSIONS

V.A Introduction

Ray tracing analysis provides several insights into the operation and optimization of the two-port "buried-antenna" magnetoelastic delay line. As a result, bandwidth and dynamic range can be optimized, and the effects of several different material parameters are explained. A simple predictive model is developed.

V.B Summary of Previous Work

Borgeaud [3] built and tested a two-port "buried-antenna" magnetoelastic delay line (Figure 3.4) designed to the following parameters:

TD(f) = 500 f - 200 [nsec]

C = -1000

Rod radius = 1.5 [mm]

Rod length = 5 [mm]

Axial antenna locations = +/- 1.0 [mm]

The value of C = -1000 was chosen to demonstrate that a nonlinear field profile would produce a linearly dispersive delay function. His results can be summarized as follows:

Range of detectable signal = 3.1-3.6 [GHz]

Detectable signal bandwidth = 500 [MHz]

Range of linear dispersion = 3.2-3.5 [MHz]

Linearly dispersive signal bandwidth = 300 [MHz]

Actual delay function implemented = 500 f - 500 [nsec]

Borgeaud found that the range of frequencies which propagate is determined by the antenna location. Only those frequencies falling within the range defined below can propagate:

$$f_z \leq f \leq \sqrt{f_z(f_z + f_M)} \tag{5.1}$$

This region is the spin wave manifold and is bounded by the dispersion relation curves shown in Figure 5.1. In this case ω_z is defined by the local field, H_0, at the antenna. Borgeaud's selection of antennas at +/- 1.0 [mm] explicitly defined the available range of frequencies for the given magnetic field profile. For $\omega \rightarrow \omega_z$, the frequency of propagation is already at the turning point and the rays propagate immediately toward regions of lower magnetic field (Figure 5.2a); as frequencies increase the rays spend more time as a backward magnetostatic wave and propagate closer to the z-axis (Figure 5.2b). Rays which propagate away from the z-axis, however, show large deviations from the desired linear time response (Figure 5.2a,b).

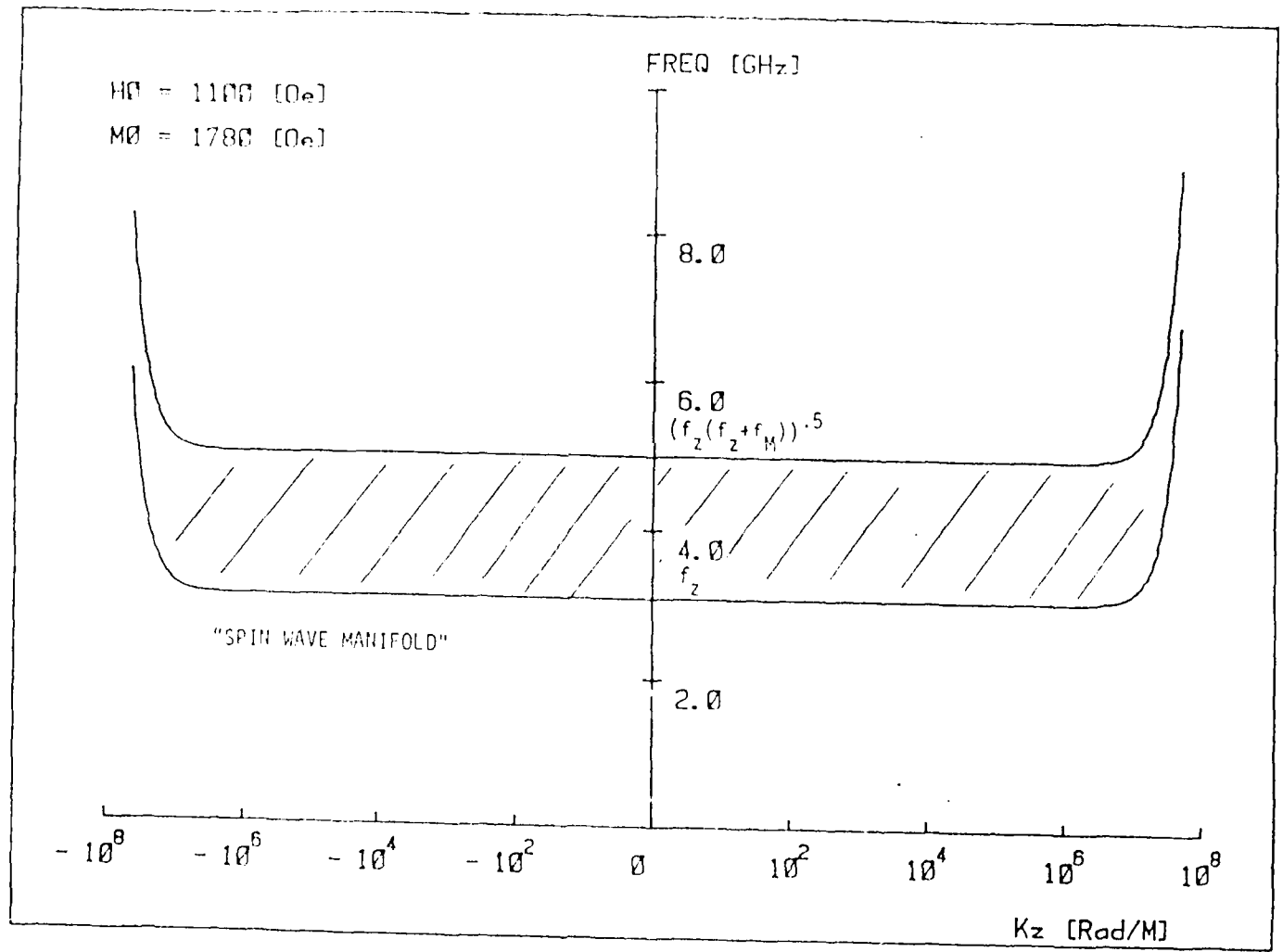

Figure (5.1) - Magnetostatic dispersion relation - "Spin Wave Manifold"

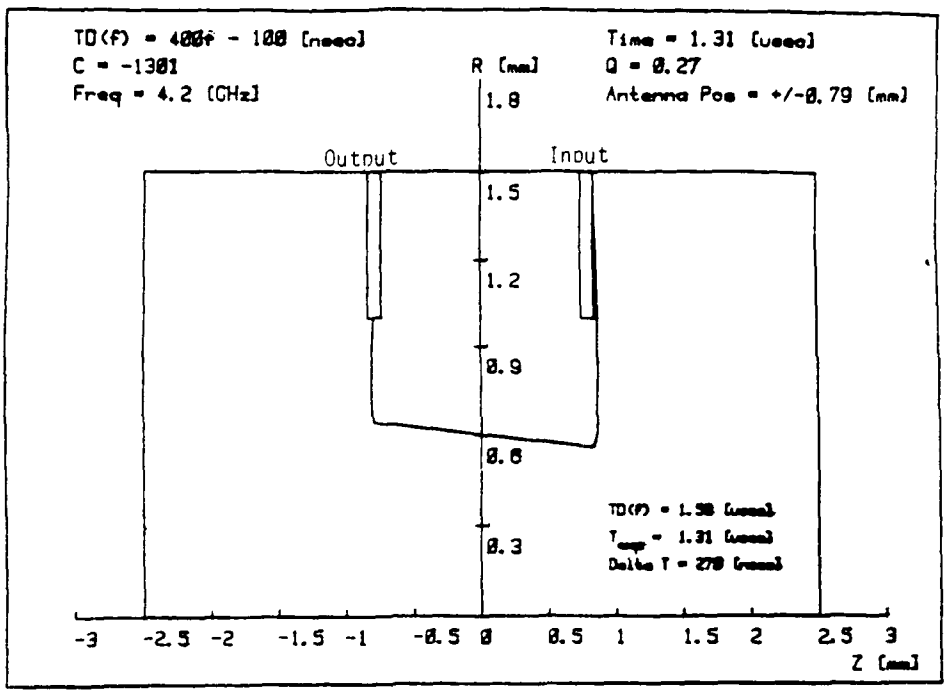

A. Ray propagating away from z-axis - large time deviation

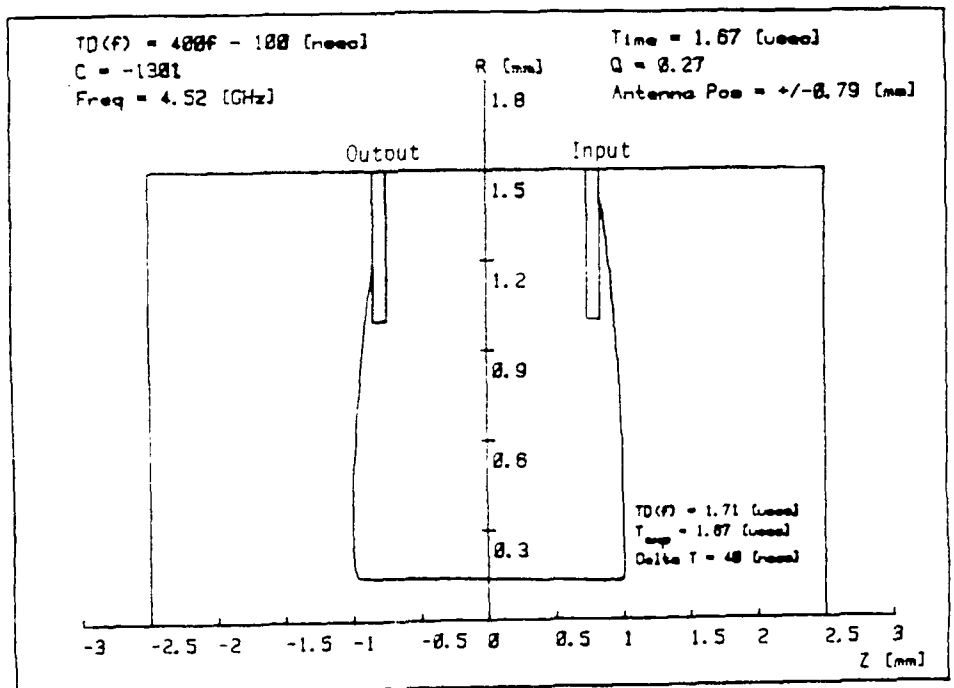

B. Ray propagating near z-axis - small time deviation

Figure (5.2) - Ray propagation times compared

V.C Bandwidth Analysis

In order to analyze the bandwidth obtained by Borgeaud, it was necessary to create a computer program which would conduct the appropriate ray tracing. This program, described in Section IV.F, meets design goals of (a) a 10X increase in computation speed over earlier ray tracing routines, and (b) automatic bandwidth analysis. Overall program speed is improved by hosting on a faster microcomputer, writing computationally intensive routines in C language (instead of Basic), and optimizing code structure.

For the range explored by Borgeaud (a bottom frequency of 3.1 [GHz]), it is apparent that larger bandwidths are obtainable by changing the value of the field profile constant, C. Figure 5.3 shows how bandwidth varies as a function of C for several different delay functions and the same bottom frequency. The antenna location explicitly defines the resonant frequency for the given frequency range. A relation giving bandwidth as a function of C and D, however, is not readily apparent.

Although the choice of D, the dispersive delay, has a marked effect on bandwidth, the choice of the fixed delay T_0 has no effect on bandwidth (Figures 5.4a and 5.4b). This implies that the bandwidth is independent of the location of the crossover point (Equation 3.7) -- an intuitively appealing result since the elastic wave portion of a ray path tends to be roughly parallel to the central axis. The elastic wave portion of the propagation does not constrain bandwidth and the fixed delay T_0 is contained entirely in the elastic wave propagation.

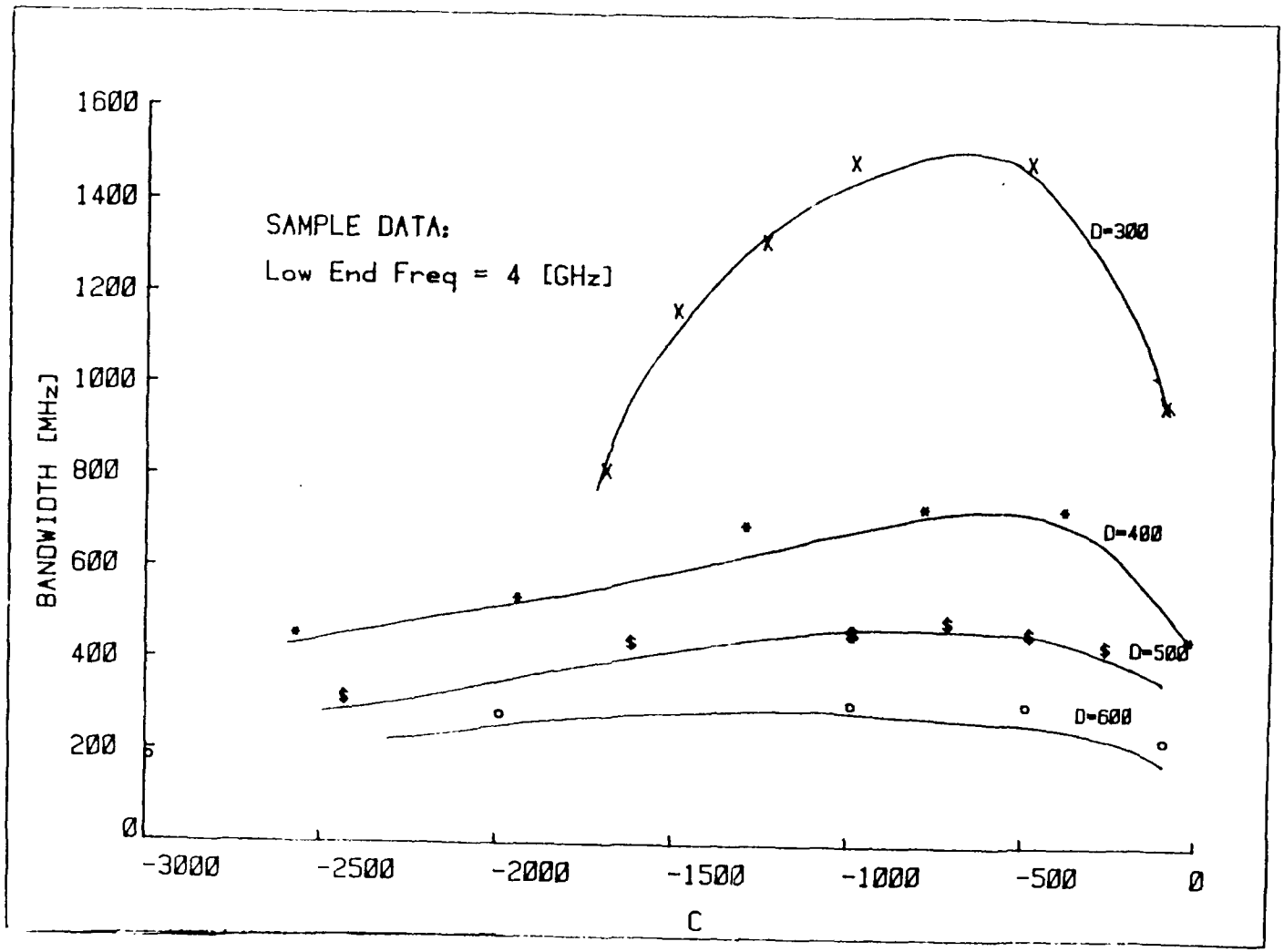

Figure (5.3) - Bandwidth as a function of D and C

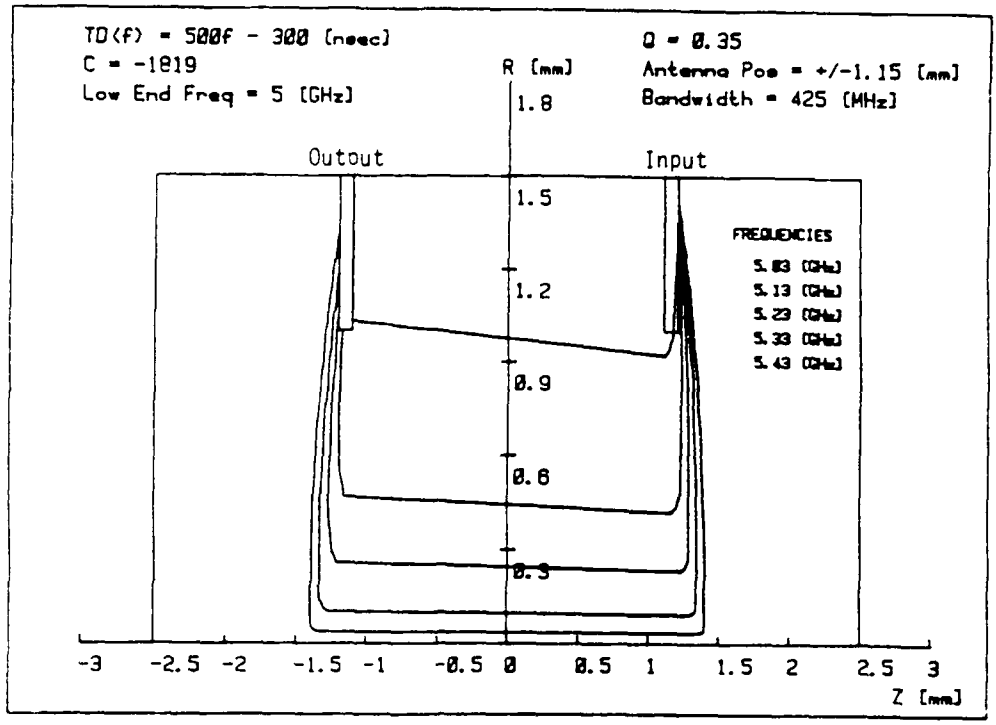

A. Bandwidth=425 MHz; T_0=-300 nsec; All other parameters fixed

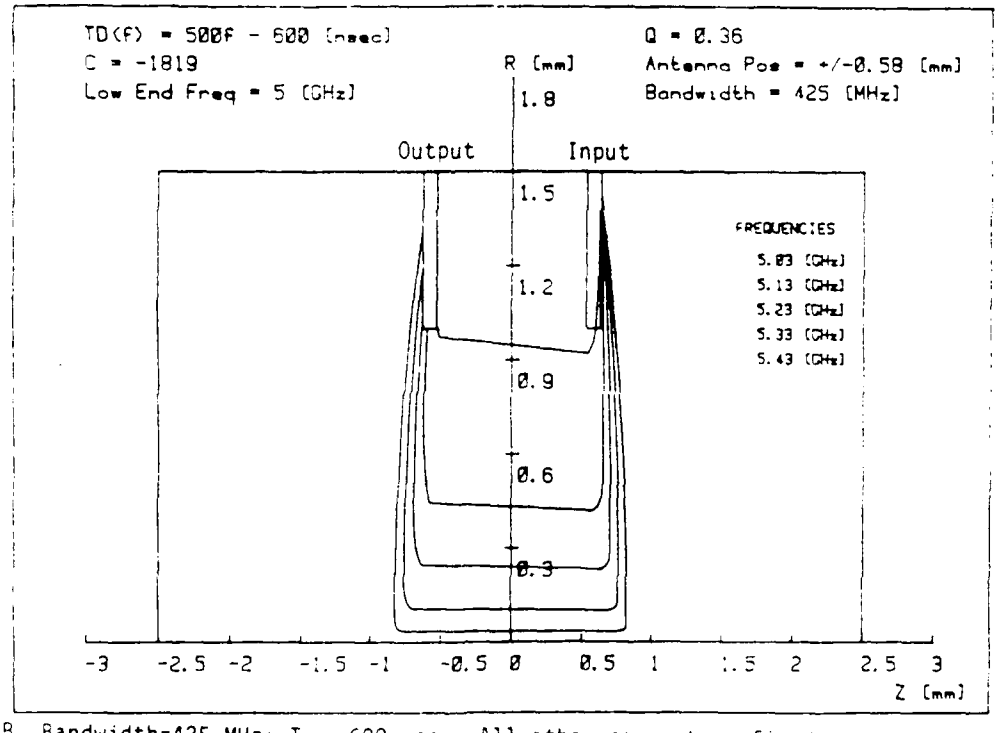

B. Bandwidth=425 MHz; T_0 =-600 nsec; All other parameters fixed

Figure (5.4) - Bandwidth as a function of T_0

Figure 5.3 illustrates that, for each value of dispersive delay D, the bandwidth reaches a maximum for some value C_{max} (Figure 5.5a-c). For values of C more negative than C_{max}, higher frequency rays collide with the z-axis and never reach the output antenna (Figure 5.6). For values of C greater than C_{max}, rays between the second turning point and the output antenna experience abrupt, unusual changes in direction (Figure 5.7). The former case is clear from ray tracing; the latter effect appears due to the interaction between $\bar{k}$ (which evolves asymmetrically) and the radial components of $\bar{M}$.

It was suggested by Morgenthaler [30] that bandwidth maxima might be dependent upon Q, the focusing parameter discussed in Section III.E. Figure 5.8 shows this to be the case, with maximum values of bandwidth consistently occurring for $0.4 < Q < 0.5$. Rays with a value of Q greater than 0.5 tend to show the abnormal changes in direction between the second turning point and the output antenna. Frequencies whose rays have values of Q less than 0.5 obey a regular trend.

V.D A Simple Predictive Model

The independence of bandwidth from T_0 leads to the following hypothesis: Bandwidth is a function of dH/dz. The inference is made because the slope of the magnetic field at crossover, $dH(r=0,z)/dz$ at $z = z_{cp}$, is also independent of T_0 (Equation 3.12):

$$\left.\frac{\partial H(r=0,z)}{\partial z}\right|_{z=z_{cp}} = \frac{2}{v_{ew}\frac{\gamma\mu_0}{2\pi}}\left[\frac{Df}{2} - \frac{C}{f}\right]^{-1} \qquad (5.2)$$

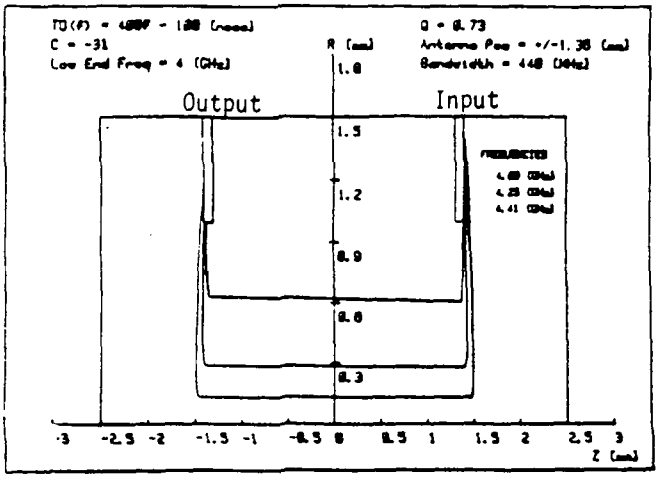

A. $C > C_{max}$; Bandwidth=440 MHz; all other parameters fixed

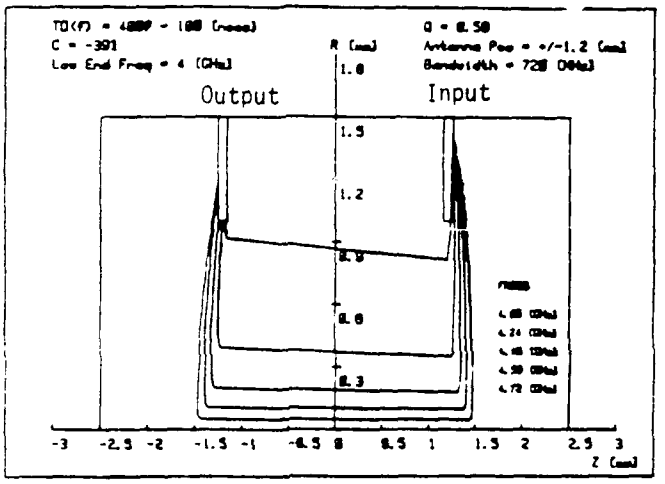

B. $C \sim C_{max}$; Bandwidth=720 MHz; all other parameters fixed

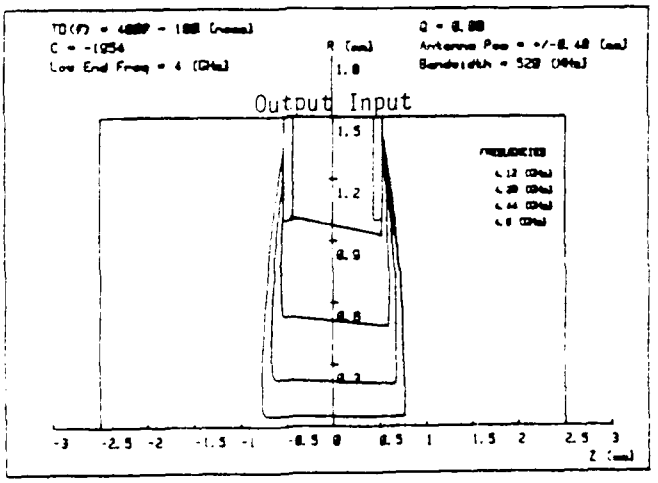

C. $C \ll C_{max}$; Bandwidth=520 MHz; all other parameters fixed

Figure (5.5) - Bandwidth as a function of C

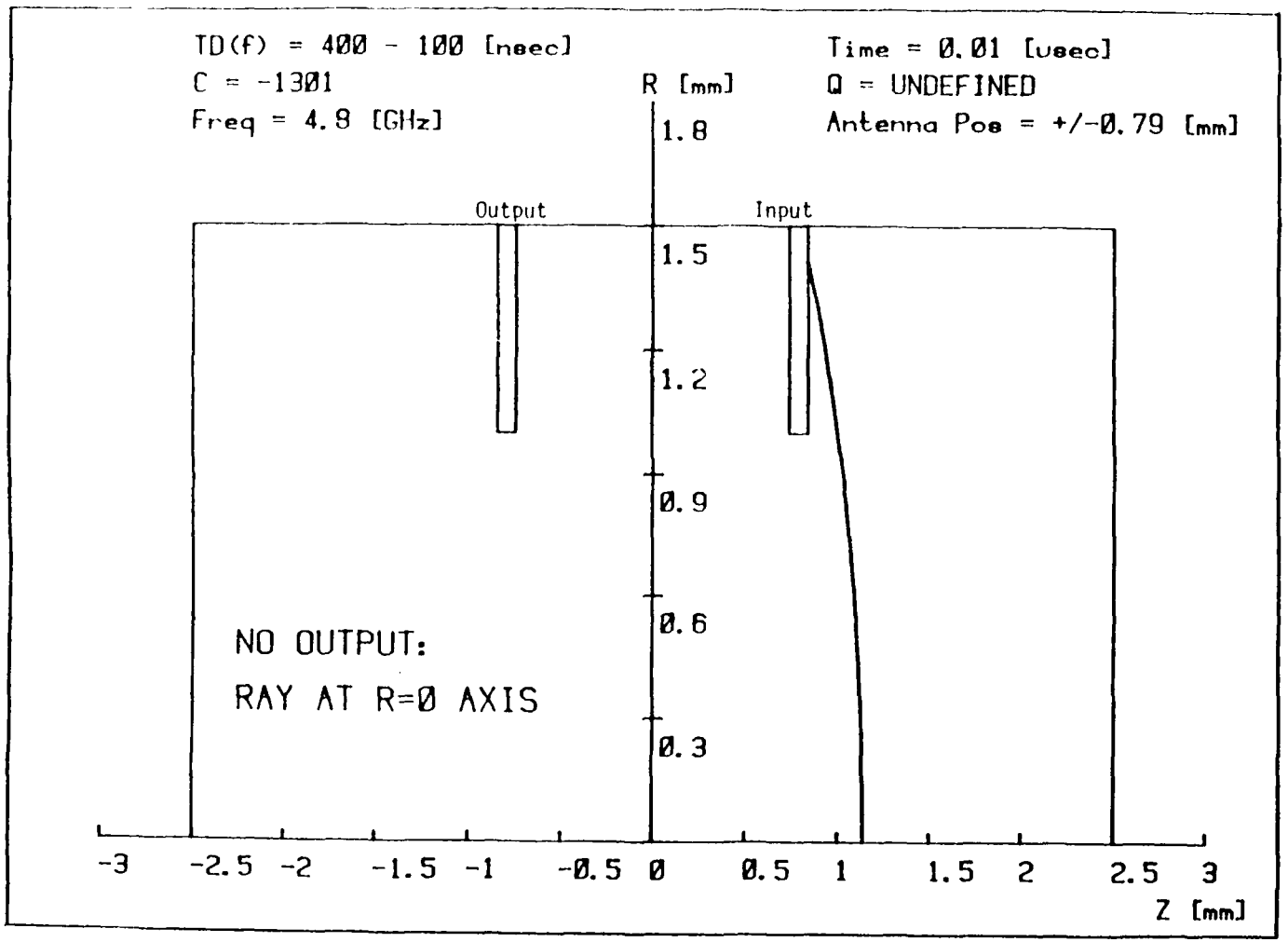

Figure (5.6) - Ray propagates directly from antenna to z-axis

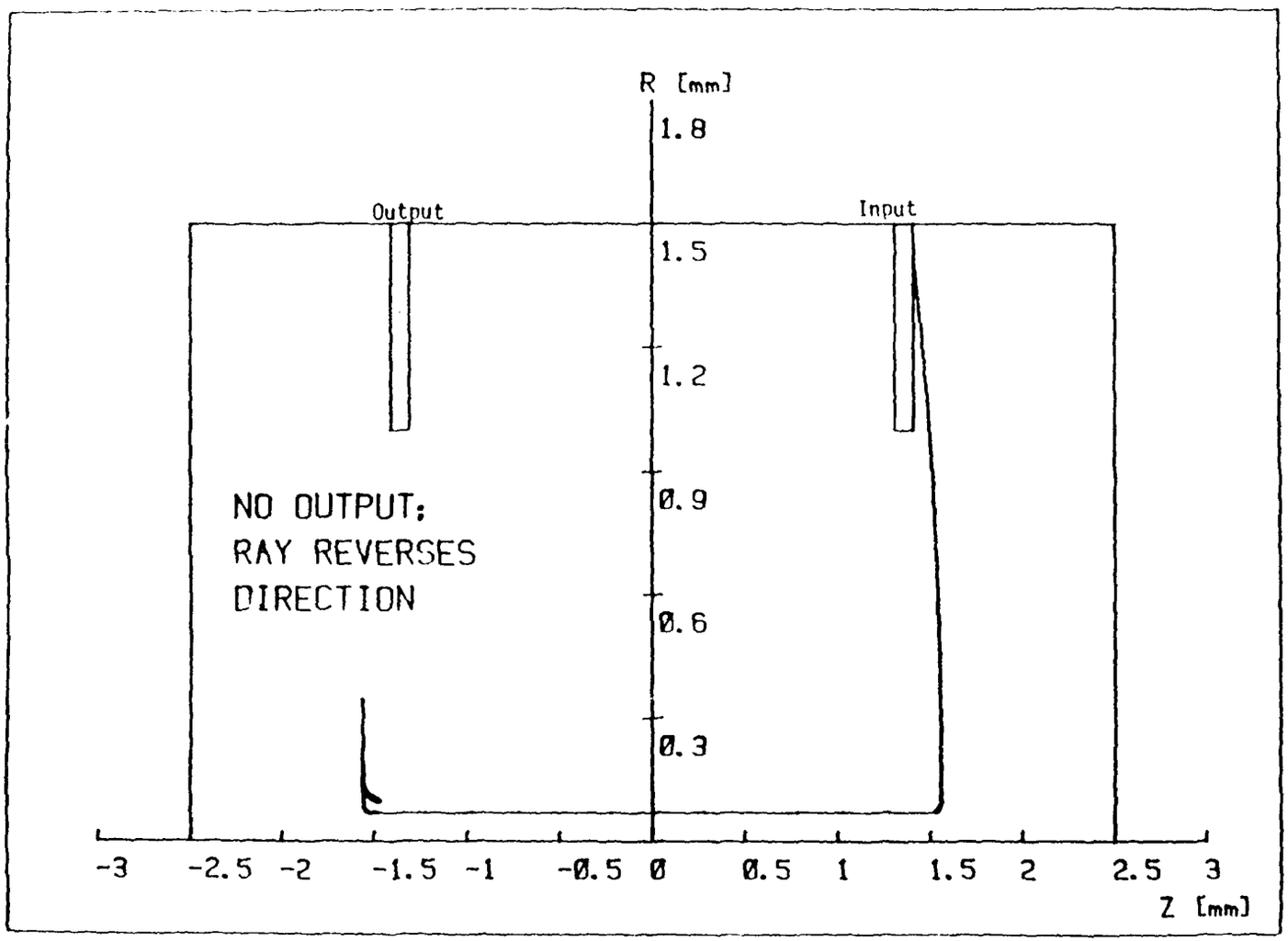

Figure (5.7) - Ray changes direction after second turning point

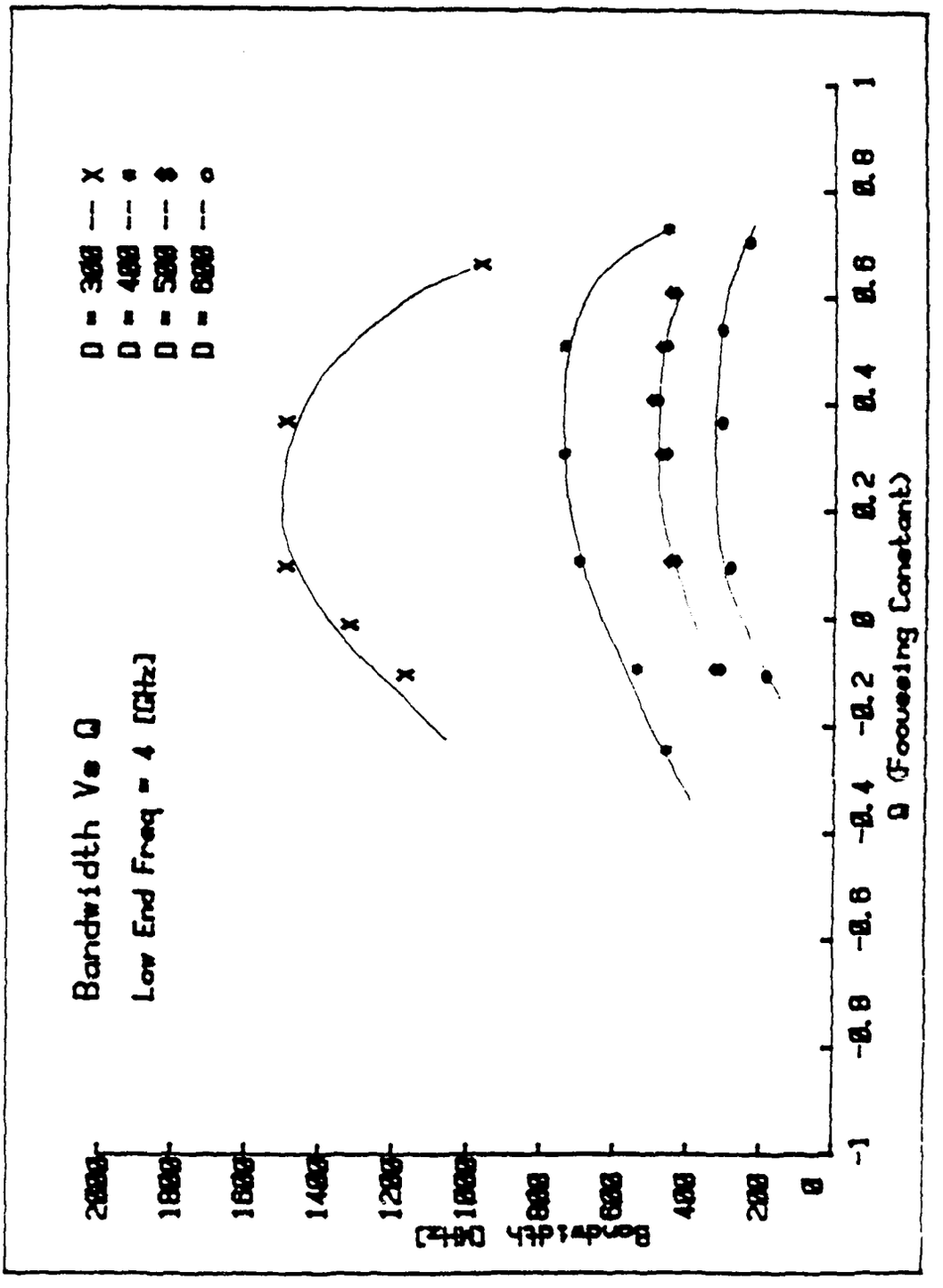

Figure (5.8) - Bandwidth as a function of Q and D

The derivative of magnetic field in Equation 5.2 is a function of D and C, and it remains constant to within an order of magnitude throughout the rod. A Log-Log plot of bandwidth versus dH/dz (excluding points with $Q > 0.5$) shows a straight line relationship (Figure 5.9a) with a slope of 2.3 (from least mean square line fitting). A linear plot of bandwidth versus $(dH/dz)^{2.3}$ gives a percentage standard deviation of 10%, small enough for predictive use (Figure 5.9b).

The dependence of bandwidth on the slope of the magnetic field profile seems reasonable because dk_z/dt and dk_r/dt are proportional to, respectively, dH/dz and dH/dr (Equation 4.6):

$$\frac{dk_z}{dt} = -\gamma\mu_0 \frac{\partial H}{\partial z} \tag{5.3}$$

$$\frac{dk_r}{dt} = -\gamma\mu_0 \frac{\partial H}{\partial r} \tag{5.4}$$

Recall also that dH/dr, from Equation 4.7, can be expressed as a function of the <u>axial</u> field derivative.

$$\left.\frac{\partial H}{\partial r}\right|_{r=0} \approx -\frac{1}{4}\left(\frac{1}{a+1}\right)\left.\frac{\partial H}{\partial z}\right|_{r=0} \tag{5.5}$$

As mentioned above, the higher the frequencies radiated from a fixed antenna location, the closer the rays propagate to the z axis. Above the upper edge of the frequency band, rays collide with the z axis. The controlling factor for the backward magnetostatic wave is thus the evolution of v_r (Equation 2.21):

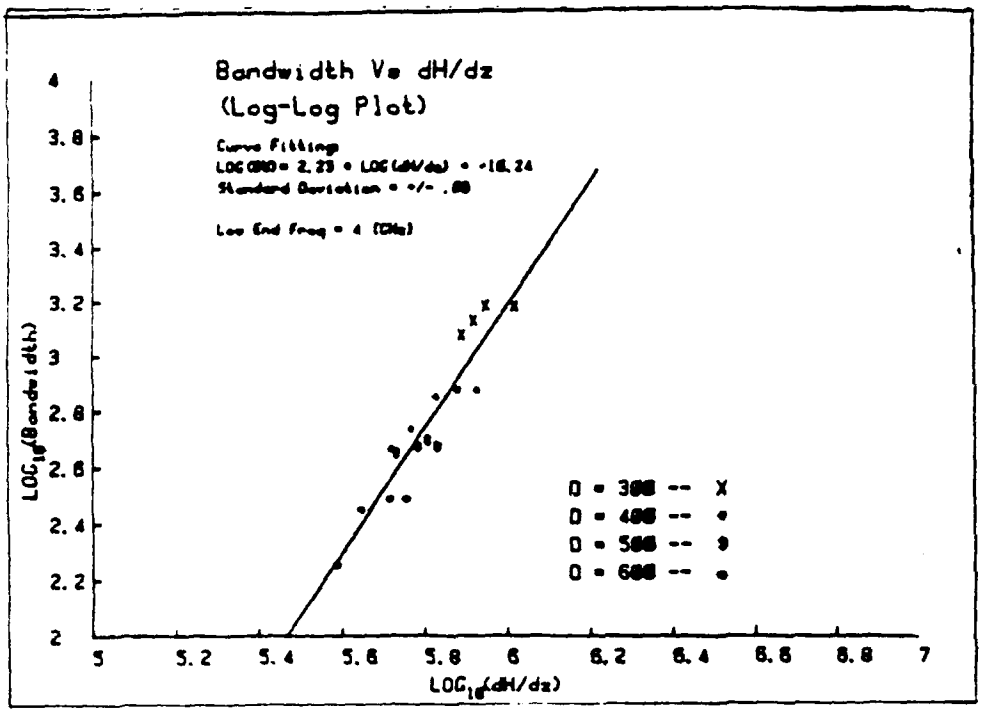

A. LOG-LOG plot of bandwidth vs dH/dz

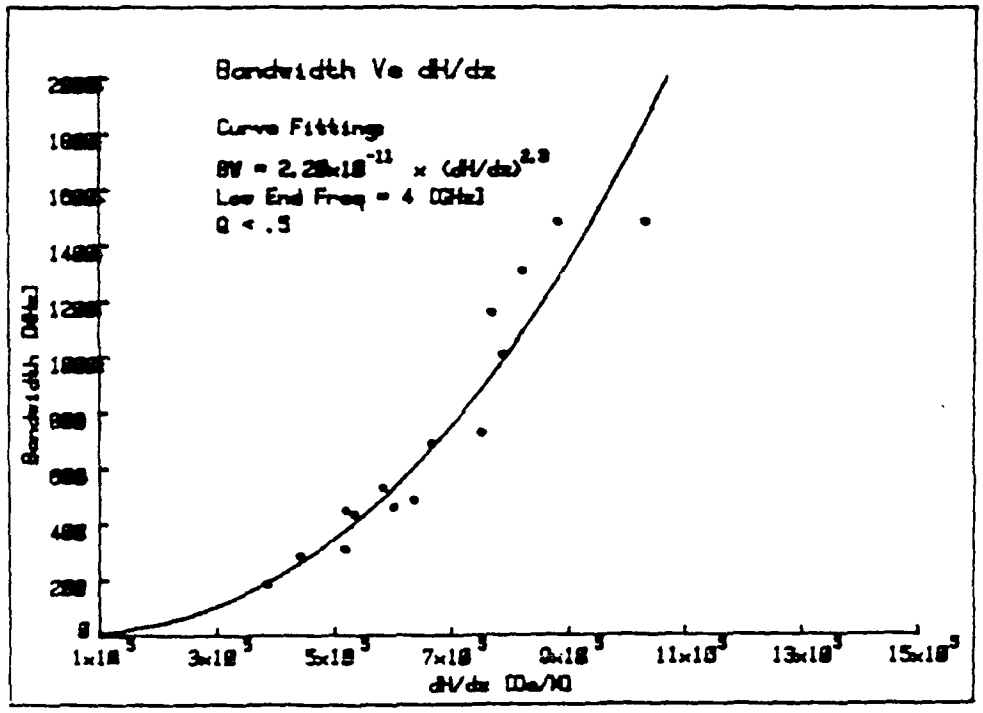

B. Linear plot of bandwidth vs dH/dz

Figure (5.9) - Bandwidth as a function of dH/dz

$$v_r \propto \frac{k_r}{k_z^2} \tag{5.6}$$

All other things being equal, the faster the magnitude of v_r approaches zero and/or becomes positive, the less likely the ray is to collide with the z-axis. For $z > 0$: k_r and k_z are initially negative; $dk_z/dt < 0$; $dk_r/dt > 0$; and larger magnitudes of dk_r/dt and dk_z/dt improve the likelihood of a ray reaching the turning point and, ultimately, reaching the output antenna.

Borgeaud's assumption that rays reaching the z-axis propagate no further is an intuitive consideration of energy flow. Rays reaching the z-axis from opposite ends of the same antenna tend to intersect there and ray paths can no longer be defined. Ray tracing analysis of rays reaching the z-axis confirms the assumption on different grounds. Those rays which have $v_r < 0$ at the z axis do not appear to ever leave the axis. Figure 5.10 shows the behavior of such a ray -- v_r remains negative and the ray oscillates about the z axis with increased attenuation.

Experimenting with bandwidth data and Equations 5.2 and 5.5 leads to the following proportionality:

$$BW \propto \left(\frac{dk_r}{dt}\right)^{1.3}\left(\frac{dk_z}{dt}\right)^{1.0} = \left[-\frac{1}{4}\bullet\frac{1}{a+1}\right]^{1.3}\left\{\frac{1}{v_{ew}}\left[\frac{Df}{2} - \frac{C}{f}\right]^{-1}\right\}^{2.3} \tag{5.7}$$

$$a = \frac{\omega_M}{\omega} = \frac{\gamma\mu_0}{2\pi} \bullet \frac{M_0}{f}$$

This relation preserves the order of the proportionality between bandwidth and dH/dz, and it allows prediction of bandwidth as a function

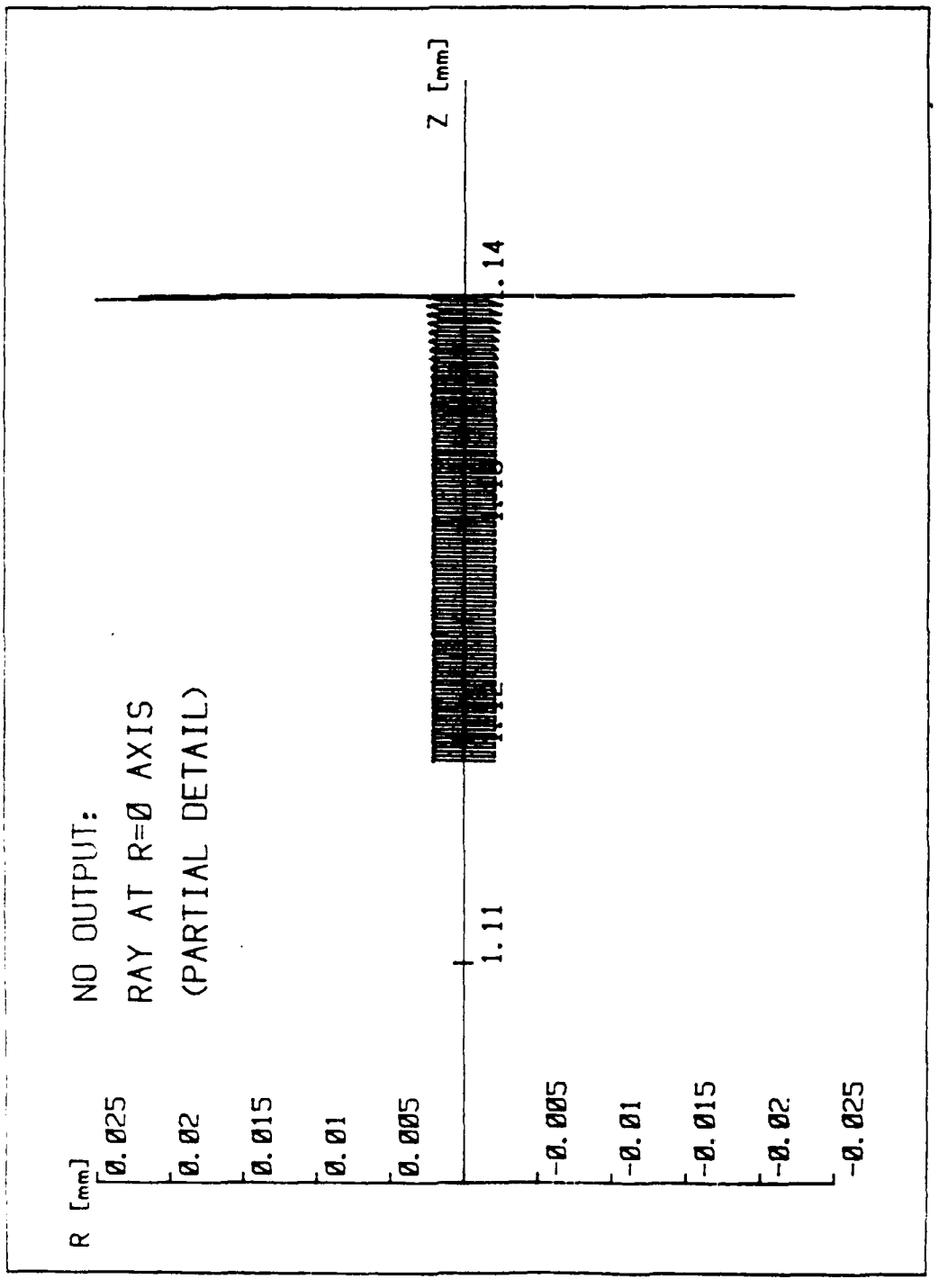

Figure (5.10) - Detail of ray reaching z-axis and oscillating

of several other variables: (a) M_0, the saturation magnetization; (b) v_{ew}, the elastic wave velocity; and (c) $\gamma\mu_0$, the gyromagnetic constant. Figures 5.11a-c show ray tracing bandwidth data which are in accordance with expected values.

As a result of this work, optimizing bandwidth for a given delay function becomes a trivial calculation. Recasting Equation 3.14 to give C, the field profile constant, as a function of Q allows immediate calculation for Q = 0.5:

$$C = \frac{Df^2}{2}\left[\frac{Q(a+1)^2 - 3a}{Q(a+1)^2 - 3a - 4a(a+1)}\right] \tag{5.8}$$

This value optimizes bandwidth.

V.E Dynamic Range

A second goal of this thesis is to determine if the dynamic range of the magnetoelastic delay line can be optimized as well. Dynamic range is defined here in the sense of a saturation point since no study has yet been made of noise floor and Minimal Discernible Signal (MDS). As discussed in Section IV.C, power flow can be viewed as a function of the distance between rays emanating from opposite ends of the transmit antenna. The power handling capability is proportional to the product of cross-sectional area between rays and the group velociy, assuming the fields are of constant amplitude.

Figure 5.12 shows the paths of rays for the same frequency and delay functions but in magnetic fields with different values of C. The distance between the rays decreases as C approaches zero and the

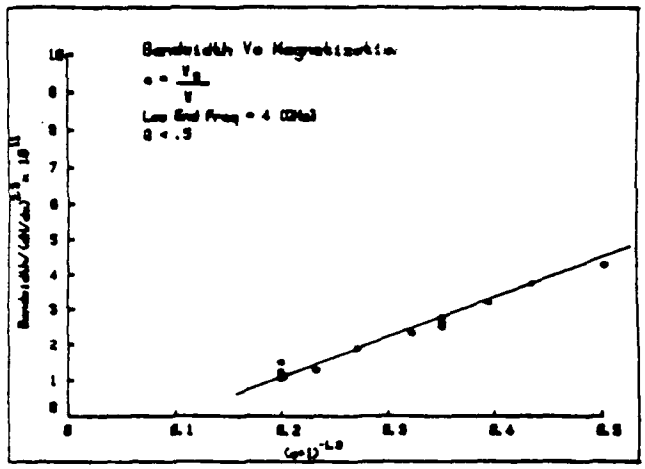

A. Bandwidth as a function of magnetization M_0

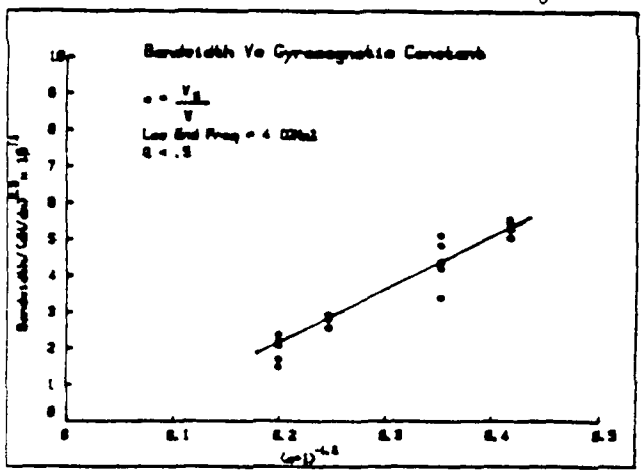

B. Bandwidth as a function of the gyromagnetic constant

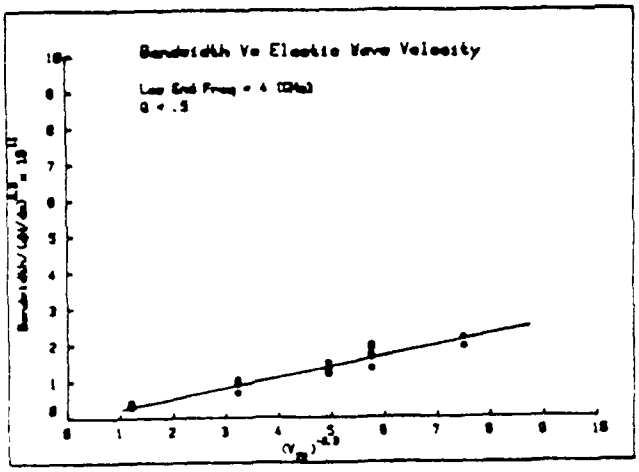

C. Bandwidth as a function of elastic wave velocity

Figure (5.11) - Bandwidth dependence on material constants

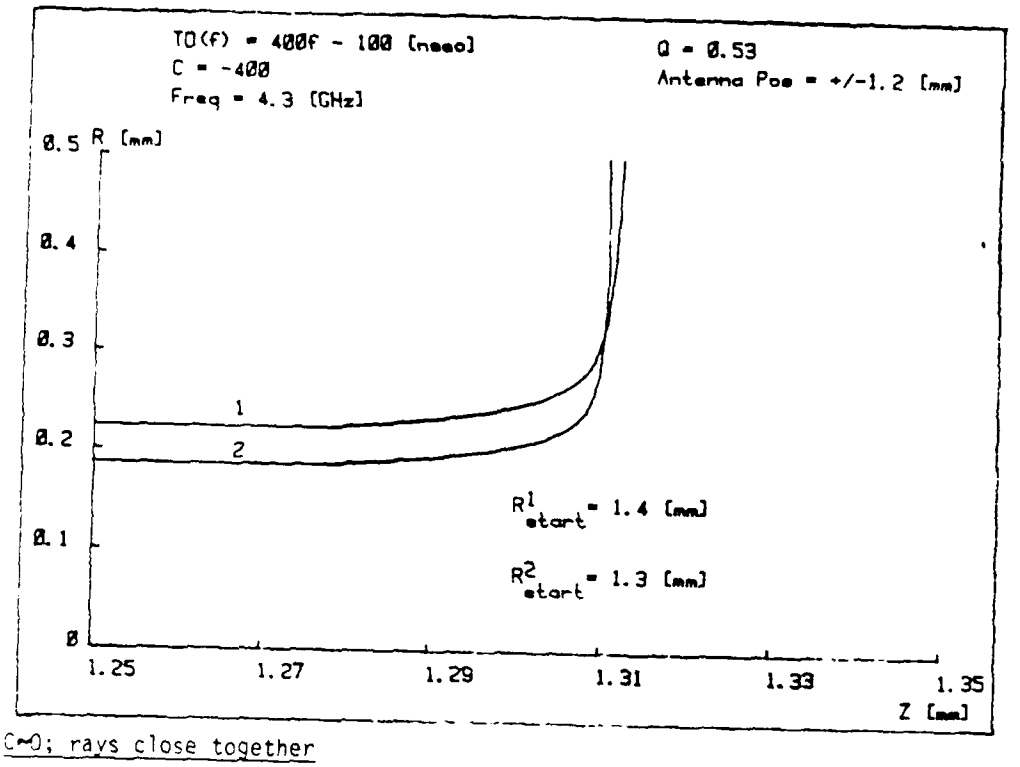

A. C~0; rays close together

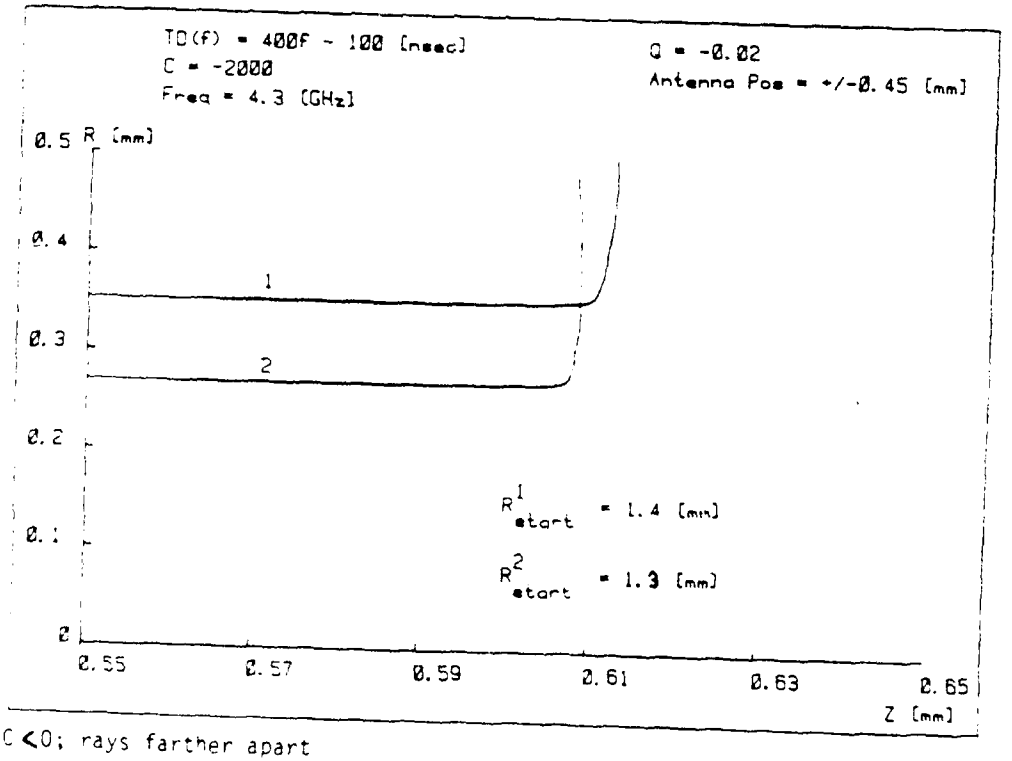

B. C<0; rays farther apart

Figure (5.12) - Ray tracing for power handling estimation

distances remain relatively constant past the turning point. Since the group velocity at the turning points is very small and similar for both sets of ray paths (~ 1 [m/sec]), dynamic range should be improved for the magnitude of C increasing. This is opposite to the results for bandwidth.

V.F Consequences of Field Asymmetry

The development of a comprehensive ray tracing program has allowed several other aspects of magnetoelastic delay line behavior to be explored. One issue of interest is the asymmetry between ray paths in the delay line. In defining the delay line, the magnetic and magnetization fields are defined as vectors whose axial components are directed in the +z direction. The results of Sections V.B-C, however, are only for rays injected at the antenna in +z half plane and whose axial component of the elastic wave velocity vector is negatively directed.

The absence of axial magnetic and magnetization field symmetry about $z = 0$ implies that ray paths will not be symmetric. Likewise, the Taylor series expansion of the on-axis magnetic and magnetization fields through the rod gives radial field components which are odd with respect to $z = 0$. These conditions cause differences in (a) the initial conditions of k_z and (b) the values of $\bar{k} \times \bar{M}$ and $\bar{k} \cdot \bar{M}$ in the different half-planes.

Comparing bandwidth ray tracing for rays starting at the +z and -z antennas under otherwise identical conditions shows that the behaviors are very similar, if not identical. Intuitively again, this is appealing since dk_z/dt and dk_r/dt are roughly symmetric about $z = 0$ and the change

in initial value of k_z is small compared to the magnitude of the total change. The changes in the vector products have minimal impact on both the group velocity and $d\bar{k}/dt$. This result has strong practical implications: the delay line can be used in either a forward or backward sense with respect to the direction of magnetic field. Choice of antenna terminal has no apparent effect.

V.G Comparison to Single-Ended Delay Line

Strauss type delay lines with a synthesized magnetic field can also be analyzed by the ray tracing program. In fact, the differences in computer analysis of the two-port "buried-antenna" and two-port, single-ended Strauss type lines are trivial; the latter merely fixes the antenna at $z = 0$ and requires elastic wave reflection at $z = 0$. The delay line built by Platzker and Morgenthaler [2] can be considered in this manner and good correlation with experimental results is found.

Ray tracing demonstrates that the two-port "buried-antenna" design provides an additional degree of freedom in design as well as substantially larger bandwidths. The degree of freedom results from being able to locate the antenna so that the local magnetic field is at the resonant frequency. In the Strauss type line, the antenna is fixed at $z = 0$, and T_0 and C cannot be set independently.

The lower bandwidths evidenced for the Strauss type delay line are a result of waves at frequencies near the bottom of the spin wave manifold not reaching a crossover point (Figure 5.13a). Absent this low frequency range effect, the bandwidths of the "buried-antenna" and Strauss type

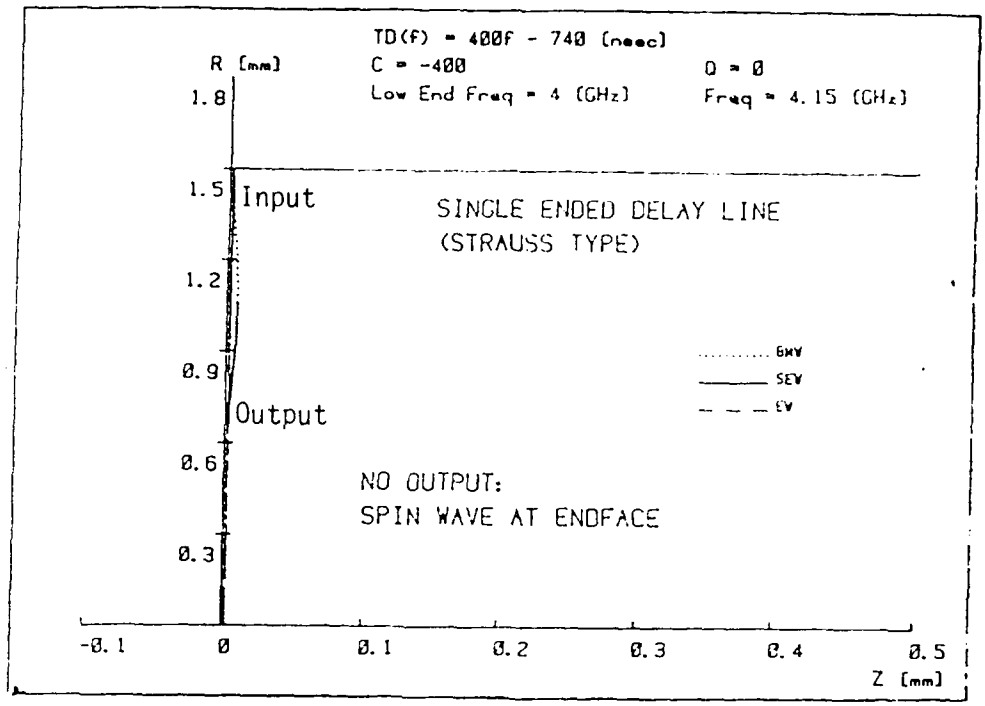

A. Strauss type delay line - ray does not reach crossover

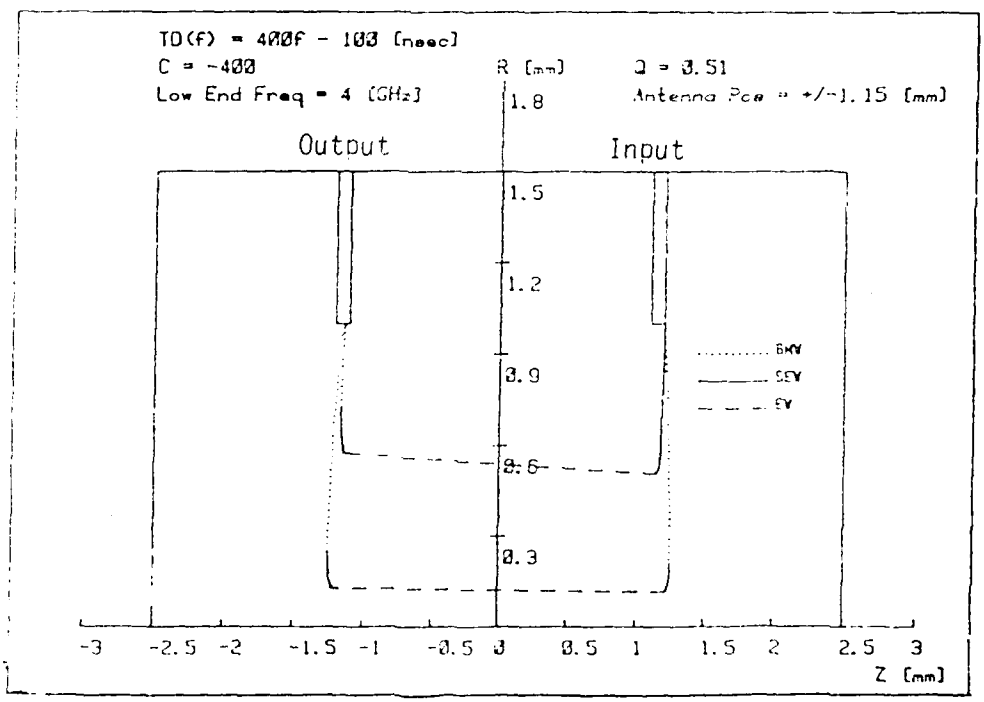

B. "Buried-antenna" delay line - ray proceeds directly from turning point

Figure (5.13) - Low-end frequency propagation

delay lines would be the same. As described in Section V.A, spin waves at or near the local resonant frequency in the two-port "buried-antenna" line are immediately at the turning point and propagate towards regions of lower magnetic field (Figure 5.13b). In the Strauss line, however, there is no region of lower magnetic field since the antenna is at z = 0. Waves at or near this frequency cannot reach a crossover point and simply return to the output antenna as a magnetostatic wave.

Analysis of the Strauss type delay line also suggests that rays which originate near the center of the endface are less likely to propagate than rays starting at greater radial distance. As with the two-port "buried-antenna" delay line, the radial velocity of a ray must reach zero before the ray collides with the z axis. Rays starting at greater radial distance have greater likeihood of reaching a turning point (Figures 5.14a and 5.14b). Rays returning from reflection, however, reach the endface at lesser radial distances (Figure 5.14b). This suggests that endface antenna designs should be optimized for maximum coupling at different radial distances.

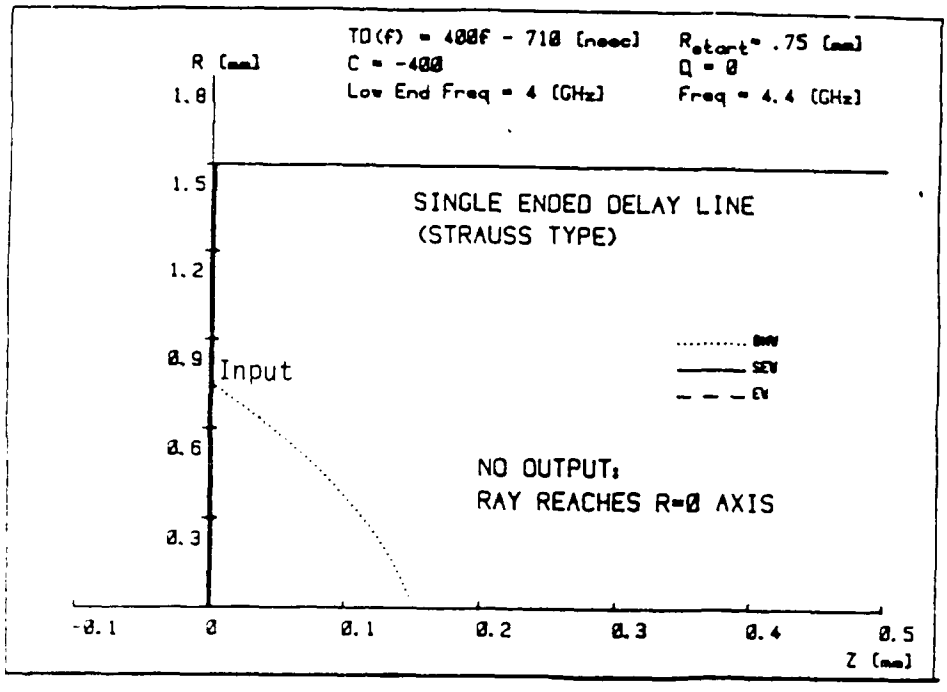

A. Ray start at radius/2

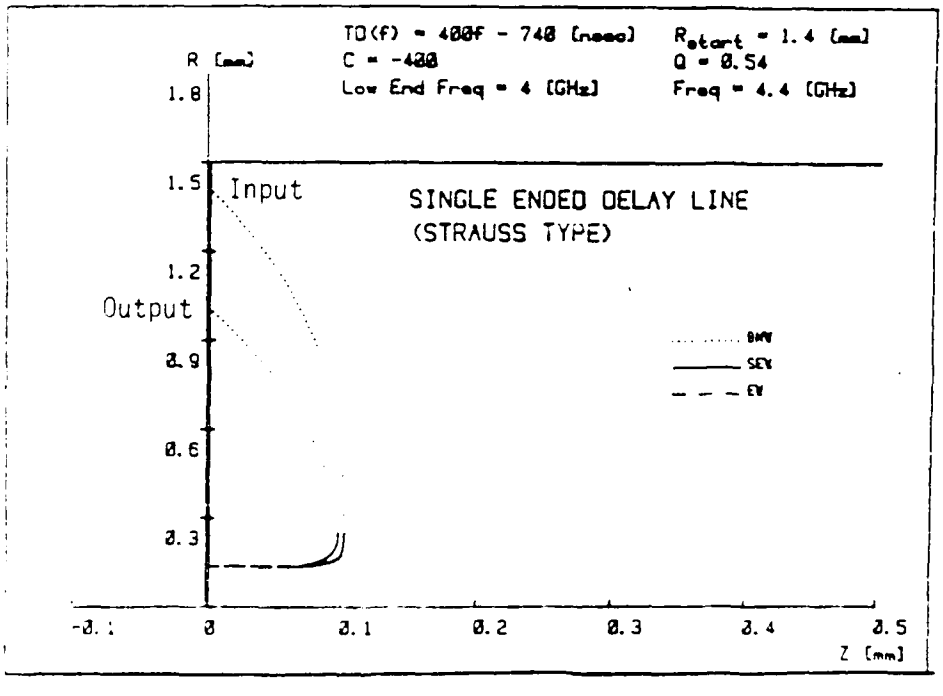

B. Ray start near radius

Figure (5.14) - Ray starting points in Strauss type delay line

Chapter VI

CONCLUSIONS AND RECOMMENDED FUTURE WORK

A ray tracing analysis of "buried-antenna" and, to a lesser extent, Strauss type linearly dispersive, two-port magnetoelastic delay lines has been performed. It has been found that either operating bandwidth or dynamic range can be maximized with respect to the choice of internal magnetic field profile. Also, differences in bandwidth performance between the types of delay line have been resolved and the "buried-antenna" design has been shown to be superior. Ray tracing results have been correlated with an experimental result from each type of delay line.

Delay line performance is typically characterized by a time-bandwidth product which delineates the trade-off between bandwidth and total delay time. Magnetoelastic delay lines, however, should be capable of large time-bandwidth products and, realistically, are not well characterized by this quantity. The bandwidth of magnetoelastic delay lines is apparently relatively insensitive to the frequency range of operation and, since delay times are directly proportional to frequency, design of delay lines with large time-bandwidth products should be possible. This should be especially true at high frequencies and for delay functions with low values of the dispersive delay rate, D.

Consequently, linearly dispersive magnetoelastic delay lines can now be designed with an a priori knowledge of the attainable bandwidth and time-bandwidth product, and the required magnetic field profile. As described in Chapter V, bandwidth is maximized for magnetic field profiles which cause the focusing parameter Q to be restricted to a limited range. For a given dispersive delay function, the value of Q

is determined by the magnetic field profile nonlinearity constant C, and a closed form expression for C as a function of Q is available. The selection of C in turn allows direct estimation of attainable bandwidth and, ultimately, time-bandwidth product.

Validation of the ray tracing approach comes from previous experimental work. In 1983 Borgeaud [3] constructed a "buried-antenna" delay line prior to the development of the described ray tracing tools. His selection of a nominal field profile constant was motivated by the simple requirement to demonstrate that nonlinear magnetic fields could produce linear dispersion. Subsequent bandwidth analysis of his experimental work (a) is validated for his experimental case and (b) shows that his choice of field profile constant was slightly off optimum. Earlier, Platzker [2] had built and tested a Strauss type delay line with synthesized magnetic field. He selected a linear field profile (C = 0), also without any *a priori* method of estimating bandwidth. His measured bandwidth matches ray tracing analysis, and a larger bandwidth could have been attained with a different value of C.

The differences in bandwidth performance between the "buried-antenna" and Strauss type delay lines can also be explained by ray tracing. The Strauss type delay line operates over a narrower band because low end frequencies cannot reach crossover points. This effect is apparently the sole factor in Strauss type lines exhibiting reduced bandwidths.

The continued analysis of magnetoelastic delay lines requires further correlation of ray tracing with experimental results. Although the validity of ray tracing in magnetoelastic media is well established, predictive properties should be based upon a variety of experimental

cases. Cases of special interest include very low values of D, the dispersive delay rate, for which extremely large bandwidths are expected; values of C close to zero; and values of C very large negative. Additionally, the bandwidth dependence on frequency range should be examined for X-band and above. The case of D very small is of special interest since previous work [31] has shown that a constant delay profile is when focusing. As discussed in Section III.E, a limit on D for Q > 0 can be defined; it therefore should be possible to design delay lines with relatively small fractional changes in dispersive delay time.

A desirable upgrade to the existing capability would be the ability to predict attenuation in the delay ine. The existing computer program contains an attenuation calculation subroutine (adapted from Addison et al. [23]). There are, however, very few experimental data to confirm the quality of the approximations.

Physical improvements to the "buried-antenna" magnetoelastic delay line construction are also desirable. These improvements would provide some form of shielding between the antenna wires to improve isolation. Also, adding a conducting sheath around the YIG crystal between the antenna holes would provide a "waveguide" in which electromagnetic radiation would experience cutoff. Antenna-antenna isolation would be improved with minimal effect on magnetoelastic wave propagation.

Appendix A

MAGNETOELASTIC WAVE THEORY

A.1 Complete Magnetic Spin Wave Theory and Dispersion Relations

Magnetic spin waves in ferrimagnetics are the result of the magnetization field and its incorporation into the constitutive relations. This magnetization field is induced by the precession of electron spin moments about an applied axis of magnetization. When a strong enough magnetic field is applied, all the magnetic moments precess around the same axis of static magnetization.

Maxwell's Equations (in MKS units) for a ferrimagnetic are those of a sourceless, materially isotropic medium:

$$\bar{\nabla} \cdot \bar{B} = 0 \tag{A.1}$$

$$\bar{\nabla} \cdot \bar{D} = 0 \tag{A.2}$$

$$\bar{\nabla} \times \bar{H} = \partial \bar{D}/\partial t \tag{A.3}$$

$$\bar{\nabla} \times \bar{E} = -\partial \bar{B}/\partial t \tag{A.4}$$

The constitutive relations vary from the isotropic case in that the precession of magnetic moments produces time varying magnetic fields each of which generates a torque on its respective magnetization vector. This introduces a time dependence into the constitutive relations (Figure 2.2):

$$\bar{B} = \mu_0(\bar{H} + \bar{M}) \tag{A.5}$$

$$\partial \bar{M}/\partial t = \gamma \mu_0(\bar{M} \times \bar{H}_{eff}) \tag{A.6}$$

$$\bar{H}_{eff} = \bar{H}_{ext} + \bar{h}_{rf} + \bar{H}_{EX} + \bar{H}_{A} + \bar{H}_{DEM} + \bar{h}_{damp} + \bar{h}_{me} \qquad (A.7)$$

$$\bar{H}_{EX} = \lambda_{ex} \nabla^2 \bar{M}$$

$$\bar{H}_{A} = -\frac{1}{\mu_0} \frac{\partial W_A}{\partial \bar{M}} \qquad W_A = \text{cubic anisotropy energy}$$

$$\bar{h}^{i}_{me} = -\frac{1}{\mu_0} b_{ijk} \frac{\partial \rho_j}{\partial x_k}$$

b_{ijk} = magnetoelastic coupling constant

ρ_j = elastic displacement

x_k = unit vector

$\bar{H}_{DEM} = \bar{\bar{N}}_d \cdot \bar{M}$ $\qquad \bar{\bar{N}}_d$ = demagnetizing tensor (geometry dependent)

$\bar{h}_{damp} = \frac{\alpha}{|M|} \bar{M} \times \frac{\partial \bar{M}}{\partial t}$ $\qquad \alpha$ = phenomenological damping constant

Equation A.6 defines the interaction between the internal magnetic field and the magnetization. $\bar{H}_{eff}$, the effective internal magnetic field, includes several terms which act to produce torques in the magnetization vector and can be modeled as effective magnetic fields:

(a) $\bar{H}_{ext}$ -- the applied, external static magnetic field;

(b) $\bar{h}_{rf}$ -- the time varying component of applied magnetic field;

(c) $\bar{h}_{damp}$ -- a phenomenological damping term which accounts for losses. This term is ignored in the further derivations as it can be accounted for with a straightforward addition of an imaginary wavevector component in the final dispersion relations;

(d) $\bar{H}_{EX}$ -- the quantum mechanical exchange force has no analog in classical physics. This force acts to align nearest neighbor spin moments and is required for ferro-, antiferro-, and ferrimagnetic behavior;

(e) $\bar{H}_{DEM}$ -- demagnetizing magnetic field caused by the occurrence of volume divergence and surface dipole magnetic terms in finite ferrite samples;

(f) $\bar{h}_{me}$ -- the magnetic field induced by the elastic strain of the lattice. This term can be treated as negligible, although it is the mechanism for coupling between spin and acoustic waves. The coupling will be introduced subsequently through a coupling of modes method;

(g) $\bar{H}_A$ -- the anisotropy field which depends upon the orientation of the external magnetic field with respect to the crystal lattice structure.

Morgenthaler has developed the full theory incorporating all these magnetoelastic terms [20].

Neglecting the smaller terms leaves the simplified constitutive relation:

$$\frac{d\bar{M}}{dt} = \mu_0 \gamma \left(\bar{M} \times (\bar{H}_{ext} + \bar{h}_{rf} + \bar{H}_{EX}) \right) \tag{A.8}$$

Assuming that (a) the DC components of the magnetization and magnetic fields are z-directed, and (b) the DC components are much larger than the time varying components:

$$\bar{M} = M_z \bar{z} + \bar{m} \qquad |\bar{M}| = M_z \tag{A.9}$$

$$\bar{H} = H_z \bar{z} + \bar{h} \qquad |\bar{H}| = H_z \qquad \bar{h} = \bar{h}_{rf} + \lambda_{ex} \nabla^2 \bar{m}$$

then substitution of the above into the constitutive relation yields the small signal constitutive relation which explicitly defines the relation between the time varying components of $\bar{M}$ and $\bar{H}$:

$$\frac{\partial \bar{m}}{\partial t} = \gamma\mu_0 \bar{z} \times (\omega_M \bar{h}_{rf} - \omega_z \bar{m} - \omega_M \lambda_{ex} \nabla^2 \bar{m}) \tag{A.10}$$

$$\omega_z = \gamma\mu_0 H_0 \qquad \omega_M = \gamma\mu_0 M_0$$

Assuming a slowly varying plane wave nature for the time varying components:

$$\bar{h} \approx \bar{h}_0 e^{j(\omega t - \bar{k}\cdot\bar{r})} \tag{A.11}$$

$$\bar{m} \approx \bar{m}_0 e^{j(\omega t - \bar{k}\cdot\bar{r})}$$

$$\bar{e} \approx \bar{e}_0 e^{j(\omega t - \bar{k}\cdot\bar{r})}$$

$$\bar{b} \approx \bar{b}_0 e^{j(\omega t - \bar{k}\cdot\bar{r})}$$

and equating the differential operators with their equivalents:

$$\bar{\nabla} \leftrightarrow -j\bar{k} \tag{A.12}$$

$$\frac{\partial}{\partial t} \leftrightarrow j\omega$$

then the tensor relation between the small signal magnetization and the local magnetic field can be defined. The coefficient matrix $\bar{\bar{x}}$ is the Polder Tensor.

$$\bar{m} = \bar{\bar{x}}\cdot\bar{h} \tag{A.13}$$

$$\bar{\bar{x}} = \begin{pmatrix} \dfrac{\omega_z \omega_M}{\omega_z^2 - \omega^2} & j\dfrac{\omega\omega_M}{\omega_z^2 - \omega^2} \\ -j\dfrac{\omega\omega_M}{\omega_z^2 - \omega^2} & \dfrac{\omega_z\omega_M}{\omega_z^2 - \omega^2} \end{pmatrix}$$

The small signal magnetic flux is:

$$\bar{b} = \mu_0(\bar{h} + \bar{m}) = \bar{\bar{\mu}} \cdot \bar{h} \qquad (A.14)$$

$$\bar{\bar{\mu}} = \mu_0(\bar{\bar{x}} + \bar{\bar{I}})$$

Since the relation defines the extent of an induced magnetization as a function of applied field, the Polder Tensor terms are susceptibilities.

Applying the plane wave approximation to Maxwell's Equations in the ferrimagnetic yields:

$$-j\bar{k} \cdot \epsilon\bar{e} = 0 \qquad (A.15)$$

$$-j\bar{k} \cdot \bar{b} = 0 \qquad (A.16)$$

$$-j\bar{k} \times \bar{h} = j\omega\epsilon\bar{e} \qquad (A.17)$$

$$-j\bar{k} \times \bar{e} = -j\omega b \qquad (A.18)$$

The RF magnetic and electric fields can be defined as a function of the small signal magnetization field:

$$\bar{h} = \frac{-\bar{k}(\bar{k} \cdot \bar{m}) + k_0^2\bar{m}}{k^2 - k_0^2} \qquad (A.19)$$

and:

$$\bar{e} = \frac{-k_0^2(\bar{k} \times \bar{m})}{k^2 - k_0^2} \frac{1}{\omega\epsilon} \tag{A.20}$$

and substitution of A.19 into A.10 yields a complete magnetic spin wave dispersion relation (Figure A.1):

$$k = k_0\left[\frac{(\mu^2-\mu-\kappa^2)\sin^2(\theta)+2\mu \pm \{(\mu^2-\mu-\kappa^2)\sin^4(\theta)+4\kappa^2\cos^2(\theta)\}^{1/2}}{2[(\mu-1)\sin(\theta)+1]}\right]^{1/2} \tag{A.21}$$

$$\mu = 1 + \frac{\omega_z\omega_M}{\omega_z^2 - \omega^2} \qquad \sin(\theta) = \frac{|\bar{k} \times \bar{M}|}{|\bar{k}||\bar{M}|} \qquad k_0 = \omega(\mu_0\epsilon)^{1/2}$$

$$\kappa = \frac{\omega\omega_M}{\omega_z^2 - \omega^2} \qquad \cos(\theta) = \frac{|\bar{k}\cdot\bar{M}|}{|\bar{k}||\bar{M}|}$$

The dispersion relation provides for an ordinary wave with "EM-like" characteristics and an extraordinary wave which is the magnetic spin wave. The extraordinary wave is right-hand elliptically polarized.

A.2 The Magnetostatic Approximation

From Equations A.19 and A.20, for the case $|\bar{k}| >> k_0$, the magnetic and electric fields are approximately:

$$\bar{h} \approx \frac{-\bar{k}(\bar{k}\cdot\bar{m}) + k_0^2\bar{m}}{k^2} \tag{A.22}$$

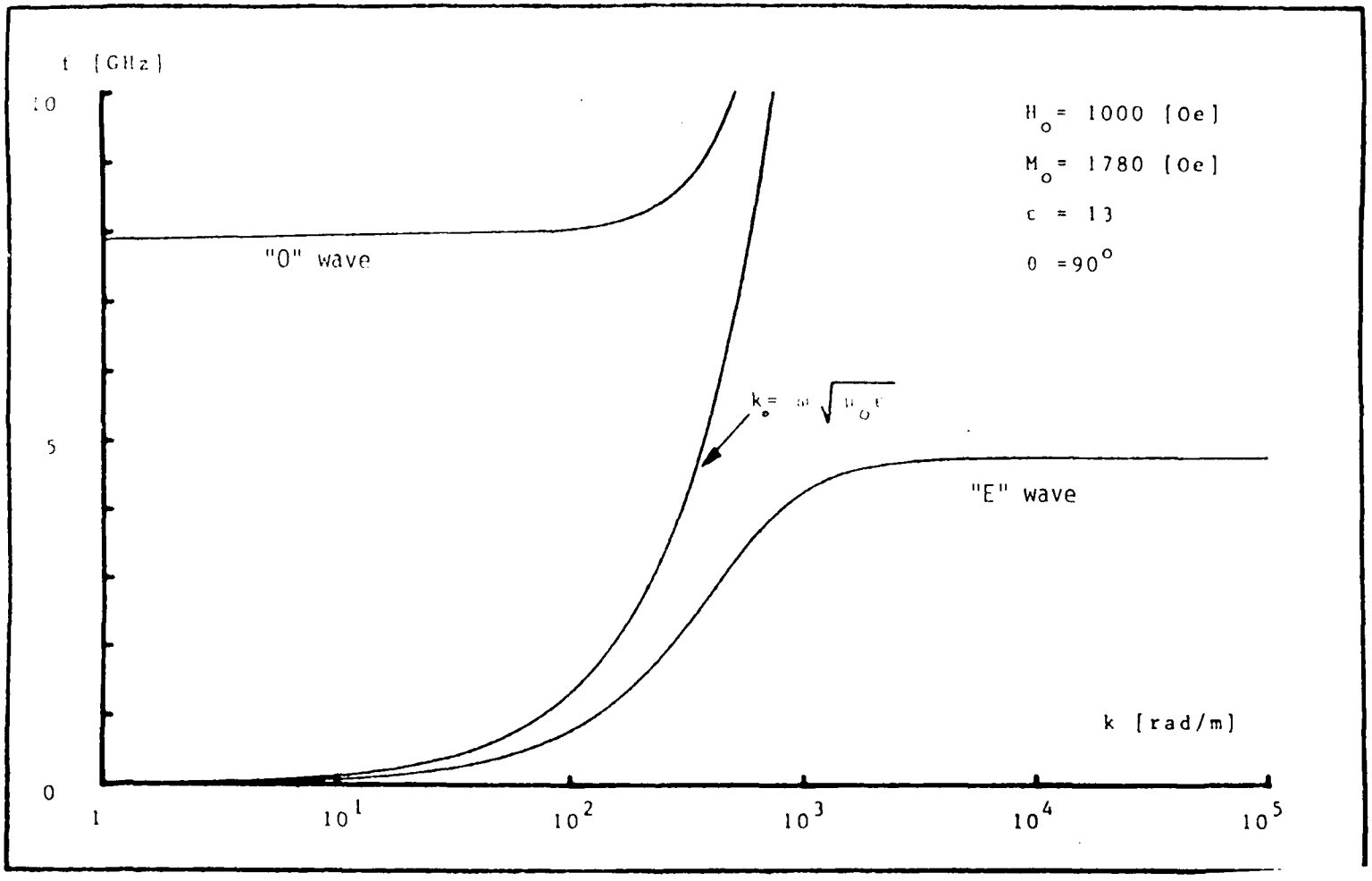

Figure (A.1) - Magnetic spin wave dispersion relation

and:

$$\bar{e} \approx \frac{-k_0^2(\bar{k} \times \bar{m})}{k^2} \frac{1}{\omega\epsilon} \tag{A.23}$$

The electric field is proportional to 1/k and, as $|\bar{k}|$ becomes very large, a magnetostatic approximation can be made:

$$\bar{e} \approx 0 \tag{A.24}$$

$$\bar{\nabla} \times \bar{h} \approx 0 \tag{A.25}$$

The magnetic field can be modeled as the gradient of a scalar magnetic potential field and a simplified approximation to h_{rf} thus becomes available:

$$\bar{h} = -\nabla\psi \tag{A.26}$$

$$\psi = \frac{j\bar{k}\cdot\bar{m}}{k^2} \tag{A.27}$$

$$\bar{h} = \frac{-(\bar{k}\cdot\bar{m})\bar{k}}{k^2} \tag{A.28}$$

Substituting Equation A.28 into Equation A.10 produces an equation which is homogenous in $\bar{m}$ and whose secular determinant gives the dispersion relation for an infinte ferrite under the magnetostatic approximation:

$$\omega^2 = (\omega_z + \omega_M\lambda_{ex}k^2)\left(\omega_z + \omega_M\lambda_{ex}k^2 + \omega_M\sin^2(\theta)\right) \tag{A.29}$$

$$\sin^2(\theta) = \frac{|\bar{k} \times \bar{M}|^2}{|\bar{k}|^2 |\bar{M}|^2}$$

A.3 Elastic Waves in YIG

The existence and propagation of elastic waves in isotropic YIG are governed by Newton's force law:

$$D_0 \frac{\partial^2 \bar{\xi}}{\partial t^2} = C_{44} \nabla^2 \bar{\xi} + (C_{12} + C_{44}) \nabla (\bar{\nabla} \cdot \bar{\xi}) \qquad (A.30)$$

$\bar{\xi}$ = elastic vector displacement

D_0 = density

C_{12}, C_{44} = Lamé constants

Equation A.30 can be simplified by noting that (a) the YIG crystal is a [100] crystal, and (b) coupling between longitudinal elastic and magnetic spin waves along crystal axes is negligible. The force law equation can be simplified to a simple second order differential equation and, assuming coupling to a transverse plane elastic wave [32]:

$$\bar{\xi} = \bar{\xi}_0 e^{j(\omega t - \bar{k} \cdot \bar{r})} \qquad (A.31)$$

$$\omega = \sqrt{\frac{C_{44}}{D_0}} \cdot k \qquad (A.32)$$

A.4 Magnetic Spin Wave and Elastic Wave Interconversion

Having separately derived the equations for the magnetic spin wave and elastic wave systems, the coupling of modes approach can be used to

define their interaction. This treatment is equivalent to including an $\bar{h}_{me}$ term in Equation A.5. The complete approach has been extensively developed and yields the approximate dispersion relation [7]:

$$(\omega - \omega_{sw})^2(\omega - \omega_{ew})^2 = \frac{1}{4} b^2 \tag{A.33}$$

Conversion between spin and elastic waves occurs when:

$$\omega \approx \frac{k}{v_{ew}} \qquad v_{ew} = \text{elastic wave velocity} \tag{A.34}$$

Although the splitting term b^2 is proportional to frequency, it is generally of an order of 10^7 Hz at room temperature, typically less than 1% of the unperturbed frequency value. The dispersion relation is shown in Figures 2.8 and 2.9.

The efficiency of coupling is determined by the ratio of local magnetic field slope to a critical value [20]:

$$\eta = 1 - e^{-(H'_{crit}/H')} \tag{A.35}$$

As pointed out by Wadsworth [33], this condition is easily met and is not a good design criterion.

Appendix B

MAGNETIC FIELD REQUIRED FOR LINEAR DISPERSION

The time spent by magnetoelastic waves propagating through the delay line can be accounted for by two wave behaviors: (a) spin exchange wave and (b) elastic wave. Transitions between wave types are assumed to occupy negligible time. The backward magnetostatic wave contribution to total propagation time is also neglected because the wave has very high group velocity.

$$TD(f) = T_{sew} + T_{ew} \tag{B.1}$$

The time spent as an elastic wave which has fixed velocity is:

$$T_{ew} = \frac{2 \cdot z_{cp}}{v_{ew}} \tag{B.2}$$

The group velocity of the spin exchange wave is a function of position since the magnetic field is inhomogenous. The time spent as a spin exchange wave is calculated as follows:

$$T_{sew} = 2 \int_{z_{tp}}^{z_{cp}} \frac{dz}{v_g} \tag{B.3}$$

Differentiating the approximate spin exchange wave dispersion relation of Equation 2.22 gives:

$$-2\omega_M \lambda_{ex} k_z \cdot dk_z = \gamma \mu_0 H'(z) dz \tag{B.4}$$

and, for a spin exchange wave, the axial group velocity is (Equation 2.23):

$$v_z = \omega_M \lambda_{ex} k_z \tag{B.5}$$

Substituting Equations B.4 and B.5 into Equation B.3 gives a solvable integral in the variable k_z instead of z:

$$T_{sew} = 2 \int_{k_{tp}}^{k_{cp}} \frac{dk_z}{\gamma \mu_0 H'(z)} = \frac{2[k_{cp} - k_{tp}]}{\gamma \mu_0 H'(z)} \approx \frac{2k_{cp}}{\gamma \mu_0 H'(z)} \tag{B.6}$$

For $|k_{cp}| >> |k_{tp}|$ and, from Equation 2.28, the spin wave propagation time can be estimated:

$$T_{sew} \approx \frac{2}{v_{ew}} \frac{\omega}{H'(z_{cp})} \tag{B.7}$$

The magnetic field at the crossover point can be explicitly calculated from Equations 2.22 and 2.27:

$$H(z_{cp}) = \frac{1}{\gamma \mu_0} \left[\omega - \omega_M \lambda_{ex} \left(\frac{\omega}{v_{ew}}\right)^2 \right] \tag{B.8}$$

The second term represents a very small contribution to the field strength at crossover (~1%) and can be neglected (as done in Equation 3.5). The field strength at crossover can therefore be considered to be proportional to frequency and the total time spent is:

$$\omega \approx \gamma \mu_0 H(z_{cp}) \tag{B.9}$$

$$T_{sew} \approx \frac{2}{v_{ew}} \left[\frac{H(z_{cp})}{H'(z_{cp})} \right] \tag{B.10}$$

From Equation B.9, the spatial derivative of H_z (z_{cp}) can be thought of as proportional to a spatial derivative of f, and substituting into Equation B.10 with Equations B.1 and B.2 gives an exact differential:

$$\frac{df}{dz} \propto H'(z_{cp}) \tag{B.11}$$

$$TD(f) = \frac{2}{v_{ew}} \left[z_{cp} + f \cdot \frac{dz_{cp}}{df} \right] = \frac{2}{v_{ew}} \frac{d}{df} [z_{cp} f] \tag{B.12}$$

Equating this function of frequency to the desired linear delay function in Equation 3.1 and integrating gives:

$$\int (Df + T_0)df = \frac{2}{v_{ew}} \int \frac{d}{df} [z_{cp} f]df \tag{B.13}$$

$$\frac{Df^2}{2} + T_0 f + C = (z_{cp} \cdot f) \frac{2}{v_{ew}} \tag{B.14}$$

$$z_{cp} = \frac{v_{ew}}{2} \left[\frac{Df}{2} + T_0 + \frac{C}{f} \right] \tag{B.15}$$

It is apparent that appropriately locating the crossover point z_{cp} as a function of frequency allows the linear dispersion to be obtained. The field strength at crossover is directly proportional to frequency (Equation B.9) and a straightforward substitution into Equation B.15 can be made:

$$z_{cp} = \frac{v_{ew}}{2}\left[\frac{D\,\frac{\gamma\mu_0}{2\pi}\,H(z_{cp})}{2} + T_0 + \frac{C}{\frac{\gamma\mu_0}{2\pi}\,H(z_{cp})}\right] \tag{B.16}$$

Rearranging Equation B.16 and solving the quadratic for $H(z=z_{cp})$ yields an expression for the magnetic field strength required for the linear delay:

$$H(z_{cp}) = \frac{(2z_{cp} - v_{ew}T_0) \pm \sqrt{(2z_{cp} - v_{ew}T_0)^2 - 2v_{ew}^2DC}}{\frac{\gamma\mu_0}{2\pi}\,v_{ew}D} \tag{B.17}$$

Generalizing z_{cp} to cover all values along the z-axis completes the derivation of the required one-dimensional magnetic field.

$$H(z) = \frac{(2z - v_{ew}T_0) \pm \sqrt{(2z - v_{ew}T_0)^2 - 2v_{ew}^2DC}}{\frac{\gamma\mu_0}{2\pi}\,v_{ew}D} \tag{B.18}$$

The fixed delay, T_0, must be negative for the magnetic field to be positive everywhere in the rod. A change of sign in the magnetic field implies that domains might form.

The magnetic field prescribed above is for $z > 0$, where $z = 0$ is the midpoint of the rod. Replacing z with $|z|$ gives a function which is symmetric in z but has discontinuous derivatives at $z = 0$. Since continuity in $H(r,z)$ and its derivatives inside the rod is required by Maxwell's Equations, an approximation near $z = 0$ is required. A

simple solution is to substitute a polynomial for $H(0,z)$ for $|z| < z_0$. Continuity is assured by matching the polynomial and its derivatives with $H(0,z)$ and its derivatives at $z = z_0$.

Appendix C

MAGNETIC FIELD FOR A YIG ROD

C.1 Magnetic Field in a YIG Rod

Ray tracing in the magnetoelastic delay line requires knowledge of the static magnetic field everywhere within the YIG rod. Morgenthaler has devised a method for estimating this magnetic field by expanding the specified on-axis field subject to certain constraints [1].

Maxwell's equations for static fields inside a ferrimagnetic yield the following constraints:

$$\bar{M} \times \bar{H} = 0 \tag{C.1}$$

$$\bar{M} \cdot \bar{H} > 0 \tag{C.2}$$

$$|\bar{M}| = M_0 \tag{C.3}$$

$$\bar{\nabla} \times \bar{H} = 0 \tag{C.4}$$

$$\bar{\nabla} \cdot \bar{B} = 0 \tag{C.5}$$

Since $\bar{\nabla} \times \bar{H}$ is zero, both $\bar{H}$ and $\bar{M}$ can be expressed as the gradient of a scalar field:

$$\bar{H} = -\nabla\psi \tag{C.6}$$

$$\bar{M} = \frac{-\nabla\psi}{|\nabla\psi|} M_0 \tag{C.7}$$

The scalar field can be expanded as a series:

$$-\psi = \sum_{n=0}^{\infty} a_{2n}(z)r^{2n} \tag{C.8}$$

Although $\bar{H}$ and $\bar{M}$ could be expanded in terms of the same coefficients, they can also be expressed as follows:

$$\bar{H}(r,z) = \bar{z} \sum_{n=0}^{\infty} a'_{2n}(z)r^{2n} + \bar{r} \sum_{n=0}^{\infty} 2(n+1)a_{2n+1}(z)r^{2n+1} \tag{C.9}$$

$$\bar{M}(r,z) = M_0 \left[\bar{z} \sum_{n=0}^{\infty} b_{2n}(z)r^{2n} + \bar{r} \sum_{n=0}^{\infty} b_{2n+1}(z)r^{2n+1} \right] \tag{C.10}$$

The coefficients a_n and b_n are functions of z and can be determined by the following expressions:

$$b_1(z) = \frac{-\frac{1}{2} a''_0(z)}{a'_1(z) + M_0} \tag{C.11}$$

$$a_2(z) = \frac{1}{2} b_1(z)a'_0(z) \tag{C.12}$$

$$b_2(z) = -\frac{1}{2} b_1^2(z) \tag{C.13}$$

$$b_{2s+1} = \frac{\frac{-1}{2(s+1)}(a''_{2s}+M_0 b'_{2s}) + \sum_{k=1}^{s} [2(s-k+1)a_{2(s-k+1)}b_{2k} - a'_{2k}b_{2(s-k)+1}]}{a'_0 + M_0} \tag{C.14}$$

$$a_{2(s+1)} = \frac{a'_0 b_{2s+1} - \sum_{k=1}^{s} [2(s-k+1)a_{2(s-k+1)}b_{2k} - a'_{2k}b_{2(s-k)+1}]}{2(s+1)} \tag{C.15}$$

$$b_{2(s+1)} = -\left[\sum_{k=1}^{s} b_k b_{2s-k+2} + \frac{1}{2} b_{s+1}^2 \right] \tag{C.16}$$

The solution is implemented by invoking:

$$b_0 = 1 \tag{C.17}$$

$$a_0'(z) = H(z) \tag{C.18}$$

$$a_0''(z) = H'(z)$$

$$\vdots$$

$$\frac{d^{n}\left(a_0(z)\right)}{dz^{n}} = \frac{d^{n-1}H(z)}{dz^{u-1}} \tag{C.19}$$

$$a_0(z) = \int H(z)dz \tag{C.20}$$

C.2 External Potential Field

C.2.A Outer Field Expansion

Morgenthaler's method for synthesizing a desired magnetic field in a rod or disc requires the calculation of equipotential surfaces outside the rod [1]. Once the magnetic field expansion for the interior of the rod is known, an expression for a scalar potential field outside the rod can also be found. From this scalar potential, the required equipotentials can be found.

The magnetic scalar potential field outside the rod must be a solution to the Laplacian in cylindrical coordinates:

$$\nabla^2\psi_{ext} = 0 \tag{C.21}$$

The conventional selection of Bessel functions, however, becomes difficult to solve. Alternatively, the potential field can be expanded:

$$-\psi_{ext} = \sum_{n=0}^{N} c_n P_n^*(r,z) + \sum_{n=0}^{n-1} C_n' Q_n^*(r,z) \tag{C.22}$$

and, with solutions using $a_0(z) = z^n$, a linear sum of mixed polynomials each of which is a solution to the Laplacian can be derived:

$$P_0^* = 1 \tag{C.23}$$

$$P_1^* = z$$

$$P_2^* = z^2 - \frac{1}{2} r^2$$

$$P_3^* = z^3 - \frac{3}{2} zr^2$$

$$P_4^* = z^4 - 3z^2r^2 + \frac{3}{8} r^4$$

These polynomials resemble the Legendre polynomials. A second set of polynomials is also included:

$$Q_0^* = \ln(r) + 1 \tag{C.24}$$

$$Q_1^* = z \ln(r) + 1$$

$$Q_2^* = z^2 \ln(r) - \frac{1}{2} r^2 \ln(r) + z^2$$

$$Q_3^* = z^3 \ln(r) - \frac{3}{2} zr^2 \ln(r) + z^3$$

$$Q_4^* = z^4 \ln(r) - 3z^2r^2 \ln(r) + \frac{3}{8} r^4 \ln(r) + z^4 - \frac{3}{16} r^4$$

Recursion relations which explicitly define these functions are described by Morgenthaler [1].

C.2.B Boundary Conditions

The coefficients in the outer field expansion are found by solving the boundary conditions at the rod's cylindrical surface. The boundary conditions for magnetic fields are continuity of (a) tangential $\bar{H}$ and (b) normal $\bar{B}$. The outer field potential can then be expressed directly as a function of the inner field.

In order to simplify the calculation, the internal tangential $\bar{H}$ and normal $\bar{B}$ fields are approximated by polynomials in z at the surface. The conversion from the nonlinear expansion inside the rod to a polynomial at the inner surface of the rod uses an integral mean square error minimization:

$$H_z^{int}(R,z) = \sum_{n=0}^{N} \alpha_n \left(\frac{z}{L}\right)^n \qquad B_R^{int}(R,z) = \sum_{n=0}^{N} \beta_n \left(\frac{z}{L}\right)^n \tag{C.25}$$

$$E = \int_{-length/2}^{length/2} \left(H_z^{int}(R,z) - \sum_{n=0}^{N} \alpha_n \left(\frac{z}{L}\right)^n \right)^2 dz + \int_{-length/2}^{length/2} \left(B_R^{int}(R,z) - \sum_{n=0}^{N} \beta_n \left(\frac{z}{L}\right)^n \right)^2 dz \tag{C.26}$$

$$B_R^{int}(R,z) = H_R^{int}(R,z) + M_R^{int}(R,z)$$

R = rod radius

Minimizing the error with respect to each set of the polynomial coefficients gives N linear equations of the form:

$$0 = \frac{\partial E}{\partial \alpha_i} = \int_{-length/2}^{length/2} 2 \left(H_z^{int}(R,z)\left(\frac{z}{L}\right)^i - \left(\frac{z}{L}\right)^i \sum_{n=0}^{N} \alpha_n \left(\frac{z}{L}\right)^n \right) dz \tag{C.27}$$

The first term in each integral is solved by normalizing the length to [-1,1] and applying a Gauss-Legendre series approximation:

$$\int_{-1}^{1} f(u)du \sim \sum_{i=0}^{N} f(u_i)w_i \tag{C.28}$$

u_i = zeroes of Gauss-Legendre function of order N

w_i = weights of Gauss-Legendre function of order N

The second term is directly integrable:

$$\int_{-length/2}^{length/2} \sum_{n=0}^{N} \alpha_n \left(\frac{z}{L}\right)^{n+i} dz = \sum_{n=0}^{N} \frac{\alpha_n L}{n+i+1} \left(\frac{z}{L}\right)^{n+i+1} \Bigg|_{-length/2}^{length/2} \tag{C.29}$$

$$\int_{-length/2}^{length/2} \sum_{n=0}^{N} \beta_n \left(\frac{z}{L}\right)^{n+i} dz = \sum_{n=0}^{N} \frac{\beta_n L}{n+i+1} \left(\frac{z}{L}\right)^{n+i+1} \Bigg|_{-length/2}^{length/2}$$

$$= \sum_{n=0}^{N} \begin{cases} \frac{2\beta_n L}{n+i+1} \left(\frac{1}{2}\right)^{n+i+1} & n+i+1 \text{ odd} \\ 0 & n+i+1 \text{ even} \end{cases}$$

The coefficients α_i and β_i are found by equating the two expressions and solving two systems of N linear equations. This approximation to the internal field at the surface is readily found by computer.

Calculation of the external field requires fulfilling the boundary conditions at the rod radius:

$$\psi^{int}(R,z) = \psi^{ext}(R,z) \Leftrightarrow H_z^{int}(R,z) = H_z^{ext}(R,z) \tag{C.30}$$

$$B_R^{int}(R,z) = B_R^{ext}(R,z) \tag{C.31}$$

The mean square error at the boundary can be expressed as:

$$E = \left(\psi^{int} - \sum_{j=1}^{N} C_j f_j \right)^2 + \left[\left(1 + \frac{M_0}{|\nabla \psi^{int}|} \right) \frac{\partial \psi^{int}}{\partial r} - \sum_{j=1}^{N} C_j \frac{\partial f_j}{\partial r} \right]^2 \tag{C.32}$$

$$\frac{\partial E}{\partial C_i} = 0$$

With the inner field defined as a polynomial in z, the least squares method can be applied. An error expression is formed and differentiated with respect to each of the outer field coefficients (with equal weighting of the boundary conditions in the error expression). Morgenthaler and Platzker demonstrated the closed form solution for the outer field coefficients [2]:

$$C_p = \frac{\alpha_{p-1}}{pL^{p-1}} - (\ln(R) + 1)C'_p$$

$$- \sum_{k=1}^{N-p} R^{2k} A_{p+2k,k}[C_{p+2k} + (\ln(R) + \phi_k)C'_{p+2k}] \qquad (C.33)$$

$$C'_p = \frac{R\beta_p}{L^p} - \sum_{k=1}^{N-p} R^{2k} A_{p+2k,k}\{2k[C_{p+2k} + (\ln(R) + \phi_k)C'_{p+2k}] + C'_{p+2k}\} \qquad (C.34)$$

$$C'_N = 0$$

$$A_{n,k} = (-1)^k \frac{n!\ 4^{-k}}{(n - 2k)!\ (k!)^2} \qquad (C.35)$$

$$\phi_k = \begin{cases} 1 & k = 0 \\ 1 - \sum_{i=1}^{k} \frac{1}{i} & k > 0 \end{cases} \qquad (C.36)$$

The procedure involves assuming that $C'_N = 0$, and subsequently finding C_n, C_{n-1}, C'_{n-2}, C_{n-2}, ... , C'_0. Once these coefficients have been found, the external potential field and its gradient, the magnetic field, are defined.

Wadsworth has noted an interesting correlation between external field and delay function [33]. He found that the coefficients for delay function 1000 f - 200 were approximately twice those of the delay function 500 f - 200. Doubling the external field coefficients corresponds roughly to doubling the energizing field.

BIBLIOGRAPHY

[1] Morgenthaler, F.R., "The Synthesis of Cylindrically Symmetric Static Magnetic Fields in a Locally Saturated Ferromagnet," AIP Conference Proceedings No. 24, Magnetism and Magnetic Materials, pp. 503-504, 1974.

[2] Morgenthaler, F.R., and Platzker, A., "Magnetic Field Synthesis Procedures for Magnetostatic and Magnetoelastic Devices," Proceedings of the 1978 International Symposium on Circuits and Systems, New York, pp. 574-581, May 17-19, 1978.

[3] Borgeaud, M., "An Improved Two-Port Magnetoelastic Delay Line," Technical Report 47 (S.M. Thesis), Microwave and Quantum Mechanics Group, Massachusetts Institute of Technology, January 1984.

[4] Schlömann, E., Advances in Quantum Mechanics, Columbia University Press, New York, p. 437, 1961.

[5] Eshbach, J.R., "Spin Wave Propagation and the Magnetoelastic Interaction in Yttrium Iron Garnet," Journal of Applied Physics, Vol. 34, No. 4, Part 2, pp. 1298-1304, April 1962.

[6] Schlömann, E., Joseph, R.I., and Kohane, T., "Generation of Spin Waves in Nonuniform Magnetic Fields, with Application to Magnetic Delay Lines," Proceedings of the IEEE, Vol. 53, No. 10, pp. 1495-1507, October 1965.

[7] Strauss, W., "Elastic and Magnetoelastic Waves in Yttrium Iron Garnet," Proceedings of the IEEE, Vol. 53, No. 10, pp. 1485-1495, October 1965.

[8] Auld, B.A., and Strauss, W., "Internal Magnetic Field Analysis and Synthesis for Prescribed Magnetoelastic Delay Characteristics," Journal of Applied Physics, Vol. 37, No. 3, pp. 983-987, March 1966.

[9] Bierig, R.W., Joseph, R.I., and Schlömann, E., "Magnetoelastic Propagation in YIG Rods Surrounded by Magnetic Sleeves," IEEE Transactions Sonics and Ultrasonics, Vol. SU-13, pp. 82-84, August 1966.

[10] Dotsch, H., "Magnetoelastic Delay Lines with Linear Dispersion," Journal of Applied Physics, Vol. 43, No. 4, pp. 1923-1927, April 1972.

[11] Itano, L., "Microwave Delay Line with Thin Film Antennas," Technical Report 43 (S.M. Thesis), Microwave and Quantum Mechanics Group, Massachusetts Institute of Technology, August 1981.

[12] Collins, J.H., and Webb, D.C., "Magnetoelastic Delay Line Employing YIG-YAG-YIG Configuration," Proceedings of the IEEE (Letters), Vol. 55, pp. 1492-1493, August 1967.

[13] Lax, B., and Button, R.J., Microwave Ferrites and Ferrimagnetics, McGraw-Hill Book Company Inc., New York, 1962.

[14] Sodha, M.S., Microwave Propagation in Ferrimagnetics, Plenum Press, New York, 1981.

[15] Kedzie, R.W., "Magnetostatic Mode Propagation in Axially Magnetized YIG Rod Containing a Turning Point," Journal of Applied Physics, Vol. 39, No. 6, pp. 2731-2734, May 1968.

[16] Kittel, C., and Fletcher, P.C., "Considerations on the Generation and Propagation of Magnetostatic Waves and Spin Waves," Physical Review, Vol. 120, No. 6, pp. 2004-2006, December 1960.

[17] Kales, M.L., "Modes in Wave Guides Containing Ferrites," Journal of Applied Physics, Vol. 24, No. 5, pp. 604-608, May 1953.

[18] Damon, R.W., and Van de Vaart, H., "Propagation of Magnetostatic Spin Waves at Microwave Frequencies in a Normally Magnetized Disk," Journal of Applied Physics, Vol. 36, No. 11, pp. 3453-3458, November 1965.

[19] Schlömann, E., Joseph, R.I., and Kohane, T., "Generation of Spin Waves in Nonuniform Magnetic Fields. I. Conversion of Electromagnetic Power into Spin Wave Power and Vice Versa," Journal of Applied Physics, Vol. 35, No. 1, pp. 159-166, January 1964.

[20] Morgenthaler, F.R., "Dynamic Magnetoelastic Coupling in Ferromagnets and Antiferromagnets," IEEE Transactions on Magnetics, Vol. MAG-8, No. 1, pp. 130-151, March 1972.

[21] Morgenthaler, F.R., "Waves in Ferrites," Course Material (Unpublished), Department of Electrical Engineering, Massachusetts Institute of Technology, 1967.

[22] Doane, J.L., "Reflection and Transmission Coefficients in Multi-Wave Inhomogenous Media," Technical Report 29 (Ph.D. Thesis), Microwave and Quantum Mechanics Group, Massachusetts Institute of Technology, June 1970.

[23] Addison, R.C., Auld, B.A., and Collins, J.H., "Ray Theory Analysis of Magnetoelastic Delay Lines," Journal of Applied Physics, Vol. 39, No. 3, pp. 1828-1839, February 1968.

[24] Morgenthaler, F.R., "Magnetostatic Spin Wave Focusing and Defocusing in Cylindrically Symmetric Non-Laplacian Magnetic Fields," IEEE Transactions on Magnetics, Vol. MAG-8, No. 3, pp. 550-551, September 1972.

[25] Deschamps, G.A., "Ray Techniques in Electromagnetics," Proceedings of the IEEE, Vol. 60, No. 9, pp. 1022-1035, September 1972.

[26] Auld, B.A., "Geometrical Optics of Magnetoelastic Wave Propagation in a Nonuniform Magnetic Field," The Bell System Technical Journal, pp. 495-507, March 1965.

[27] Suhl, H., "The Nonlinear Behavior of Ferrites at High Microwave Signal Levels," Proceedings of the IRE, Vol. 44, No. 10, pp. 1270-1284, October 1966.

[28] Kong, J.A., Electromagnetic Wave Theory, John Wiley & Sons, New York, 1986.

[29] Skolnick, M.I., Introduction to Radar Systems, McGraw-Hill Inc., New York, 1980.

[30] Morgenthaler, F.R., Private Communication, November 1987.

[31] Damon, R.W., and Van de Vaart, H., "Magnetic Field Shaping for Linear Dispersion in YIG Pulse Compression Filters," Proceedings of the IEEE, Vol. 55, No. 7, pp. 1231-1232, July 1967.

[32] Hu, H.L., "Studies of Magnetostatic Waves and Magnetoelastic Waves in YIG Using Optical Probing and Microwave Techniques," Technical Report 25 (Ph.D. Thesis), Microwave and Quantum Mechanics Group, Massachusetts Institute of Technology, February 1971.

[33] Wadsworth, A.K., "Improvements in the Design of Microwave Magnetoelastic Delay Lines," Technical Report 46 (S.M. Thesis), Microwave and Quantum Mechanics Group, Massachusetts Institute of Technology, January 1982.

BIOGRAPHICAL NOTE

Bruce Feldman is a Captain in the United States Air Force attending MIT through the Senior Commanders Sponsored Education Program. He is an electrical engineer with a professional background in the acquisition and development of advanced microwave receiving systems.

Captain Feldman received a B.A. in Chemistry and graduated magna cum laude from Yale University in 1978. His first tour in the Air Force was at the Air Force Institute of Technology where he received a BSEE and was honor graduated in 1983. Prior to coming to MIT, he was stationed at the 6940th Electronic Security Wing at Ft. Meade, Md.